THE ROLE OF VANADIUM IN MICROALLOYED STEELS

Rune Lagneborg
Bevis Hutchinson
Tadeusz Siwecki
Stanislaw Zajac

Dedicated to the Memory of
Michael Korchynsky

KIMAB-2014-115

Swerea KIMAB
Box 7047, SE-164 07 Kista
SWEDEN
June 2014

ABSTRACT

The present monograph concerns the role of vanadium as a microalloying element in structural steels. A brief historical outline is followed by three chapters that are of a didactic nature, introducing the physical and chemical properties of vanadium in steels and, in particular, its reactions together with the elements carbon and nitrogen. Basic thermodynamic concepts and their application presented in chapter 2 where vanadium is also compared with other microalloying elements, titanium and niobium. The different behaviours of these elements in steel processing are shown to depend on the varying solubilities of their carbonitrides in austenite. The relatively high solubility of V(C,N) in austenite means that vanadium plays only a minor role during hot deformation and mostly remains available for precipitation strengthening during subsequent cooling. Chapters 3 and 4 discuss the precipitation behaviour of carbonitrides in austenite and ferrite respectively. Co-precipitation of VN together with TiN is often an important factor since TiN is the more stable compound and frequently acts as a substrate for VN in austenite. A relatively recent finding is the ease with which ferrite nucleates on VN particles, thus providing scope for grain refinement and improved mechanical properties. Mechanisms of precipitation of V(C,N) during or after the phase transformation to ferrite are described and analysed in relation to their strengthening contributions, including inter-phase precipitation and the symbiotic effects of carbon and nitrogen contents on uniform precipitation in ferrite.

Effects of vanadium and also other elements are described in connection with the structures and ductility problems encountered during continuous casting of conventional and thin slabs in chapter 5. Principles of thermomechanical controlled processing (TMPC) are outlined in chapter 6 with special reference to vanadium and the benefits of recrystallization controlled rolling (RCR) for optimisation of final strength and toughness. The most important factors are the deformation schedule, the steel composition, especially the nitrogen content, and the cooling conditions through the austenite to ferrite transformation range. Following these general principles, chapter 7 takes up specific product types where vanadium enhances their properties and discusses how the TMPC is most suitably carried out in each case. The product types considered are (i) heavy plate, (ii) strip, (iii) long products, (iv) seamless pipes and (v) forgings. In all of these, the presence of nitrogen plays an important role for enhancing strength through precipitation of V(C,N) in ferrite while in several cases grain refinement by nucleation of ferrite on VN particles in austenite contributes both strength and toughness.
The weldability of vanadium microalloyed products is discussed in chapter 8 in relation to microstructures and toughness properties of the heat affected zones (HAZs). In most situations, vanadium and the higher nitrogen levels used in these steels pose no problems for HAZ toughness. With high heat input welding there is loss of toughness caused by coarse grained ferrite formation but for low heat input conditions the HAZ toughness is remarkably high for both single and multipass welds.

TABLE OF CONTENTS **PAGE**

1. PROLOGUE

1.1 The discovery of vanadium and the evolution of its use

Vanadium was discovered by the Swedish scientist and doctor Nils Gabriel Sefström in 1830. In his studies of ductile iron originating from iron ore of the Taberg mine he obtained a residue which he concluded contained a compound with a previously unknown element, vanadium. At this point, Sefström's master, the famous Swedish chemist Jöns Jacob Berzelius, took up interest in the new element. He announced Sefström's discovery internationally and also initiated a large research programme on vanadium salts. Sefström's and Berzelius' work was, however, confined to chemical studies of a large number of vanadium compounds. It was only some 30 years later that vanadium was isolated as a metal due to work by the English chemist, Sir Henry Roscoe.

The early use of vanadium was as a chemical compound and was based on the investigations by Sefström, Berzelius and Roscoe. Examples of early applications of vanadium compound are: black colouring of ink and fixing aniline black dyes for fabrics. The function of vanadium salts as catalyst for many chemical reactions was discovered 1900 in Germany and has become the most important application of vanadium as a chemical.

In the early 20th century, the technology of process metallurgy had developed such that commercial quantities of ferroalloys could be produced. In order to exploit the opportunities for vanadium as an alloying element in steel the first production unit was set up in South Wales, Great Britain, and a special assignment was given to Professor Arnold of Sheffield College to investigate effects of V-alloying in various steels.

Arnold's research together with studies in steel works in the Sheffield neighbourhood laid the foundation for a whole range of tool and die steels, from high speed steels to both cold work and hot work die steels. Hence, in these applications the hardness of vanadium carbide and its stability at high temperatures played an essential part. The importance of V-alloying in tool steels has not diminished with time. The development of new processing technologies, especially powder metallurgy, has made it possible to increase the hard phase content in high speed and cold work steels considerably. Hence, in recent years this has rather increased the use of vanadium in tool steels.

The usefulness of vanadium in engineering steels was early recognised. Work in the first years of the 20th century, both in England and France, showed that carbon steels exhibit a considerable increase in strength by V-alloying, particularly when quenched and tempered. In the U.S. the use of vanadium for alloying of automotive steels had, as it appears, an accidental beginning. Henry Ford I watched a motor race in which a French car crashed. He examined the wreck and found a crankshaft made from Swedish iron that suffered less damage than expected. After examination in his laboratories it was reported that the steel contained vanadium. As a result Ford gave instructions to use V-steels in critical components in Ford cars 'in order to better resist shock and fatigue on American roads'. At that time, ~ 1910, an understanding of the beneficial effect of vanadium was missing. With today's knowledge we can confidently say that the strengthening was due to fine precipitation of V-carbonitrides during cooling or tempering. The improved impact resistance was due to a refined grain structure resulting from grain growth inhibition by V-nitrides at the quenching or normalising temperature. Other important applications of V-alloying, primarily developed during the first two thirds of this century, are high temperature power plant steels, rail steels and cast irons.

The most exciting and today the largest use of vanadium is in high strength low alloy (HSLA) structural steels; another name for the same group of steels and more related to their alloying is 'microalloyed steels'. The development of these materials started in the 1950's and a brief historical account of this is given below.

Beside its application in alloying of steel and cast irons, vanadium is an essential alloying addition in Ti-alloys for aircraft and aerospace applications. Although V-base alloys have been used in nuclear breeder reactors because of their nuclear, physical, mechanical and corrosive properties at high temperature and are considered as a candidate in future fusion reactors, they have at present no important application as structural materials.

1.2 Statistics of the use of vanadium

Vanadium is obtained from three main sources. Approximately 70% comes from steelmaking slags from plants using high vanadium iron ores. Around 20% arises directly from V-rich minerals while about 10% comes from certain petroleum oils. The total world consumption of vanadium is today (2013) some 79,000 tonnes per annum, more than double the amount (34,000 tonnes) when the monograph was first produced in 1999. The predominant application of vanadium is for alloying of steel, amounting to around 92% of the total, and therefore the consumption of vanadium and the production of steel are strongly interrelated. The dramatic growth of steel production in China has been the biggest driver, and in 2013 more than 35,000 tonnes of vanadium were consumed in China alone.

Most of the vanadium for alloying of steel is used in micro-alloyed structural steels in the form of both long and flat products, most notably in Chinese concrete reinforcing bar, which is the biggest single product application. Vanadium is also widely used in alloyed steels, such as high speed and tool steels, high temperature low alloyed steels etc. The specific consumption of vanadium in steel varies between countries depending on the types of steel products produced and processes employed. For example in North America approximately 0.08kgV is used per tonne of steel, whereas in China it is around 0.035kgV/tonne. In Japan and Europe specific consumption is around 0.06kgV/tonne.

The remaining eight percent of annual vanadium demand in in the chemical and titanium alloy fields. Use in titanium alloys is relatively small compared to steel and relatively stable. The alloy Ti-6%Al-4%V is the workhorse titanium alloy used in aerospace applications, and is expected to grow as commercial airplane production increases and higher proportions of Ti alloys are used in future designs. The main chemical applications include oxidation catalysts, pollution control catalysts, pigments in paints and ceramics. Energy storage represents a potential future important new application for vanadium.

China is the biggest producer, accounting for approximately 55% of global output in 2013. Other significant producers are South Africa, Russia and North America, and there are developments ongoing in Australia, Brazil and elsewhere that will eventually feed more vanadium into the market.

1.3 The development of V-microalloying for structural steels

The development of the microalloyed structural steels and the related development of controlled rolling started in the late 1950's. With the broad introduction of welded structures after the Second World War, strengthening of steel by increasing the carbon content became

practically prohibitive in view of carbon's detrimental effect on toughness of welded structures. Therefore the new knowledge that grain refinement could improve weldability at the same time as enhancing strength was a strong stimulus for developing new hot rolling practices and new steels. With time it was also recognised that strengthening by microalloy precipitation could be substituted for strengthening by carbon while weldability is improved.

In the past, normalising heat treatment was an absolute requirement for steel plate and most structural sections used in structures for heavy-duty service. In the 1960's and 70's V-microalloyed steels with 0.15-0.20% C and 0.10-0.15% V and somewhat enhanced N-content 0.010-0.015% found wide use for this type of application, e.g. thick walled gas pipelines.

In the early 1960's Bethlehem Steel developed and marketed a series of V-N steels with maximum content of C and Mn of 0.22% and 1.25%, respectively, having yield strengths ranging from 320 to 460 MPa and to be used in the as-rolled condition. The steels were offered in practically all product forms, plate, strip and structural sections. An early advanced V-strip steel was VAN80, developed at Jones & Laughlin around 1975, with a typical yield strength of 560 MPa. This was one of the first steels where in-line accelerated cooling was applied in a controlled manner to enhance both grain refinement and strengthening by microalloy precipitation. Around 1965 the development of controlled rolling had reached a level such that it was introduced in commercial production. By microalloying with Nb it was possible to prevent recrystallisation during hot rolling, thereby flattening the austenite grains progressively with reduction and in this way the austenite was conditioned to transform to very fine-grained ferrite. In order to increase strength it was soon found advantageous to also microalloy with vanadium. This type of controlled rolled Nb-V steels, with about 0.10%C, 0.03%Nb and 0.07%V, has been widely adopted for pipelines.

A different controlled rolling route later developed, ~ 1980, was recrystallisation-controlled-rolling. By allowing the worked austenite to recrystallise after each rolling reduction it was found possible to reach a similar grain refinement as with the former method. This process results in higher finishing temperatures; it therefore requires lower rolling forces and can accordingly be practised in weaker rolling mills as well as offering superior productivity. It was found that Ti-V microalloyed steels are especially suited for this process since both these elements only retard recrystallisation weakly and therefore allow repeated recrystallisation during rolling.

1.4 Scope of the present review

The first edition of this monograph (The role of vanadium in microalloyed steels) was published in the Scandinavian Journal of Metallurgy in 1999 (1.1). The copyright of that publication was acquired by the Strategic Minerals Corporation of USA who later re-printed it also in Chinese and Russian. Now that 14 years have passed and much new relevant research and development has taken place it seems appropriate to bring the content of this monograph up to date. The aim of the present paper remains as before, to review the role of vanadium in microalloyed structural steels and our understanding of how it affects microstructure evolution and mechanical properties. Its role related to thermo-mechanical processing in various product categories is especially addressed. The paper covers principally V-microalloyed structural steels with ferrite-pearlite microstructures having low to medium carbon contents. Hence, the many important uses of V-alloying in other steels, e.g. tool and high speed steels, low-alloy creep resistant steels etc., are omitted.

The review is mainly based on work carried out at the Swedish Institute for Metals Research (now Swerea KIMAB) during the last 35 years but includes also reference to other relevant, published work. It should be emphasised, though, that the intention is not to attempt to critically review all the available literature in the area. Most of the original paper has been modified; in several sections it is virtually re-written. New topics include the role of VN as a nucleant for ferrite formation on cooling and its application in several product areas such as seamless pipes and heavy sections. Microalloying with vanadium to stabilise microstructures and strength in low carbon bainitic strip steel is another example. Developments in thin slab casting which was in its infancy in 1999, are also taken up in relation to V-microalloying

A specific aim is to show the present scientific understanding of the subject. Therefore we have devoted the first 3 chapters following the introduction to our view as to how essential phenomena and properties of V-microalloyed steels should be understood and interpreted, ranging from thermodynamic predictions of relevant phase equilibria in V-steels, to microalloying effects in austenite and precipitation in ferrite and its effect on strength. The last 4 chapters are devoted to a comprehensive account for the role of V related to the most important processing steps that microalloyed structural steels are subjected to, viz. continuous casting, thermomechanical processing and welding.

As stated earlier, it has not been our intention to review comprehensively all literature on this subject. Readers are referred to other sources. In particular, the excellent recent review by Baker (1.2) covers many aspects of crystallography of V-phases in steels that are omitted here. Gladman's book on HSLA steels (2.1) makes a valuable starting point for learning about high strength low alloy steels as well as thermo-mechanical processing. As regards papers concerning vanadium in steels, a very large number of these are easily available and can be down-loaded from the Vanitec web-site (1.3).

1.5 Acknowledgments

This review rests primarily on research carried out during the last 35 years at Swerea KIMAB (formerly the Swedish Institute for Metals Research (SIMR)) with economical support by the U.S. Vanadium Corporation/ Stratcor (and its predecessor Union Carbide) and technical cooperation with the late Michael Korchynsky of that organisation. The personal interest and engagement of Michael Korchynsky through most of those years were a prerequisite for the fulfilment of that work. The authors are indebted to him for countless technical discussions, so rewarding and indeed essential for the outcome of the work. More recently, our research into vanadium-microalloying, including preparation of the present review, has been supported by Vanitec and the authors express their gratitude to that organisation and to David Milbourn who has maintained a close interest in it.

We would also like to acknowledge the financing of some of the underlying work by the General Research Programme of SIMR and by SSAB. Finally it should be noted that many researchers at SIMR, beside the present authors, have contributed to this review as investigators and authors of individual projects and papers. In this context the outstanding work of William Roberts should be given special recognition. He laid the foundation for the research on microalloyed steels and hot working at SIMR, and his research increased our understanding of the behaviour of these steels significantly and made improved alloy design and processing possible.

2. ALLOY SYSTEM AND THERMODYNAMIC BASES

The strengthening effect of microalloying additions may be produced by the dispersion strengthening effect of fine carbonitride particles or by grain refinement, i.e. inhibition of grain growth by carbonitride particles, or by a combination of these two effects. In order to maintain a fine austenite grain size prior to transformation, particles that remain undissolved in the austenite, or particles that will precipitate during hot rolling are required. To produce the very fine particles that are responsible for dispersion strengthening (i.e. particles ~ 2-5 nm in diameter), these should be freshly precipitated during or after transformation to ferrite.

To achieve the desired metallurgical states, a detailed knowledge of the solubilities of the microalloy carbides and nitrides is required, together with a knowledge of their precipitation behaviour. An understanding of the role of different microalloying elements can be gained from the solubility product data summarised in Fig. 2.1 from thermodynamic evaluation. Despite a simplification the individual solubilities of the microalloyed carbides and nitrides offer clear directions for the selection of microalloying additions for specific purposes. It is seen that TiN is extremely stable and can withstand dissolution at high temperatures during reheating prior to rolling or during welding. Niobium nitride and carbide have relatively low solubilities and may precipitate out in the later stages of rolling. Vanadium on the other hand, has a rather high solubility in austenite even at temperatures as low as 1050°C. It is also seen that the nitrides are substantially less soluble than the corresponding carbides. This is especially true for titanium and vanadium where the differences are particularly pronounced.

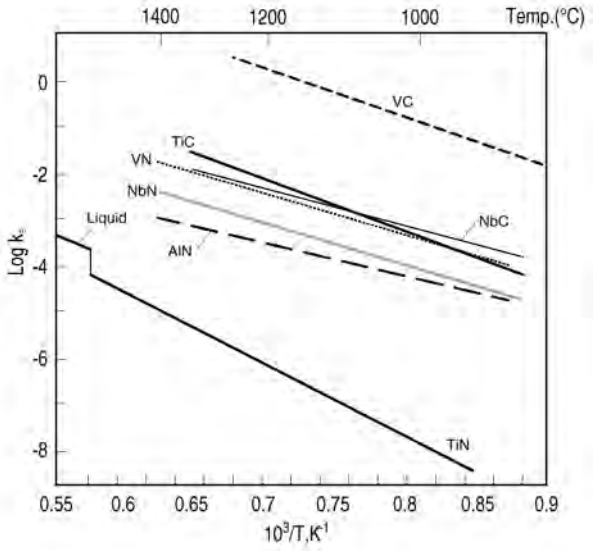

Fig. 2.1 Solubilities of microalloy carbides and nitrides.

In normal circumstances the solubility relationships shown in Fig. 2.1 represent a simplification, as steel may contain more alloying elements with high affinity for carbon and nitrogen which alter the solubility of the microalloyed carbides and nitrides.

2.1 Thermodynamic considerations

2.1.1 Approximate expression for the solubility product

As was stated above the solubility of carbides and nitrides in austenite and ferrite is usually expressed as a solubility product in terms of wt. % of microalloy element and carbon and/or nitrogen. The temperature dependence of the solubility product is expressed by the Arrhenius relationship in the form,

$$\log k_S = \log [M][X] = A - B/T \qquad 2.1$$

where k_s is the equilibrium constant, [M] is the dissolved microalloy (wt.%), [X] is the content (wt.%) of nitrogen or carbon, A and B are constants and T is absolute temperature.

Several authors have made efforts to establish the solubility of carbides, nitrides and carbonitrides in austenite, see for example, the compilation in (2.1). All of these investigations expressed their results in a form of solubility products. However, the results proposed by various authors as the "best-line" relationships sometimes differ considerably. An analysis of published data concerning the solubility of VC, VN, NbC, NbN, TiN and AlN, Fig. 2.2, show that more than ten different solubility equations exist for each carbide/nitride, and the spread between them is significant, in most cases greater than 150°C. It should be pointed out that the situation is even more complicated when more than one microalloy element is present and when the ratio of carbon to nitrogen is changed. The influence of carbon and nitrogen on carbonitride formation has been handled in different ways by different authors, (2.2). For example, for Nb-microalloyed steels the nitrogen was often considered to modify the effective carbon concentration as [C+12/14N], e.g. (2.3).

The analysis of the solubility data in terms of solubility products implicitly assumes that the activity coefficients of microalloying elements as well as carbon and nitrogen are constant while the micro-additions are treated as a dilute solutes and any interactions between solutes in the system are neglected. Therefore the individual solubility equations apply only to a particular composition investigated and are not capable of predicting the solubility at different compositions, where the effects of solute interactions become significant. The carbides and nitrides are also non-stoichiometric and, hence, their composition can vary when precipitated in steels.

The similarity of crystal structure of carbides and nitrides enables them to show mutual solubility. Except for (V,Zr)N, all other carbides and nitrides formed by Ti, Nb, Zr and V show continuous or extended mutual solubility. For V and Zr the large difference in atomic size enables their compounds only to show limited mutual solubility. It is necessary to emphasise that aluminium differs from the microalloying elements V, Nb and Ti because it does not form a carbide in steel, but only the nitride, AlN, having a different crystal structure (hexagonal close packed). Therefore, there is no mutual solubility with the carbides/nitrides of V, Nb and Ti, all of which have the NaCl cubic crystal structure.

2.1.2 ThermoCalc model

In order to accurately predict the austenite/ferrite carbonitride equilibria, expressions describing the chemical potentials of the transition metals and carbon and nitrogen in austenite and metal carbonitride are required as a function of composition and temperature. To describe the thermodynamics of austenite, ferrite and the non-stoichiometric carbonitride phase respectively, the Wagner formalism (2.4) for dilute ternary solutions or a sublattice-subregular solution model proposed by Hillert and Staffansson (2.5) can be used. The Wagner formalism is in fact identical to the regular solution model if the second-power terms are neglected.

In the sublattice-subregular model proposed by Hillert and Staffansson the partial Gibbs energy of component M in each individual phase is expressed as,

$$G_M = RT \ln a_M = RT \ln x_M + {}^{E}G_M \qquad (2.2)$$

where a is the activity and ${}^{E}G_M$ is the excess Gibbs energy.

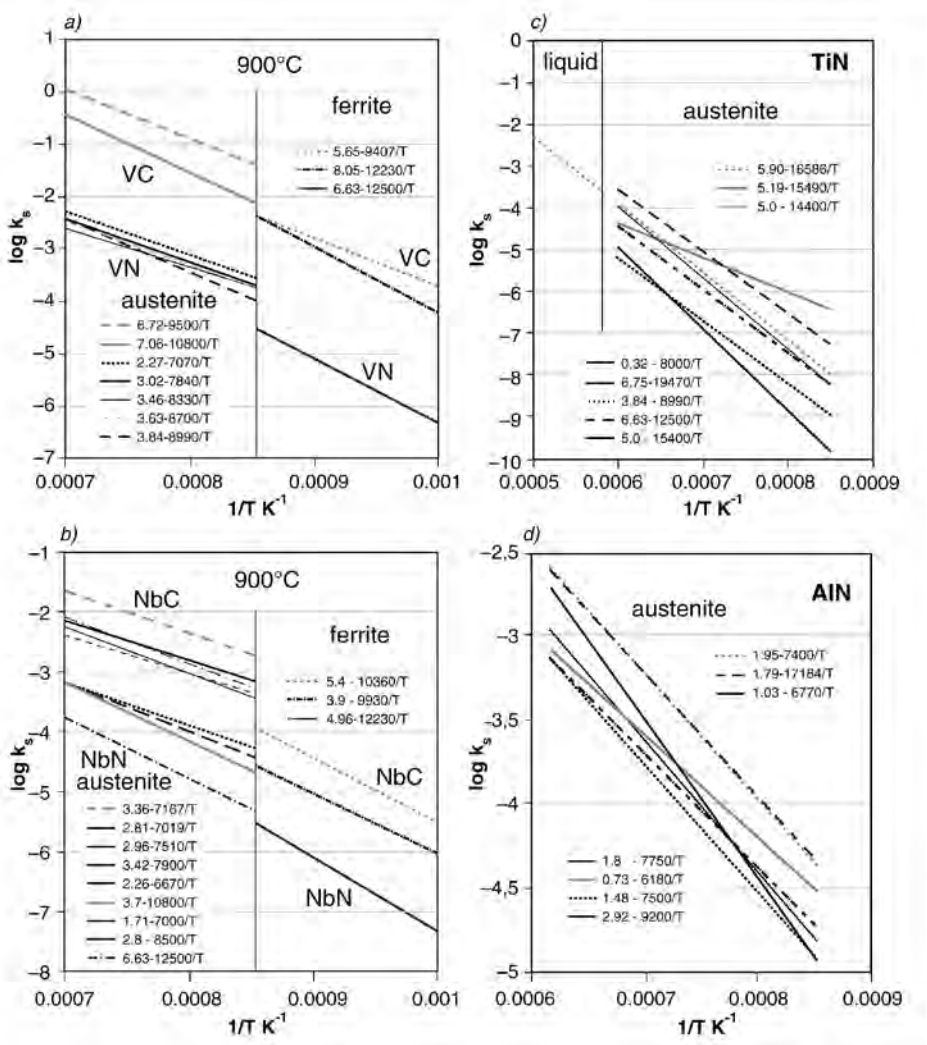

Fig. 2.2 Solubility data for (a) VC and VN, (b) NbC and NbN, (c) TiN and (d) AlN (2.1).

The real crystalline structure of nitrides and carbides is expressed in the form of two sublattices, one for the substitutional elements and one for the interstitial elements. Most of the interstitial sites are usually vacant and vacancies (Va) must thus be treated as an additional element. In principle, an interstitial solution cannot extend beyond the composition where all the interstitial sites are occupied. To take fcc V-N as an example, the model of the solution extends from pure V, which may be regarded as a V_1Va_1 to a compound V_1N_1. A general ThermoCalc database for the thermodynamic properties of microalloyed steels has been developed (2.6) which comprises the thermochemical parameters for multi-component systems of HSLA steels. In the ThermoCalc approach (2.7), the properties of elements and phases are described by the mathematical representation of their thermodynamic properties and the phase equilibria and complete phase diagrams are calculated by minimising the Gibbs energy. The database can also be used to calculate metastable equilibria since the data can be extrapolated from the regions where the phases involved are stable. Interactions between different atoms in higher-order systems are described by the mixing parameters. This model is now successfully utilised to calculate the volume fraction and compositions of particles at different temperatures as well as the driving force for precipitation. The analysis of the alloy systems of microalloyed steels described below was made with the aid of the ThermoCalc model.

2.2 Thermodynamic description of the Fe-V-C-N system

2.2.1 The Fe-V-C Ternary System

In the Fe-V-C ternary system the following phases have been considered (including a vanadium-rich eutectic); liquid, ferrite, austenite, VC_{1-x} carbide, V_2C_{1-x} carbide, V_3C_2 carbide, sigma (σ) phase, graphite and metastable phase cementite. Both V_2C and VC carbides have appreciable ranges of homogeneity due to the carbon deficit (2.8). The carbon atoms are randomly distributed in the interstitial sublattice at high temperatures. The solubility of VC carbide in the Fe-V-C system has been studied rather extensively (2.9). The experimental iso-carbon activity data in austenite were described by the ternary interaction parameter, $L^{fcc}_{Fe,V:C}$, in the form $-(7645.5 + 2.069T)[1+(y_{Fe}-y_V)]$ (2.10).

2.2.2 The Fe-V-N Ternary System

The Fe-V-N ternary system consists of two bcc phases (ferrite (α) V(b-V)), two fcc phases (austenite (γ), vanadium mononitride (VN)), two hcp phases (iron nitride (ε), vanadium dinitride (V_2N)), liquid (L), Fe_4N(γ′) and so-called sigma phase (σ), Fig. 2.3 (2.11). In addition to these phases, N_2 gas is involved in some equilibria. The VN phase has a NaCl type of structure, which can be described as fcc V with all the interstitial sites filled with N. Since this phase is isomorphous with austenite from a crystallographic point of view, the solubility of VN in austenite is described by a miscibility gap which separates the Fe-rich fcc phase (i.e. austenite) from Fe-poor fcc phase (i.e. VN).

Several reports were presented previously on the equilibrium nitrogen solubility and nitride formation in austenite (2.12) and ferrite (2.13). Considerable experimental uncertainty still remains which makes some difficulty in the accurate determination of the interaction parameters. This is mainly due to the quite narrow austenite single phase region in the experimental temperature range. The ternary interaction parameters $L_{Fe,V:C}$ were evaluated by Ohtani and Hillert (2.11) for liquid phase and fcc. Using these parameters it was possible to estimate the solubility product of VN in austenite and ferrite. The following equations were obtained,

in austenite; $\log (wt.\%V)(wt\%N) = -7600/T - 10.34 + 1.8\ln T + 7.2\times10^{-5} T$ (2.3)
and ferrite; $\log (wt.\%V)(wt\%N) = -12500/T + 6.63 - 0.056\ln T + 4.7\times10^{-6} T$ (2.4)

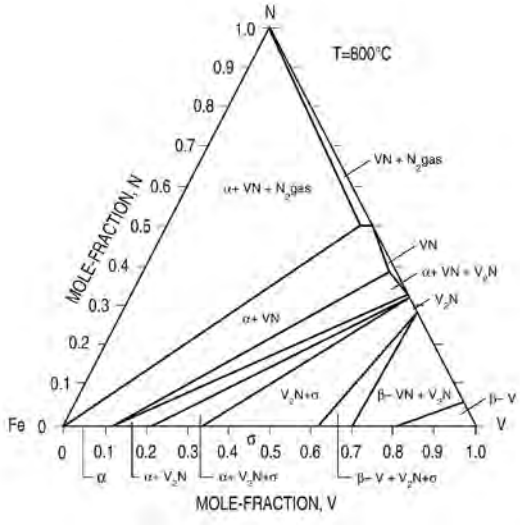

Fig. 2.3 The Fe-V-N ternary system at 800°C.

2.2.3 Solubility and composition of V(C,N) in V-microalloyed steels

ThermoCalc calculations of precipitation of V(C,N) in steels microalloyed with vanadium are shown in Fig. 2.4. For these calculations the parameters for the carbon, nitrogen and vanadium interaction with other elements present in steels have been taken from the SSOL and TCFE ThermoCalc databases (2.7). For V-microalloyed steels the effect of manganese on the activity of V is especially important. Manganese is known to increase the activity coefficient of V and at the same time decrease the activity coefficient of C. Also shown in this figure is the mole fraction of nitrogen in carbonitrides at various temperatures and for various nitrogen contents from hyperstoichiometric levels to zero. This shows that vanadium starts to precipitate in austenite as almost pure nitride, until practically all the nitrogen is consumed. When the nitrogen is almost exhausted there is a gradual transition to form mixed carbo-nitrides, Fig. 2.4(b). Nitrogen-rich vanadium carbonitrides may precipitate during or subsequent to the γ-α transformation. Precipitation during the transformation is a result of the solubility drop of the vanadium carbonitrides associated with the transformation from austenite to ferrite at a given temperature. A significant feature of the solubility of vanadium carbide in austenite is that it is considerably higher than those of the other microalloy carbides and nitrides, suggesting that vanadium carbide will be completely dissolved even at low austenitising temperatures.

2.3 The Fe-Ti-C-N system

The calculated precipitation of TiN and TiC in steels microalloyed with titanium, is shown in Fig. 2.5. Also shown in this figure is the mole fraction of nitrogen in carbonitrides at various temperatures for various nitrogen contents from hyperstoichiometric levels to zero. Titanium forms an extremely stable nitride TiN that is virtually insoluble in austenite and may be effective in restricting grain growth during processing and welding. Only a small titanium addition (~ 0.01%Ti) is required for this purpose. If larger contents are present the excess titanium can precipitate at lower temperatures as the carbide TiC which contributes a precipitation hardening effect. This shows that the solubilities of titanium nitride and titanium carbide are significantly different and the precipitates formed in the austenite are almost pure nitrides, until practically all the nitrogen is consumed. It is worth noting that in the Ti-steel containing 0.01%Ti or less for controlling austenite grain size there is usually sufficient nitrogen to combine all Ti as TiN. When the nitrogen is about to be exhausted there is a gradual transition to form mixed carbonitrides, Fig. 2.5 (b).

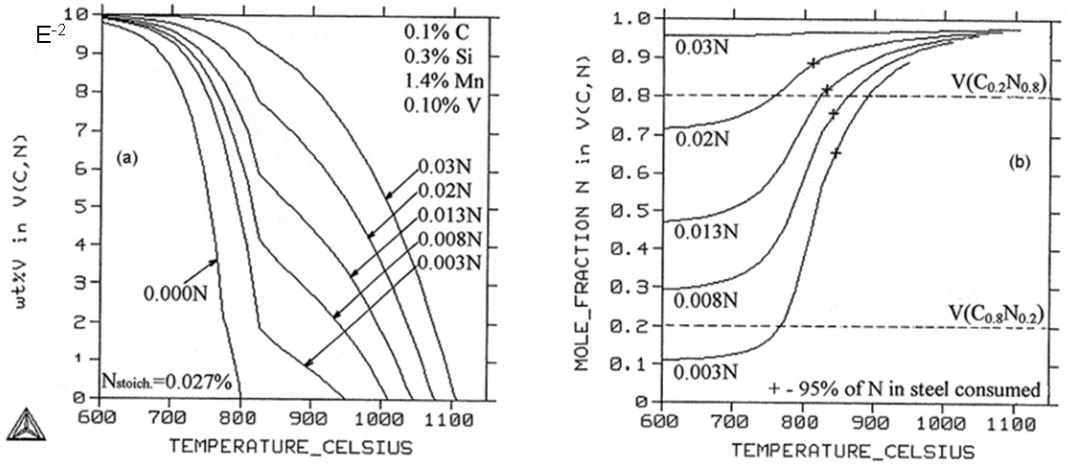

Fig. 2.4 Example showing the precipitation of nitrides, nitrogen-rich carbonitrides and carbides in 0.10% V steels at various nitrogen contents.

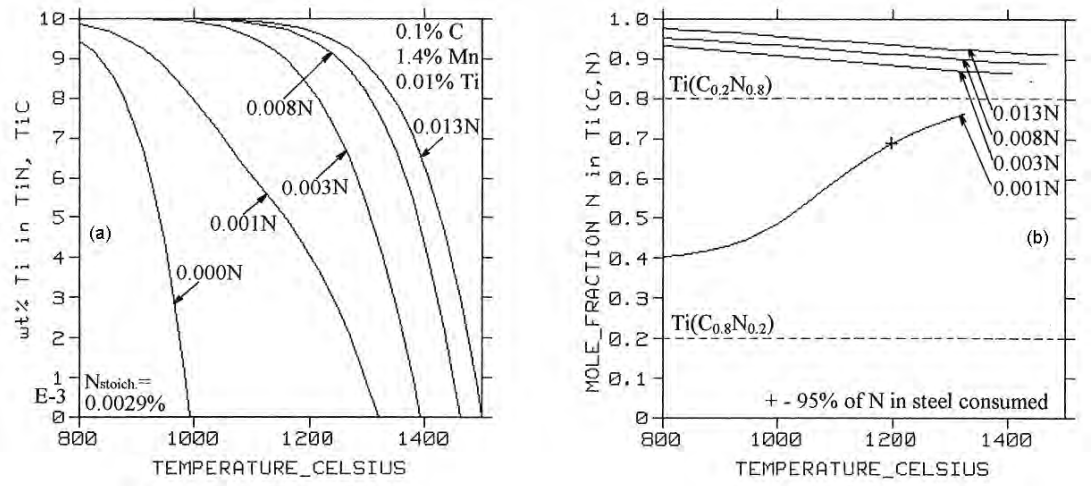

Fig. 2.5 Calculated precipitation of nitrides, nitrogen-rich carbonitrides and carbides in 0.01%Ti steels at various nitrogen contents.

Titanium exerts a strong affinity not only for carbon and nitrogen but also to other elements such as oxygen and sulphur. In Ti-microalloyed low carbon steels the carbosulphide $Ti_4C_2S_2$ or sulphide TiS may form which remain undeformed during hot rolling (2.14). According to Fig. 2.6, $Ti_4C_2S_2$, is more stable than MnS and the formation of MnS is restrained by the addition of Ti to the steels. It is also clear from this figure that the formation of Ti-sulphides or carbosulphides will decrease the amount of Ti available for TiN and TiC. Therefore for proper calculation of the precipitation of microalloyed carbides and nitrides the effect of all elements present in the steel must be considered.

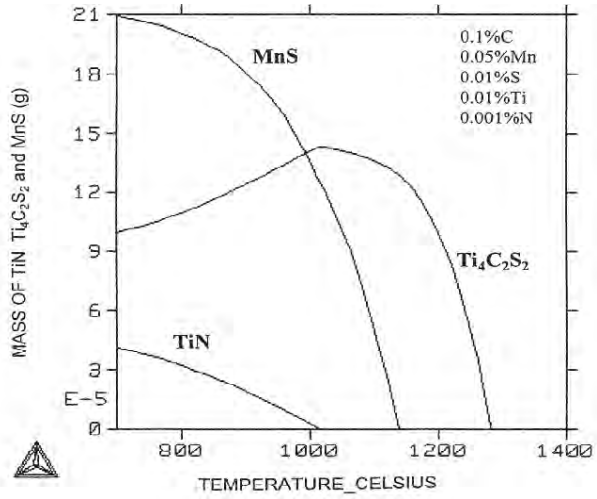

Fig. 2.6 Calculated precipitation of MnS, $Ti_4C_2S_2$ and TiN in low manganese steel.

2.4 The Fe-Nb-C-N system

For Nb-steel, Fig. 2.7 where the difference in solubility between the nitride and the carbide is relatively small, mixed carbonitrides form at all nitrogen contents, even at the hyperstoichiometric levels (2.15). Hence, for realistic contents of carbon and nitrogen in steel, relatively pure nitrides cannot form at all. Nb(C,N) is stable at low temperatures in austenite but dissolves at higher temperatures, for example, during re-heating prior to rolling. At temperatures of rolling the solubility of Nb(C,N) is exceeded, resulting in strain-induced precipitation. The deformed austenite structure transforms to fine grained ferrite on cooling, which imparts both high strength and toughness to such 'controlled rolled' steels. A further

precipitation of the remaining niobium, as smaller particles in ferrite, during cooling gives rise to additional strengthening.

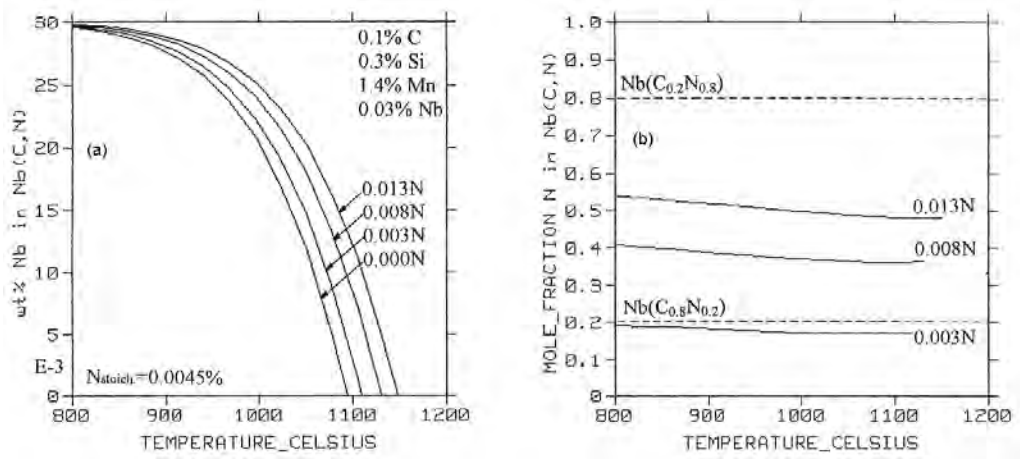

Fig. 2.7 Example showing the precipitation of Nb carbonitrides in 0.03% Nb steels at various nitrogen contents.

2.5 Chemical composition of precipitated particles in multi-microalloyed steels

The carbides and nitrides of V, Ti and Nb show extensive mutual solubilities which arises from the fact that they have the same cubic crystal structure and have very similar lattice parameters. Precipitation of carbonitrides in multiple microalloyed steels with V, Nb, Ti and Al is shown in Fig. 2.9(a), where the soluble components are expressed as a function of temperature. In Fig. 2.9 (b) the mole fraction of Ti, Nb and V in M(C,N) is also included.

As expected, the major part of the precipitate at the highest temperatures is TiN whilst further precipitation at lower temperatures is predominantly Nb(C,N). Thus, the primary precipitates to be formed in austenite are composite (Ti,Nb)-nitrides. The Ti and Nb contents of those depend on steel composition and precipitation temperature. Thermodynamic calculations imply that at the relatively high temperature of 1200°C, primary (Ti,Nb,V)N particles contain ~20% of Nb and ~5% of V for multiple microalloyed steels.

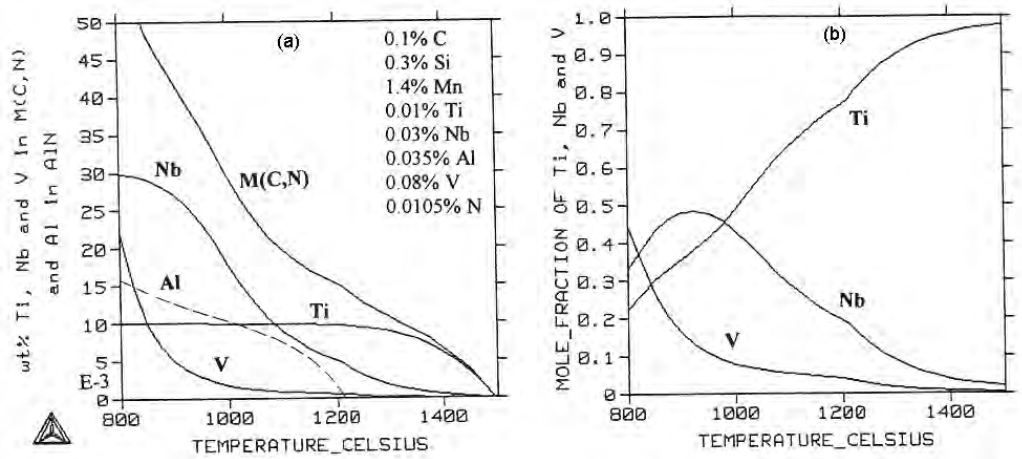

Fig. 2.9 Example of nitrides and nitrogen-rich carbonitrides in multiple microalloyed steel (a) and the mole fraction of Ti, Nb and V in M(C,N) (b).

It is clear from this figure that the volume fraction of microalloy nitrides at high temperatures will be considerably larger in the Ti-Nb-V steel than in the single microalloyed steels. It may

also be seen that AlN (with close packed hexagonal structure) has little or no solubility for other microalloying elements and starts to precipitate at approximately 1200°C in the presence of 0.035% Al, Fig. 2.9 (a).

It should be mentioned, however, that the uniform composition of second phase particles suggested from the thermodynamic calculations is often not the true situation in practice. The particles are frequently cored, reflecting the high temperature stability of a titanium-rich and nitrogen-rich compound in the interior of the particle with relative enrichment of Nb and V towards the surface of the particle. This suggests that these primary composite nitrides can act as nucleation centres for subsequently precipitation at lower temperatures, for example forming a NbN deposit around a core of TiN. Similar results have been obtained for Nb-V steels where niobium-vanadium nitrides have shown Nb and N enrichment in the precipitates, in accord with the higher thermodynamic stability of NbN. These coring effects may be a result of very slow diffusion of Ti in carbonitrides or the existence of a miscibility gap as explained further in Chapter 3.

Another important aspect of multiple microalloying is that the niobium or vanadium tied up as (Ti,Nb,V)N particles are not available for subsequent thermo-mechanical treatment. Fig. 2.9 (b) shows that a significant fraction of added niobium may remain undissolved even at high reheating temperatures and cannot contribute to retardation of recrystallisation and/or precipitation strengthening. For this reason the nitrogen content of Nb-microalloyed steels must be kept low. Vanadium, on the other hand, exhibits higher solubility and is therefore normally fully available for precipitation strengthening in ferrite.

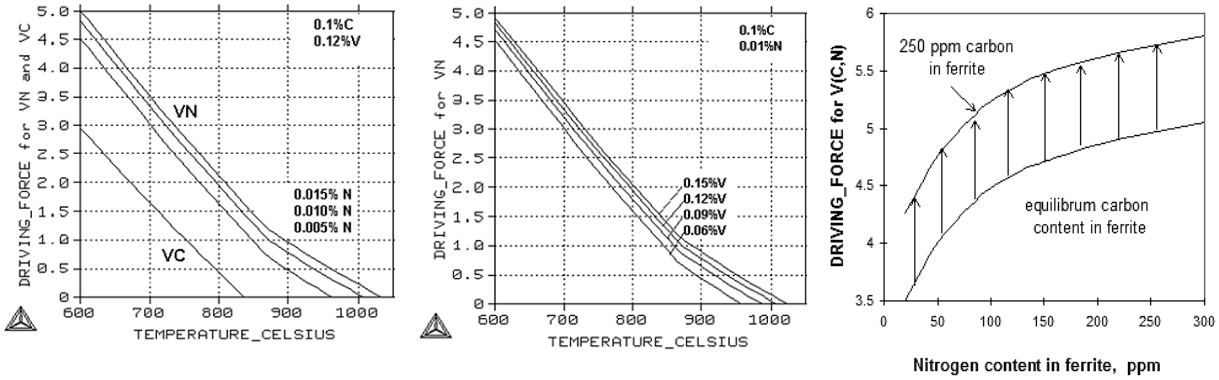

(a) (b) (c)

Fig. 2.10 (a) and (b) Chemical driving force, $\Delta G_m/RT$, for precipitation of VC and VN in 0.12% V steel. (c) effect of equilibrium and metastable carbon content in ferrite on driving force for precipitation of V(C,N) at 650°C.

2.6 Thermodynamic Driving Force for Precipitation

The precipitation process proceeds at a perceptible rate only if there is a driving force, that is, a free energy difference between the product and parent phases. This driving force enters the steady state nucleation rate in a central way and must be known with some accuracy if nucleation rates are to be calculated, or even estimated. The chemical driving force for nucleation of VN and VC in V-microalloyed steels, determined from the HSLA database are illustrated in Fig. 2.10. It can be seen in Fig. 2.10a that, as the temperature is decreased the driving force increases monotonically and changes slope after the austenite to ferrite transformation. The dominating effect of N on the driving force is clearly seen in this figure.

2.7 Practical consequences of different solubilities of V carbides and nitrides

Vanadium is the most soluble of the microalloying elements discussed here and does not readily precipitate in austenite. Since V(C,N) has high solubility in austenite it hardly affects the hot deformation process but rather precipitates during cooling in ferrite, thereby increasing the strength level of the steel by precipitation hardening. For hard particles such as microalloy carbonitrides, bypassing of dislocations is expected to occur by bowing between the particles (Orowan-mechanism) under all practical conditions. This means that there is virtually only one parameter, which determines the precipitation strengthening namely the inter-particle spacing. The smaller is the inter-particle spacing the larger is the strengthening effect.

In precipitation reactions, the decisive factor which minimises the inter-particle spacing (and maximise the precipitation strengthening) is the rate of nucleation since it determines the particle density. In turn, the most important parameter controlling the nucleation frequency is the chemical driving force for precipitation. Hence, the strong effect of N in increasing this driving force, Fig. 2.10(a), is the explanation of the well-known increase in strength by N in V-microalloyed steels (for a full discussion see Chapter 4). It should be noted, however, that the driving force can also be raised by V-addition, Fig. 2.10(b), but the effect per concentration unit is much less. Moreover, V-additions increase alloying costs significantly whereas the usage of N at the present levels is free.

A combination of V with other microalloy elements in the same steel can naturally lead to interactions since they compete for the same interstitial elements and may also form mixed compounds with one another. For example, the stable TiN phase may incorporate a significant amount of V and even AlN has sometimes been detected in complex titanium nitride particles. Since the (Ti,V)N particles are rather coarse such an effect reduces to some extent the contribution which the V can be expected to make towards precipitation strengthening.

2.8 Summary of chapter

- The solubility of V(C,N) in austenite and ferrite is much larger than that of other microalloying elements.
- The solubilities of the carbides and nitrides of V differ widely; the solubility product of VN is about two orders of magnitude lower than that of VC. This implies that N has a decisive role in V-microalloyed steels, especially for the enhancement of the driving force for precipitation.
- Interaction of V with other microalloy element leads to the formation of mixed carbonitrides and decreases the amount of vanadium dissolved in austenite.
- To accurately predict the austenite/ferrite carbonitride equilibria, expressions describing the chemical potentials of the transition metals and carbon and nitrogen in austenite and ferrite as well as metal carbonitride are required as a function of composition and temperature. Interactions between alloying elements influence significantly the solubility of V(C,N).

3. MICROALLOYING EFFECTS IN AUSTENITE

In commercial V-microalloyed steels small amounts of titanium (~ 0.01%) are commonly added to prevent excessive grain coarsening at high temperatures. The technical background to this is that titanium reacts with the nitrogen already during casting of the steel to form a fine dispersion of very stable TiN particles. For this to occur in typical HSLA plate and strip steels the normal levels of N in BOF and EAF steel making, i.e. 0.004 – 0.015%, are sufficient. However, to attain the fine TiN size necessary for effective grain growth control, fast cooling is needed during the solidification of the steel, as in continuous casting of slabs. The interest for Ti has also risen since its ´normal´ content in steel as an impurity due to recycling has increased to 30-50ppm.

The TiN precipitation may be affected by additional microalloy elements, such as vanadium, by forming compound (Ti,V) particles. This alone, but especially together with the formation of a second precipitate, may affect the grain coarsening behaviour significantly. This justifies a rather thorough discussion of the precipitation and dissolution of particles and how they affect grain coarsening during reheating before hot rolling. An important recent discovery in this area is that vanadium nitrides in austenite are effective nucleation sites for ferrite and have been demonstrated to be an effective means of grain refinement in some types of steel. Also here, V-Ti microalloying is of interest because of the early formation of V(C,N) on primary TiN during steel processing.

3.1 Precipitation and dissolution of microalloy carbonitrides in austenite

It is well established that TiN forms as a fine precipitate dispersion early after solidification in Ti-V and Ti-Nb HSLA-steels having less than about 0.02%Ti. At lower temperatures when the solubility of Nb(C,N) and V(C,N) has been exceeded, many experimental studies have shown that these phases co-precipitate to a large extent on the already existing TiN-particles. Of course, as the driving force for carbonitride formation increases at lower temperatures in the austenite regime the probability for nucleation of new carbonitrides, rich in V or Nb and eventually pure V- or Nb-carbonitrides, increases.

Figure 3.1 shows results from calculations for Ti-, Ti-V-, and Ti-Nb-steels using the thermodynamic database developed for microalloyed steels (3.1, 3.2). The graphs show the fractions of Ti, V and Nb precipitated as nitrides at equilibrium in the austenite. From this we can see that the precipitation curves, for Ti are the same for all three steels. Hence, we can conclude that the temperature for initial precipitation and complete dissolution should be the same for all of them. Furthermore, as long as all the vanadium or niobium co-precipitates on pre-existing TiN on lowering the temperature, we should expect the density of precipitates also to be the same in the steels; of course the individual particles will grow larger in the V- and Nb-steels as these elements co-precipitate. However, at lower temperatures V- and Nb-carbonitrides are expected to form as new precipitates, and indeed this has been shown experimentally (3.3, 3.4). In accordance with this reasoning it is generally observed that larger particles that formed at high temperatures are high in Ti and low in V or Nb, whereas smaller ones formed at low temperatures are low in Ti and high in V or Nb (3.3, 3.4). This is demonstrated in Fig. 3.2 for a Ti-V steel showing a gradual decline of the Ti-content in (Ti,V) N as particle size decreases (3.3). Along the same lines, Fig. 3.3 shows how the spread in V and Ti in a (Ti,V)N population decreases with increasing reheating temperature; as expected the widest spread is observed in the strand-cast condition (220mm) (3.5). The low nitrogen steel with near stoichiometric Ti/N ratio exhibits a considerably smaller spread due to the fact

that nearly all N is consumed to form TiN. From Fig 3.2 the very fine size of the TiN precipitates, in the range 5-100nm, should be noted. Comprehensive measurements of TiN size distributions show that the average particle diameter is about 10nm in 220mm slabs (3.4).

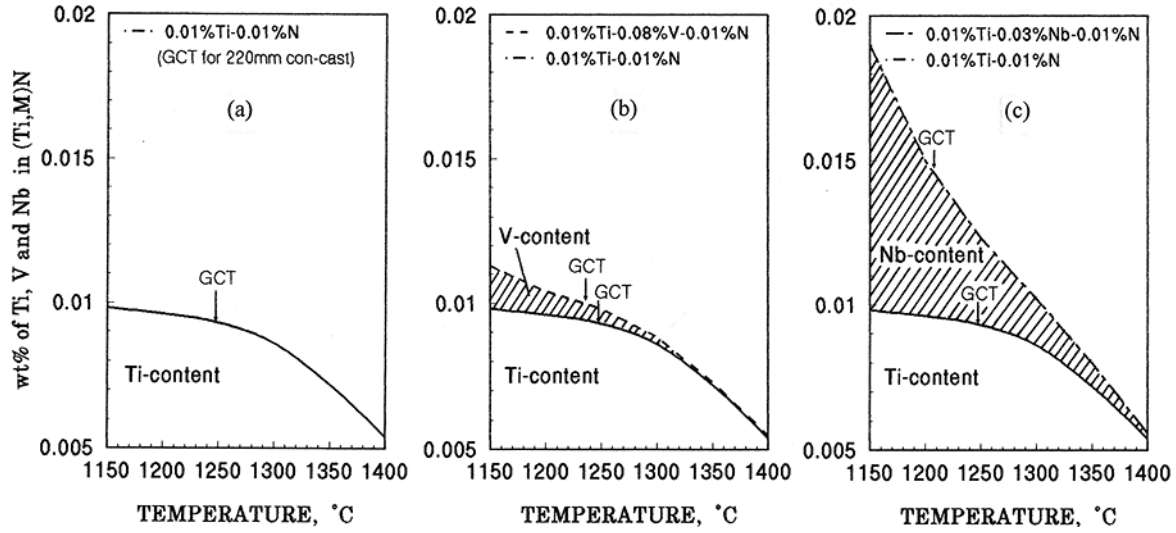

Fig. 3.1 Calculated amounts of Ti, V and Nb precipitated as (Ti,M)N in (a) Ti, (b) Ti-V and (c) Ti-Nb steel. GCT is the experimentally determined grain coarsening temperature of continuously cast 220 mm slabs (2.6).

A general conclusion is that the stability of TiN itself is not expected to change by additions of other microalloying additions, such as V or Nb. However, the separately formed V- and Nb-rich carbonitrides are less stable and dissolve at lower temperatures. This is exactly what has been found experimentally (3.6), but has sometimes incorrectly been stated as a decline of the stability of TiN.

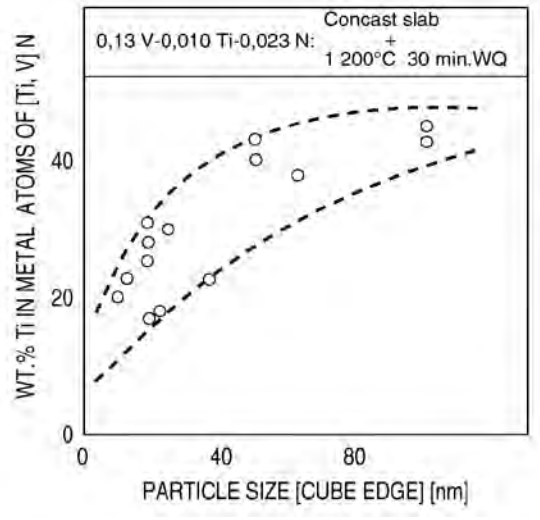

Fig. 3.2 *Relationship between composition of (Ti,V)N-precipitates and particle size in a Ti-V-steel with high V and N. The steel was laboratory cast but cooled at a rate equivalent to that of 220 mm continuously cast slab (3.3).*

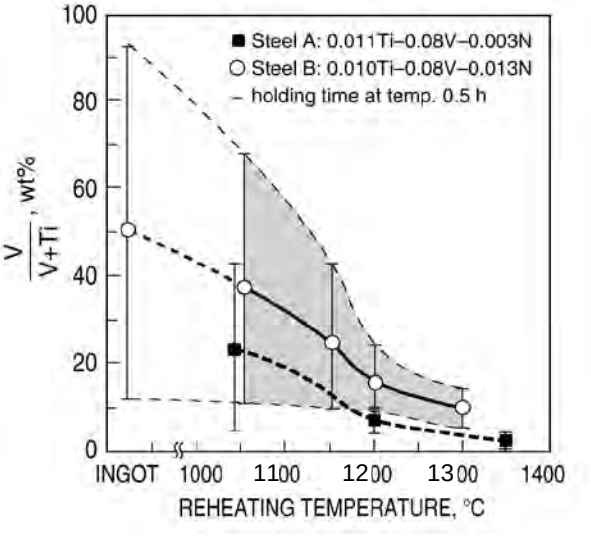

Fig 3.3 *Spread in composition of (Ti,V)N-particles in two Ti-V-steels with low and high N in the continuously cast condition and after varying reheating temperatures (3.5).*

Figure 3.4, showing the solubility curves for TiN in austenite for various temperatures, demonstrates that the Ti/N ratio affects the TiN stability in various ways (3.2). Changing the Ti and N contents along the stoichiometric lines results in the largest change in solubility. Hence, using over-stoichiometric contents of N, as indicated in the graph, gives rise to:

- a higher dissolution temperature of TiN
- a smaller fraction of dissolved TiN for a given temperature increase
- a reduction of the Ti-content in austenite in equilibrium with TiN, resulting in slower particle coarsening.

The usefulness of over-stoichiometric N-contents in Ti-V-steels for grain size control in the HAZ of welds has been demonstrated (3.2, 3.7).

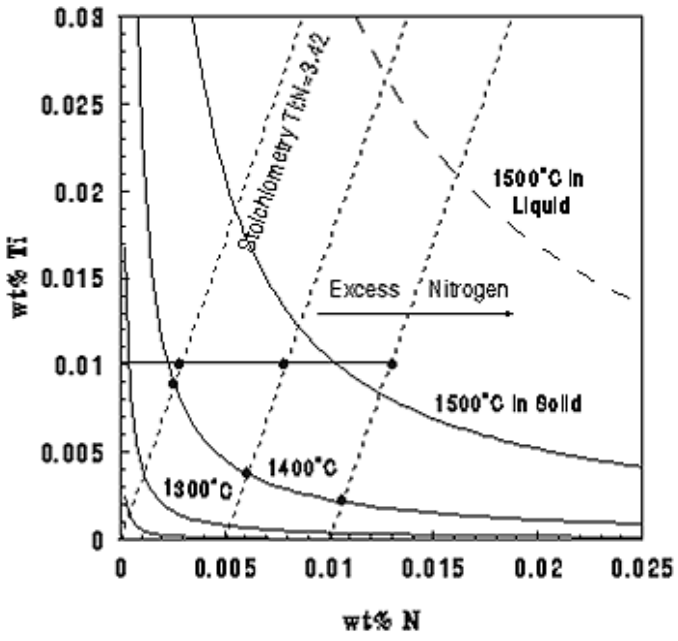

Fig. 3.4 Effect of excess nitrogen on dissolved Ti (3.2).

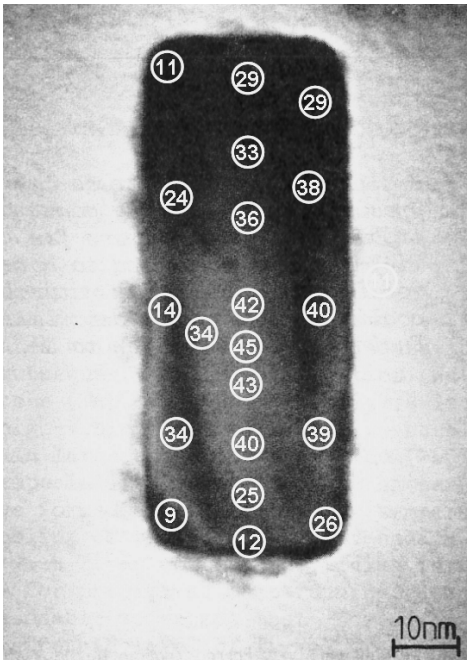

Fig. 3.5 STEM micrograph of (Ti,V)N precipitate in continuously cast and hot deformed Ti-V-N. Figures show the Ti-content as % of metal atoms (3.4).

An interesting feature of (Ti,V)(C,N) precipitation found in austenite of Ti-V steels is that the particles exhibit compositional gradients such that the external parts are richer in V and the interior is richer in Ti (3.3, 3.4, 3.6-3.8), Fig.3.5. Electron microscopy and microanalysis of the (Ti,V)-carbonitrides formed in austenite show furthermore that the compositional gradients of the particles are not always smooth. The outer V-rich part occurs commonly as dendrite arms (3.5). At first this may appear natural in view of the sequential precipitation of Ti and V during cooling. However, a prerequisite is then that the inter-diffusion of Ti and V in the (Ti,V) carbonitride is substantially lower than in austenite. Otherwise there will be ample time for homogenisation of the elements to occur. Unfortunately, the scatter of reported diffusion coefficients in refractory carbides and nitrides is very large. For instance, the self-diffusion of Ti in TiC is slower by 10^{10} than Ti in austenite, whereas the inter-diffusion of Nb in (Ti,Nb)C is only slower by 10^3 (3.9, 3.10). This implies that in the former case, any compositional gradient formed during precipitation of (Ti,V)N will be frozen whereas in the latter case there will be time for full equilibration in normal processing. In view of the fact

that it is inter-diffusion that is significant in the present situation it seems that we should give more confidence to the reported results on (Ti,Nb)C, and hence that homogenisation will occur of the (Ti,V)-particles. This, in turn, would imply that Ti-rich and V-rich carbonitrides can co-exist in equilibrium, and consequently leads to the conclusion that there is a miscibility gap in the (Ti,V)(C,N) system. In fact, this was exactly the result of a thermodynamic analysis of the Ti-V-N system (3.11). It should be borne in mind, though, that only small shifts in the input data for the thermodynamic analysis might cause a change from full inter-solubility to de-mixing.

In a recent laboratory study on simulation of thin slab casting and CSP of low carbon V-Ti steels with titanium contents less than 0.01% and normal EAF nitrogen contents it was found that no (Ti,V)N particles formed during casting but not until holding in the tunnel furnace at 1100°C (3.8). Already at this stage the precipitates exhibited compositional gradients with a higher surface content of V. At lower temperatures and longer times the relative amount of V increased and displayed a weak tendency for a maximum at 900°C.

To illustrate the time scale and the temperature dependence of the changes of the precipitation that may occur in the austenite range we have found it instructive to compute

- the time for completion (90%) of the TiN precipitation from an initial state of all Ti and N in solution
- the time for TiN dissolution (90%) from an initial state of full equilibrium between TiN and austenite at 1000°C
- the time for 50% increase of initial precipitate size by coalescence.

The computations have been carried out for different particle dispersions, expressed as inter-particle spacings, and for the cases of precipitation and dissolution; allowance is made for soft impingement of adjacent solute-enriched zones. Results are displayed in Figs. 3.6 and 3.7.

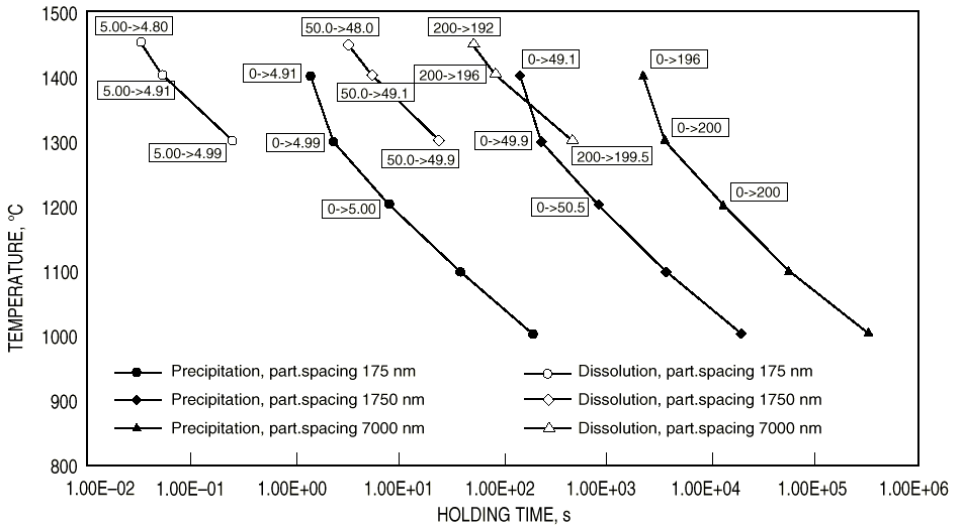

Fig. 3.6 Time for 90% completed precipitation and dissolution of TiN as a function of temperature in a 0.01%Ti, 0.01%N steel at given particle spacings (175, 1750, and 7000nm). Precipitation starts with all Ti and N in solution, whereas the dissolution starts in a state corresponding to full equilibrium between austenite and TiN at 1000°C. Labels at data points indicate changes in particle radius.

The rates of coalescence and dissolution depend critically on the solubility of TiN in austenite. The solubility data available in literature exhibit a considerable scatter, as was demonstrated in Chapter 2. In the selection of data for the present computations our preference has been to use data that produce reasonable agreement with observed ripening of TiN (3.5), although this has implied that we have chosen somewhat lower solubilities than the mean of the scatter band.

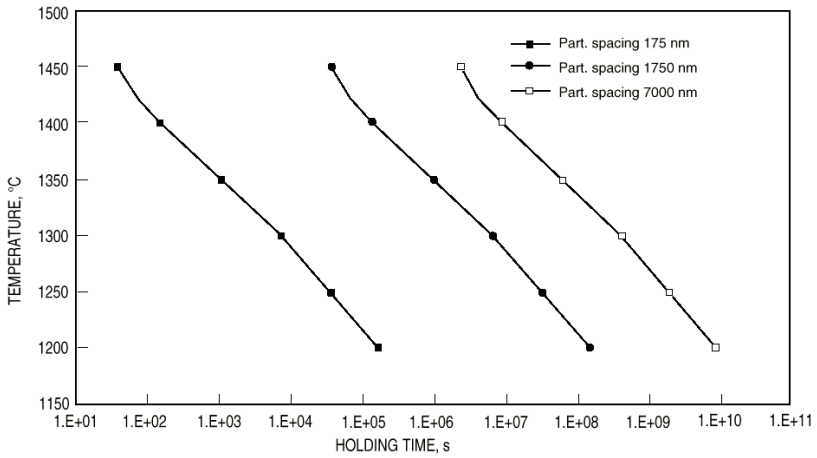

Fig 3.7 Time for 50% increase of the initial TiN size by coalescence as a function of temperature. The initial state corresponds to complete precipitation of TiN with three different particle spacings, 175, 1750, and 7000 nm.

From Fig. 3.6 we may note that very little dissolution of TiN takes place, even at the highest temperatures. At 1450°C, for instance, an initial precipitate size of 5.0 nm equilibrated at 1000°C only shrinks to 4.80 nm. The time for dissolution is about an order of magnitude faster than the time for precipitation, Fig. 3.6. The explanation is the very minute dissolution of TiN as compared to the amount of TiN transferred for complete precipitation. Obviously this effect outweighs the lower Ti-gradient in dissolution as compared to precipitation. The computations of coalescence in Fig. 3.7 show furthermore that coalescence does not produce significant particle coarsening for normal heating temperatures and times except for the finest particle dispersion with particle radius 5 nm and spacing 175 nm, and above about 1300°C.

Hence, these computations show that the grain coarsening temperatures of about 1200°C and even lower that has been observed in thermo-mechanically processed steels, to be discussed below, cannot be accounted for by TiN-dissolution or TiN-ripening. From these results one dares to say that ripening is also insignificant for V and Nb carbonitrides in steel processing because, although the solubility is larger than for TiN, the temperature ranges for their existence are much lower, implying considerably lower diffusivity.

3.2 Grain growth inhibition and grain coarsening

It is a common view that abnormal grain growth is invariably associated with dissolution or ripening of restraining particles. However, this is normally not the case for Ti-microalloyed steels since the TiN-dispersion is virtually unaltered at temperatures below about 1250ºC (3.3). To give a sound understanding of the grain coarsening behaviour of these steels and all the associated important and often intriguing experimental findings it is necessary to go back to the basics of grain growth and its dependence on impeding particles.

The growth rate for an individual grain of diameter D in a distribution of grain sizes with the mean size $\overline{D}$ and containing a dispersion of small particles with volume fraction f and mean radius r is given by (3.12) as:

$$\frac{dD}{dt} = \alpha\sigma M\left(\frac{1}{\overline{D}} - \frac{1}{D} \pm \frac{3f}{8r}\right) \tag{3.1}$$

where α is a constant (~ 1), σ the grain boundary energy, and M the grain boundary mobility. Thus the impeding effect of particles enters by the term $\frac{3f}{8r}$.

From Eq. (3.1) the following conclusions, essential in abnormal grain growth, can be drawn:

(i) Normal grain growth reaches a limiting grain size

$$\overline{D}_{\text{limit}} = \frac{8r}{9f} \tag{3.2}$$

(ii) However, if, in an assembly of grains with mean size $\overline{D}_{\text{limit}}$, there is one grain larger than $1.5\,\overline{D}_{\text{limit}}$ it can grow and with increasing speeds as it grows. Hence, a few individual grains can in this fashion cause abnormal grain coarsening.

(iii) The tendency for abnormal grain growth diminishes with increasing $\overline{D}$ and increasing 3f/8r. In fact, there is a limiting mean grain size beyond which abnormal grain growth is totally prevented

$$\overline{D}_{\substack{\text{abnorm}\\\text{limit}}} = \frac{8r}{3f} \tag{3.3}$$

Thus, a perfectly stable precipitate dispersion causing a total arrest of normal grain growth is not a guarantee against grain coarsening by abnormal growth. This is the explanation why we see grain coarsening temperatures in Ti and Ti-V steels of 1200-1250^{o}C, despite the fact that we do not observe measurable dissolution or ripening of TiN at these temperatures.

It is tempting to believe that on heating Ti-microalloyed steels into the austenite range normal grain growth occurs and the austenite reaches its limiting grain size set by the TiN-dispersion, Eq. (3.2). However, there is ample evidence from early investigations by Siwecki et al. (3.4) that the ferrite-austenite transformation produces an austenite grain size well above $\overline{D}_{\text{limit}}$. This is possible because the chemical driving force the ferrite-austenite transformation is large enough, unlike that of normal grain growth, for the ferrite-austenite interface to pass through the precipitate dispersion. In support for this it has been found that the average matrix grain size at the grain coarsening temperature is about the same in spite of large differences in amounts of TiN (3.4).

A corollary of this conclusion is that the grain coarsening temperature should be a function of the heating rate through the ferrite-austenite transition. With decreasing heating rate the grain size of the transformed austenite increases; hence the driving force for abnormal grain growth decreases, and as a result the grain coarsening temperature is raised. This explanation is confirmed by experiments the results of which are summarised in Fig. 3.8. If the grain size instead was controlled by the TiN dispersion, then the grain coarsening temperature should be independent of heating rate.

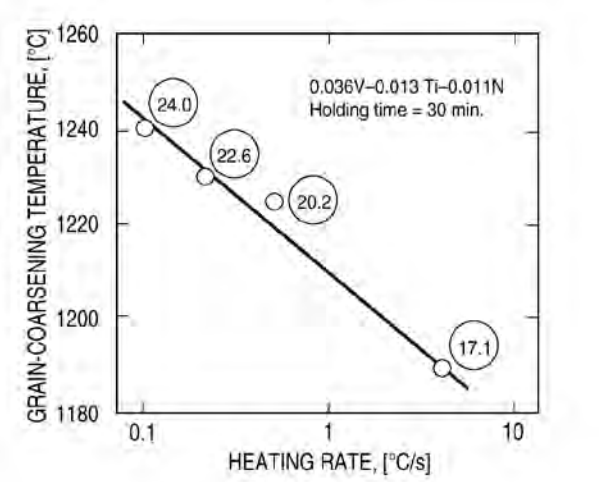

Fig. 3.8 Effect of heating rate on the grain coarsening temperature (GCT) for a 0.036V, 0.013T, 0.011N steel. Encircled numbers refer to the size of small austenite grains at the GCT (3.4).

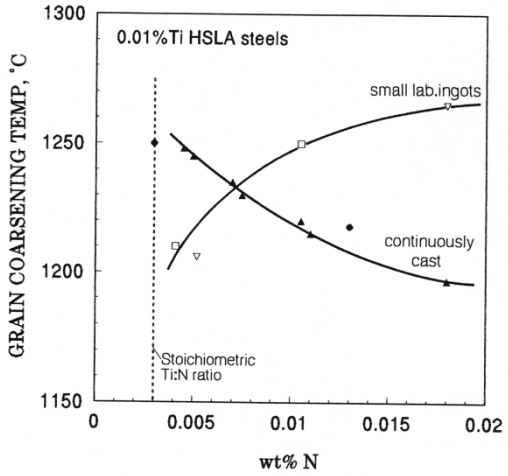

Fig. 3.9 The relationship between austenite grain coarsening temperature and N-content for continuously cast slabs (220 mm) and small laboratory ingots of 0.01%Ti HSLA steels(3.2)

Figure 3.9 summarises measurements of grain coarsening temperatures for steels with varying Ti/N ratios and cast at different cooling rates (3.2). The larger cooling rates in laboratory ingots produce a finer precipitation and a particle density increasing with the N content. The slower cooling in the continuously cast slab produces coarser TiN, and increasingly so with increasing N content due to the fact that precipitation commences at higher temperatures. The increasing precipitate density in the former case progressively prevents abnormal grain growth, and thus causes a rise in GCT. The decreasing TiN density in the slabs, on the other hand, gives the opposite behaviour.

Again, assuming that normal grain growth up to the limiting size controlled by the TiN dispersion would determine the average grain size before abnormal growth sets in, we notice that this would cause problems in explaining the observations in Fig. 3.9. As a matter of fact, if $1/\overline{D}$ were to be more decisive than 3f/8r in Eq. (3.1) for controlling abnormal growth, then we should even expect GCT to be lowered with N content for the laboratory ingots as $\overline{D}_{\text{limit}}$ is reduced with increasing particle density. In a similar way, this line of reasoning would give increasing GCT for the slab materials.

In summary, for steels with a dispersion of microalloyed nitrides stable above 1200°C, such as V-Ti steels, the austenite grain size formed on reheating will be primarily determined by the heating rate through the ferrite-austenite transformation and not by the precipitate dispersion. Normal grain growth of the austenite so formed will be totally inhibited since the grain size is larger than $\overline{D}_{limit}$. On the other hand, this structure will be exposed to abnormal grain growth occurring by accelerating growth of individual grains exceeding the mean size by about 50%. In turn, this growth will be promoted by a fine matrix grain size and impeded by a dense dispersion of precipitates, cf. Eq.3.1.

It is to be noted that the TiN dispersion in the steels discussed above is very fine. For instance, for $\overline{D}_{limit}$ to be less than all the austenite grain sizes measured in Fig.3.8 requires an average particle diameter of 13nm for a volume content of particles corresponding to 0.01%Ti. This is

also in accord with actual measurements of the TiN size distributions in these steels with an average diameter of 8nm (3.3, 3.4).

Under the very high heating rates in welding the ferrite-austenite transformation should lead to particularly fine austenite grains and therefore a strong driving force for abnormal grain growth. Still we know that Ti-microalloyed steels containing a fine dispersion of TiN exhibit very good HAZ toughness as a result of their finer austenite grain structure. This apparent anomaly is due to the fact that it takes a considerable time for the few growing grains to consume all the fine grains and thereby cause an abnormal grain size. The short dwell periods at high temperatures during welding are not long enough for this to occur. On the other hand the overwhelming majority of the grains will be inhibited from coarsening by normal grain growth since they, although finer than for slower heating rates, are still likely to be larger than $\bar{D}_{limit}$ for normal grain growth. Hence, the overall result will be a fine austenite structure. The theoretical explanations given above are therefore also consistent with the observed refined austenite in the HAZ of weldments in Ti-microalloyed steels.

The GCTs in Fig. 3.9 are assigned to both Ti and Ti-V microalloyed steels (3.5, 3.13), indicating that all observations can be understood in terms of the Ti- and N-contents and the cooling conditions during casting. So for GCT in the as-cast material, V additions to a Ti-steel seem to have no or only marginal effect. In agreement with this, Fig 3.1b exhibits a very modest decline of only 12^{o}C for the GCT of the V-Ti steel as compared with the pure Ti steel, Fig3.1a. As opposed to this, the GCT of the Nb steel in Fig.3.1c is clearly lower, by 40^{o}C, than that of the Ti steel.

It has long been known that the GCT of hot rolled Ti-microalloyed steel is lower than in the cast condition (3.4). It is also found that as the number of reheatings increases as processing proceeds the grain coarsening resistance deteriorates. This behaviour can readily be understood by the refinement of the average grain size engendered by multiple reheating, cf. Eq. (3.1). Nevertheless, Roberts et al (3.4) have convincingly shown that the grain refinement during hot rolling cannot alone explain the observed reductions in GCT for Ti-V steels in the hot rolled condition as compared to the as-cast. They designed experiments to produce TiN dispersions and austenite grain sizes at the GCT with only marginal differences, but with widely differing V-carbonitride precipitation by varying the cooling through the austenite-ferrite transformation.

Figure 3.10 shows the measured GCT for steels processed in this way with cooling rates from 220 mm slab to water quenching of 10 mm plate. In this case, the observed reduction in GCT of about 130^{o}C cannot be accounted for by the modest reduction in grain size from17μm to 11μm. Roberts et al. proposed that the occurrence of bimodal precipitate distributions of V-carbonitrides and (Ti,V)-nitrides and the rapid dissolution of the former on heating causes sufficient change in the grain size distribution to be conducive to abnormal grain growth, cf. (ii) above. It is also suggested that the observed slow increase of austenite grain size with heating temperature for the Ti-Nb, Ti-V, Ti-V-Nb steels, over that of the pure Ti steel, as demonstrated in Fig. 8.3, is due such a dissolution of Nb- and V-carbonitrides.

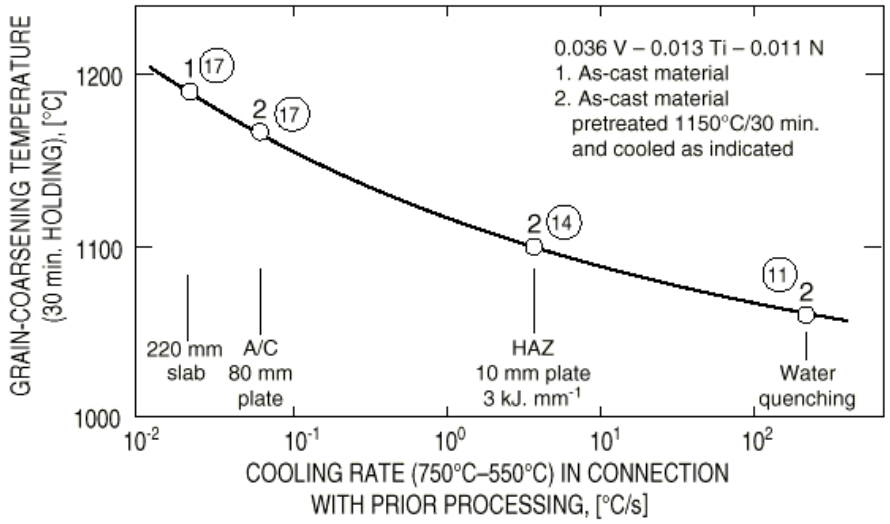

Fig. 3.10 The effect of cooling rate during previous processing on the grain coarsening temperature (GCT) of 0.036V-0.013Ti-0.011N-steel. Encircled numbers are the average diameters of the ´matrix´ austenite grains at the GCT (3.4).

3.3 Effects on recrystallization

One of the most essential features of microalloying additions is their influence on recrystallisation during controlled rolling, either to prevent recrystallisation and thereby producing 'pancaked' austenite grains during hot deformation and so conditioning the austenite to form fine ferrite grains during transformation, or to minimise their effect on recrystallisation thereby allowing repeated recrystallisation to occur during multiple deformation and a gradual refinement of austenite and the subsequent ferrite. The first case is the controlled rolling route for the Nb-bearing structural steels, and the second is the route, recrystallisation controlled rolling, adopted for the Ti-V structural steels (cf. chapter 5). The effect of the microalloying elements on recrystallization differs widely, especially so for V and Nb, as demonstrated in the classical graph due to Cuddy (3.14), Fig. 3.11; this shows the recrystallisation stop temperature as a function of the microalloy content (atom %), as dissolved when the hot deformation starts.

The mechanism by which the microalloying elements act to raise the recrystallisation stop temperature has been the subject of much debate throughout the history of microalloyed steels and numerous investigations have been performed. Mechanisms based either on solute drag or particle pinning have been proposed (3.15 - 3.24). Most of the work in this area concerns the strong impeding effect Nb has on recrystallisation. Convincing evidence has been presented that the pinning force created by the observed Nb-carbonitride dispersion at the recrystallisation stop temperature exceeds that of the driving force for recrystallisation (3.25, 3.26). So in temperature-time regimes where such precipitate dispersions are at hand this mechanism must be the controlling one, since the migration of austenite grain boundaries is then entirely stopped and hence solute drag cannot operate.

On the other hand there is today very clear experimental evidence showing that solute drag has a considerable impact on recrystallisation in niobium microalloyed steels under conditions when there is no Nb(C,N) precipitation (e.g. ref. 3.21) In an investigation from 1983, Andrade et al. (3.27) compared the effects of Nb, V and Mo on recrystallisation at 900°C and 1000°C.

The alloy elements were dissolved in all cases except in the Nb steel at 900°C where strain induced Nb(C,N) precipitation occurred during the experiment. The results of the three microalloyed steels together with the plain carbon reference steel are shown in Table 3.1 and demonstrate convincingly the strong solute drag effect of Nb and also of Mo, although the latter is somewhat weaker. Vanadium exhibits a measurable but very small solute drag effect, so will be negligible in practice. Regarding the Nb steel, the authors make the important note that even where precipitation occurs and eventually stops recrystallisation, the solute drag effect of Nb may be essential for retarding recrystallisation before the precipitation sets in.

Hence, we conclude that particle pinning is the controlling mechanism when there is an effective precipitate dispersion. At somewhat higher temperatures, when no precipitates exist, solute drag can slow down recrystallisation considerably. However, it cannot be arrested completely since solute drag can only reduce grain boundary migration and not prevent it.

Table 3.1 Recrystallisation start (R_s) and finish (R_f) times for the steels investigated in (3.27)

	1000°C		900°C	
Steel	R_s (s)	R_f (s)	R_s (s)	R_f (s)
Plain C	0,27	7,0	1,9	30
V	0,38	9,0	2,3	35
Mo	1,0	27,0	9	200
Nb-Mn	1,9	38,0	90	2800

Still this leaves us without a full explanation as to why the microalloy elements act so differently, Fig. 3.11. Normal hot rolling occurs typically in the temperature range 1100° - 900°C, but extending down to 800-750°C for controlled rolling. For preventing recrystallisation it is the lower part of this range that is of prime interest. In typical Nb-microalloyed steels the region for Nb(C,N) precipitation in austenite, including strain induced precipitation, starts at about 950°C (3.16). Hence, it matches closely the lower temperature range of hot rolling and therefore the particle pinning mechanism is expected to function well for Nb, especially for controlled rolling, cf. Fig. 3.11.

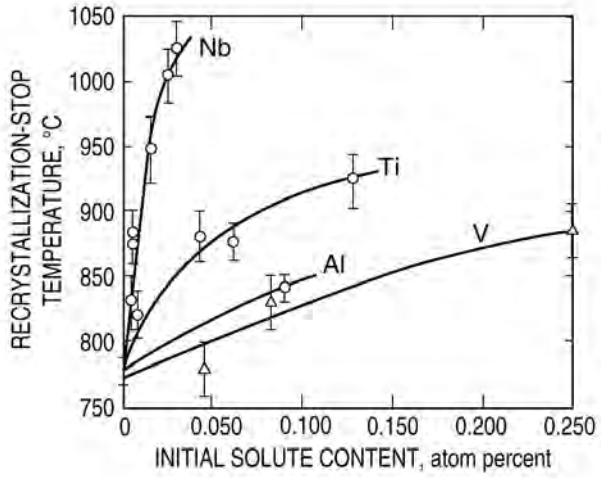

Fig. 3.11 The increase in recrystallisation-stop temperature with increase in the level of microalloy solutes in 0.07C-0.25Si-1.40Mn steel (3.14).

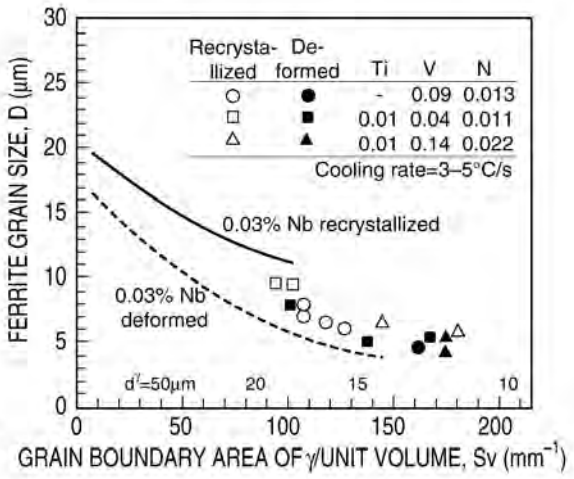

Fig. 3.12 Dependence of ferrite grain size on the area of austenite grain boundary per unit volume. Data points are for Ti-V and V-microalloyed steels. Curves refer to Nb-steels (3.28, 3.29, 3.30).

For V microalloyed steels on the other hand, no precipitation will occur until about 850°C, cf. Fig.2.4, and accordingly particle pinning cannot operate at all during normal rolling, but only during controlled rolling at low temperatures. Thus at least qualitatively, the difference between V and Nb can be understood in the case of particle pinning. At higher temperatures where the austenite is free from precipitation there will still be a considerable retardation of recrystallisation in the case of Nb due to its strong solute drag (3.21, 3.27). For V, on the other hand, experimental results show that the solute drag effect is very small and for all practical purposes is negligible, Table 3.1 (3.27). Hence, the significant difference between the effects of Nb and V on recrystallisation will be maintained at high temperatures where only solute drag can function.

3.4 Effects on the austenite-ferrite transformation

The primary parameters controlling the ferrite grain size produced in the austenite-ferrite transformation are the effective austenite grain boundary area, i.e. austenite grain boundary area/unit volume (S_v), and the cooling rate.

However, for Nb-microalloyed steels it has been shown that for a given S_v the ferrite grain size is smaller when transformed from unrecrystallised, deformed and flattened austenite grains than from recrystallized, equiaxed grains (3.28). Traditionally this difference has been accounted for by the additional ferrite nucleation that takes place in the deformation bands of heavily deformed austenite. Interestingly though, when the same type of experiments are conducted for V- and Ti-V-microalloyed steels no difference is found (3.29, 3.30). Deformed, unrecrystallised austenite grains transform to ferrite with virtually the same grain size as that produced from equiaxed, recrystallized austenite, Fig. 3.12. Thus, for the V-steels the ferrite grain size is found to be independent of austenite grain shape and processing method.

As can be seen from the figure, the V-steels occupy an intermediate position between the lines for recrystallized and unrecrystallised Nb-steels. An essential result is that the same degree of ferrite grain refinement can be achieved for the V-steels as for the Nb-steels, viz. about 4 μm, provided the effective austenite grain boundary area is large enough.

An important and interesting feature of Ti-V and V-steels is that additional nitrogen further refines the ferrite during the austenite-ferrite transformation (3.5, 3.31, 3.32), as shown in Fig. 3.13 for recrystallisation controlled processing and in Fig. 3.14 for normalising. During the last decades a great number of data have been collected at Swerea KIMAB for many different steel compositions concerning transformed ferrite grain structures as a function of the prior austenite structure and the cooling rate through the transformation. By multiple regression analysis the following equation has been deduced for the grain refinement ratio D_{γ}/D_{α}

$$D_{\gamma}/D_{\alpha} = 1+(0{,}0026+0{,}053\%C+0{,}006Mn+0{,}009\%Nb+4{,}23\%V*N-0{,}081\%Ti)*(1.5+\alpha^{1/2})*D_{\gamma} \qquad (3.4)$$

where D_{α} and D_{γ} are given in μm and the cooling rate α in °C/s (3.33). Again this shows the strong effect of vanadium and the synergy between V and N. The reason for this grain refinement, demonstrated in many investigations (3.34-3.37), is that V(C,N) precipitates in austenite are preferential nucleation sites for ferrite. These V(C,N) particles exhibit an atomic mismatch of only 2.1% along two directions perpendicular directions, $[001]_{VN}//[011]_{\alpha}$ and $[010]_{VN}//[01\text{-}1]_{\alpha}$, so allowing epitaxial growth of ferrite on edges of VN according to the Baker-Nutting relationship. A beautiful example of this phenomenon is shown in Fig. 3.15 (3.34).

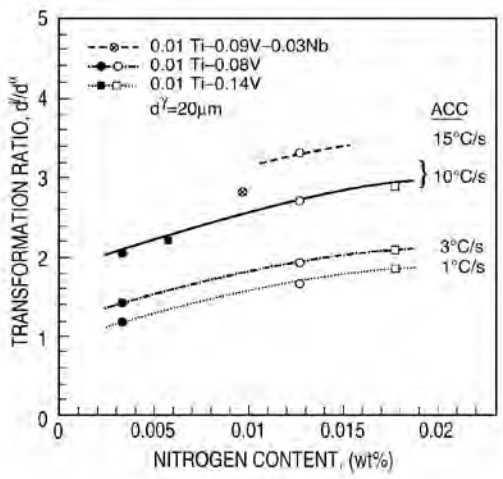

Fig. 3.13 The effect of N on the refinement of ferrite during the austenite-ferrite transformation in Ti-V-(Nb)-N steels (3.31).

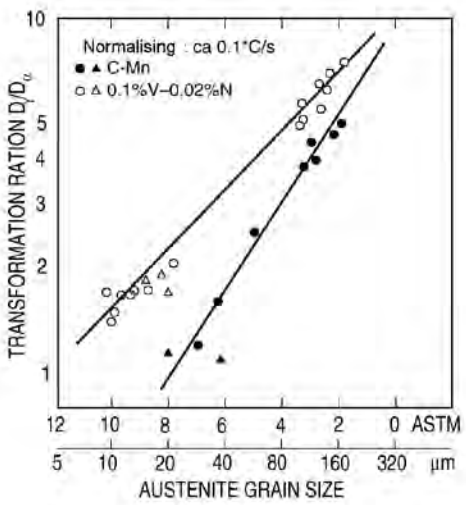

Fig. 3.14 The effect of V and high N in refining the polygonal ferrite grain size produced during the austenite-ferrite transformation (3.5, 3.32).

With enhanced levels of N the precipitates have a strong tendency to form as pure VN already in austenite and then with falling temperatures as V(C,N) with gradually increasing C contents. The preferred sites for these VN particles are the austenite grain boundaries and therefore this generates a dense array of ferrite grains along the boundaries. An interesting feature is that these ferrite grains are crystallographically much more randomly oriented than those formed in V free steels (3.35), both effects being beneficial for strength and toughness.

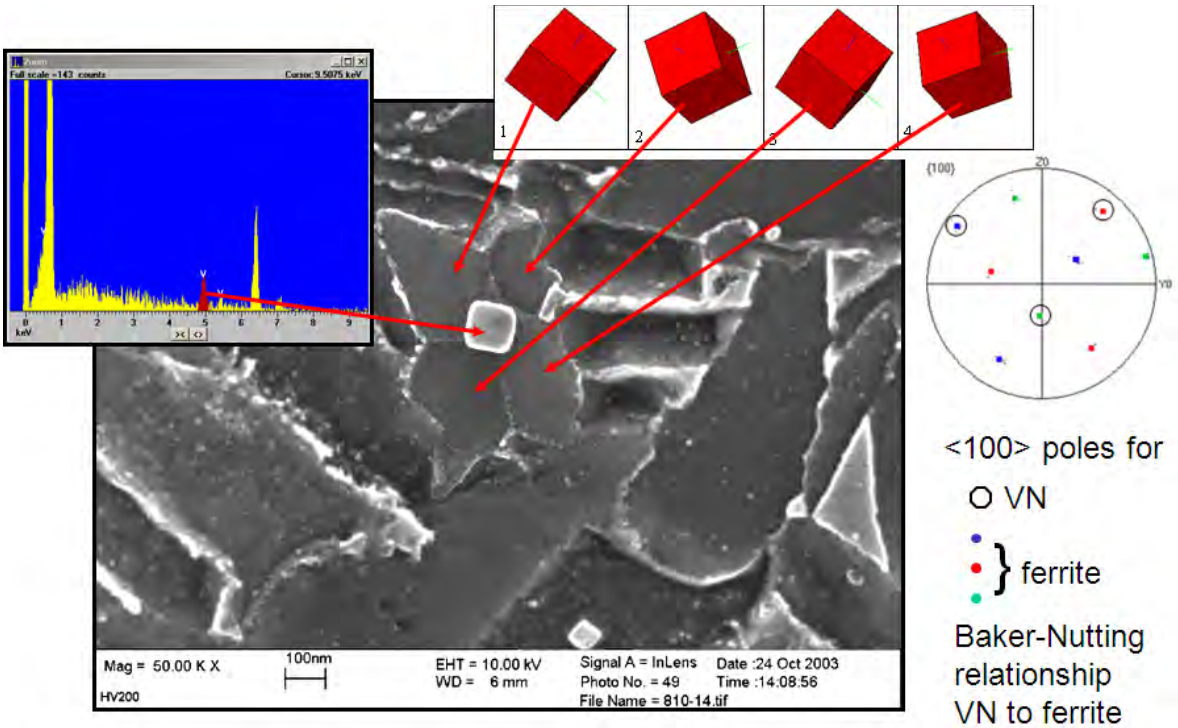

Fig. 3.15 Formation of four intra-granular ferrite grains on a VN particle(3.34)

Another possible route is to utilise particles in the austenite upon which VN precipitation occurs preferentially. MnS inclusions serve this purpose, as clearly demonstrated metallographically in Fig. 3.16 (3.34, 3.36, 3.37). However, since a low sulphur content is often a strict requirement for steel grades this method is not useful in many cases.

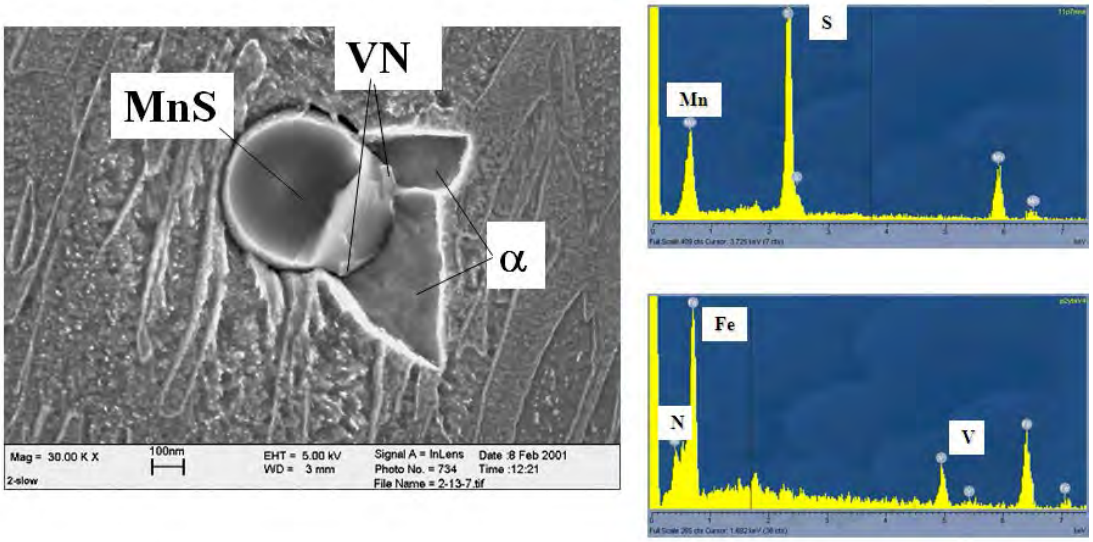

Fig. 3.16 Formation of intra-granular ferrite on a MnS+VN duplex particle in steel containing 0.1%C, 0.12%V and 0.025%N (3.34).

In a comprehensive study (3.34), strain induced precipitation of V(C,N) was applied for intra-granular ferrite grain refinement in microalloyed steels for heavy beam and thick plates. For a fully effective ferrite nucleation it appears that a high density of VN particles larger than about 10nm is required. A 0.10%V, 0.020%N steel was deformed by 50% at 900°C followed by slow cooling at 0.5°C/s, generating a high density of VN with sizes in the range 20-80nm (3.34). This resulted in a very pronounced ferrite grain refinement, a grain size of 4μm, as compared to 12.5μm for the reference steel, Fig.3.17. It was also found that a high content of aluminium, >0.03% Al, has to be avoided, since at these levels most of the nitrogen is consumed by AlN formation and therefore prevents formation of VN in the austenite

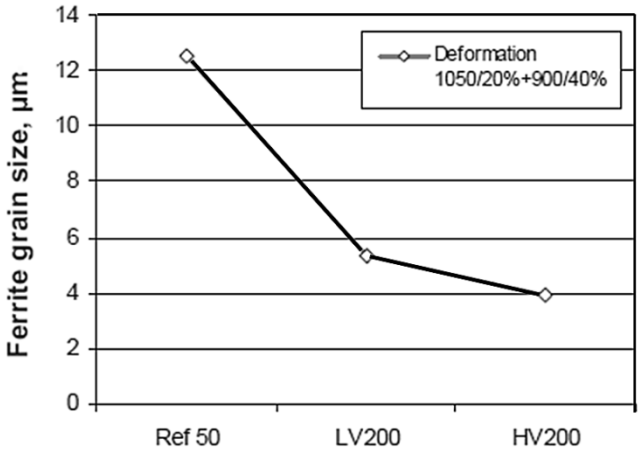

Fig.3.17 Ferrite grain sizes of V- and C-Mn steels after 40% deformation at 900°C.
Prior treatment involved 20% deformation at 1050°C followed by cooling at 0.5°/s down to 900°C (3.34)

REF50 0.005%N
LV200 0.05%V, 0.020%N
HV200 0.10%V, 0.020%N

Also in the case of intra-granular nucleation, the ferrite orientations become more randomised (3.37). Moreover, it has been shown (3.38, 3.8) that the coarse grain fractions are reduced, which should promote a lowering of the ductile-brittle fracture transition temperature. Several investigations have shown significant ferrite grain refinement by intra-granular ferrite nucleation on VN particles e.g. (3.34, 3.38). It should be borne in mind that such intra-

granular refinement is normally accompanied by a similar refinement of the grain boundary ferrite. A consequence of the strong influence of V and N on ferrite nucleation is that the transformation curves in TTT and CCT diagrams are shifted to shorter times and to considerably higher temperatures in certain intervals of cooling rates with increasing contents of N or V (8.3, 8.6), Figs. 8.9 and 8.10.

Application of the well known fact that VN co-precipitates on the interfaces of TiN particles already formed during casting, cf. section 3.1, appears to be a more attractive way to shorten the time to form effective VN nucleants for ferrite and hence should be more widely useful in commercial steel processing. This idea has been tested successfully during laboratory simulation of seamless pipe processing (3.39). A ferrite grain refinement 2.5 times larger than that of C-Mn steels of the same austenite grain size could be reached in this way and, at the same time, the processing time could be shortened considerably, Fig 7.19. It is to be noted that the observed grain refinement is derived both from the intra-granular and the grain boundary ferrite, hence showing that the VN-TiN compound particles act as nucleants both in the austenite interior and the grain boundaries (3.39). An attempt has been made to apply the same type of ferrite grain refinement in thick (16 mm) hot strip steels processed by thin slab casting and CSP (3.8). However, in these cases the TiN particles were very fine, with 90% of them being smaller than 10nm, due to the fast solidification rate. Such small particles, even when plated with VN are probably to be too small for effective ferrite nucleation.

Acicular ferrite has been of commercial importance since the 1970´s because of its use in low alloy high strength plate steels. Lately this microstructure has attracted an increasing interest and it has today a rather comprehensive literature (3.40-3.44). The term refers to ferrite plates nucleated intra-granularly with different orientations, hence producing a fine grained structure with interlocking morphologies with high strength and toughness. Acicular ferrite is formed in the same temperature range as bainite, 400-600°C, and is effectively intra-granular bainite nucleated on inclusions and precipitates. Particles of V(C,N) acting as nucleants are especially interesting since they are easier to control during steel processing than inclusions and other precipitates. Also V(C,N) is already an established nucleant for polygonal ferrite.

The CCT diagrams, Figs. 3.18, from a study by Capdevilla et al. (3.42), give a good picture of the conditions under which acicular ferrite is formed and the factors that are essential for its existence in two low carbon 0.25%V steels, one with low N content, 0.0016% (a and b) and the other with 0.018% (c and d). A key factor to understand the shifts between bainite and acicular ferrite is that bainite nucleates exclusively on austenite grain boundaries as opposed to acicular ferrite forming primarily on particles in the austenite interior. For the fine grained austenites, bainite formation is promoted in the low N steel, Fig. 3.18a, because there are few V(C,N) nucleants for acicular ferrite and a large austenite grain boundary area free for bainite nucleation.

For the high N steel, Fig. 3.18c, grain boundary ferrite is promoted and this quickly covers the boundaries, thereby preventing bainite formation. At the same time, this material contains a large number of V(C,N) particles, so favouring acicular ferrite formation. For the coarse grained variants the picture is somewhat similar, Figs. 3.18c and d. Note, in particular, that when the region for polygonal and grain boundary ferrite moves to shorter times, when going from the low to the high N steel, the region for acicular ferrite is shifted to shorter times in exactly the same way.

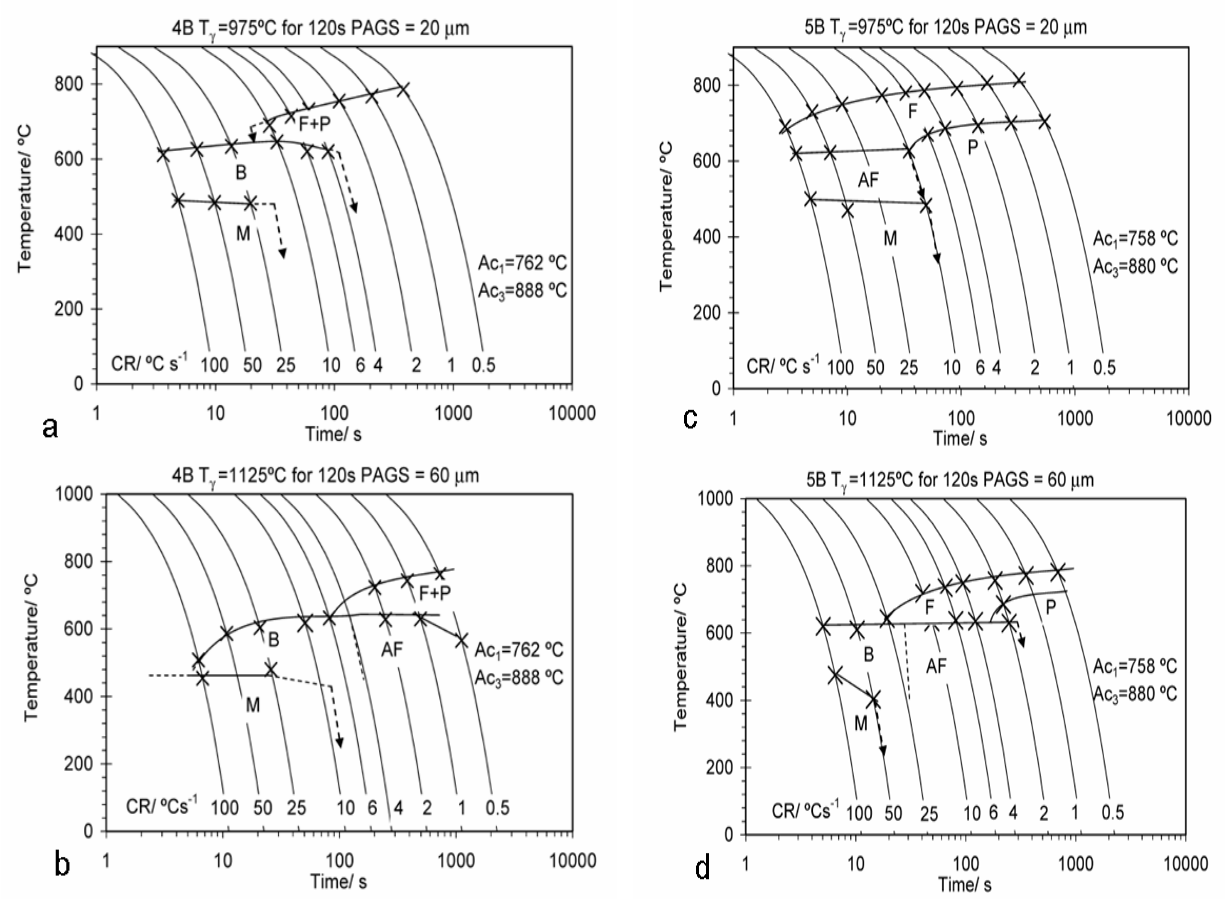

Fig.3.18 CCT diagrams for 0.08%C-0.25%V- 0.0016%N steel (a and b) and 0.08%C-0.25%V- 0.018%N steel (c and d), T_γ and PAGS are the austenitising temperature and prior austenite grain size. P, F, B and AF stands for pearlite, proeutectoid ferrite, bainite and acicular ferrite, respectively (3.42).

A general conclusion to be drawn from these CCT diagrams is that acicular ferrite forms only when austenite grain boundaries have been covered by proeutectoid ferrite whereas bainite forms normally when the austenite boundaries are free from ferrite. A particularly important result of this work (3.44) is the strong grain refinement obtained for combined additions of V and N. The grain size of acicular ferrite, defined by boundaries with misorientations larger than 15°, was 3.5µm in the high N steel, three times smaller than in the low N steel. A similar effect was observed in ref.3.8.

At first sight it seems surprising that ferrite which nucleates epitaxially on VN should be capable of developing into acicular ferrite since this necessitates a special orientation relationship for growth within the parent austenite. The growth relationships that have been observed for acicular ferrite lie in the small angular range between Kurdjumov-Sachs (KS) and Nishiyama-Wassermann (NW) (3.45). These relationships can be described respectively as $\{110\}_\alpha//\{111\}_\gamma$ with $<111>_\alpha//<110>_\gamma$ and $\{110\}_\alpha//\{111\}_\gamma$ with $<110>_\alpha//<112>_\gamma$. This poses the question as to how the ferrite can satisfy the separate conditions for both nucleation on VN and growth into austenite simultaneously. However, when microalloy nitrides precipitate in austenite they do so in cube-cube registry (3.46). The Baker-Nutting relationship for ferrite nucleation on VN is then identical with the Bain relationship for ferrite formed from austenite, i.e. $\{100\}_\alpha//\{100\}_\gamma$ with $<011>_\alpha//<001>_\gamma$. Although the Bain conditions are not identical with KS or NW, each of them is only about 8º away from 8 KS or

4 NW variants so may be able to accommodate this, especially when the austenite is deformed and contains dislocation substructure with lattice curvatures.

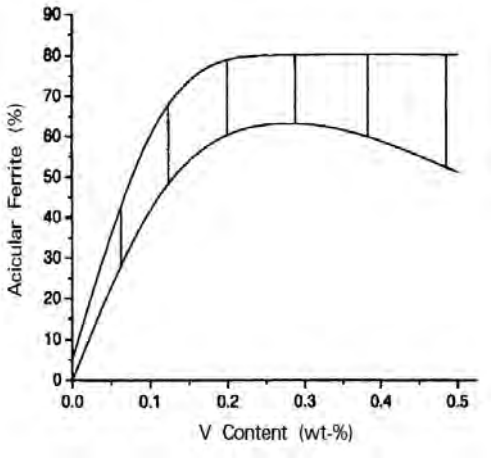

Fig. 3.19 Fraction of acicular ferrite in V- microalloyed 0.1%C, 1.2%Mn steels cooled at rates between 4 and 11°/C through the γ/α transformation (3.40).

Although the evidence for acicular ferrite being nucleated on particles is very convincing there are investigations showing that particles are not the major source for nucleation. For instance, He and Edmonds (3.40) found in a study on V-microalloyed structural steels with N contents in the range 0.003-0.019% a very strong impact of the vanadium content on the formation of acicular ferrite, Fig.3.19, but could not see any strong correlation between precipitates or inclusions and the formation of acicular ferrite. Instead they suggested that segregations of V, to form clusters rich in V, may be sites for the intra-granular nucleation. Observations by Zajac (3.41) show also that there are other sources than V(C,N) precipitates for nucleation of acicular ferrite.

3.5 Summary of chapter

- V-microalloyed steels are frequently co-alloyed with Ti to inhibit excessive austenite grain growth both during hot working and welding, thereby ensuring a refined microstructure in the finished product. This is attained by small controlled contents of Ti and N and the fast cooling during continuous casting resulting in a very fine and stable dispersion of TiN precipitates. Due to their high chemical stability and therefore low solubility these undergo practically no coarsening during reheating below 1300°C, even for the most dense dispersions. Vanadium and Niobium co-precipitate on TiN formed at higher temperatures. This does not, however, reduce the stability of the original TiN dispersion on subsequent reheating. The typical content of Ti in steel has increased to about 30-50ppm as an impurity due to recycling and therefore Ti has become a general concern in microalloying of steel.
- It is shown that the austenite grain size formed on reheating is primarily determined by the ferrite-austenite transformation and its heating rate through the transformation. Its chemical driving force is large enough for the ferrite/austenite interface to pass through the dense TiN precipitation. The austenite grain size is, for all normal heating rates, larger than the limiting grain size for normal grain growth, so impeding such growth completely. Thus, in the presence of dense TiN precipitation, abnormal grain growth is the only mechanism for grain growth, and this is a rather slow process. With the very short heating periods during welding this precipitation prevents effectively all grain growth. Prolonged heating times can, on the other hand, give some grain coarsening by abnormal grain growth, even below 1300°C. For less dense

precipitations, grain coarsening occurs by normal grain growth but will be impeded more or less, depending on the density of the precipitate dispersion.

- It appears that the widely different abilities of V, Nb, and Ti to retard recrystallisation during hot working are associated with the varying solubilities of their carbonitrides as well as the resulting temperature ranges where effective microalloy precipitation can occur to affect recrystallisation, together with their capacities to induce solute drag on migrating austenite boundaries. The temperature range for strain induced Nb(C,N) precipitation and for strong solute drag effect of Nb matches the temperature range of controlled rolling almost perfectly, whereas effective V(C,N) precipitation occurs at lower temperatures and the solute drag of V is practically negligible.
- Experiments have provided conclusive evidence that the recrystallization controlled-rolling route (RCR), involving repeated recrystallisation during working, can produce ferrite grain sizes in Ti-V-steels with virtually the same size as those produced from heavily deformed, unrecrystallised Nb-microalloyed austenite.
- A relatively new discovery in V-microalloying is that VN precipitates may act as nucleants for ferrite, so providing a new method for ferrite grain refinement. VN forms preferentially in austenite boundaries and so refines grain boundary ferrite quite effectively. Intragranular precipitation is sluggish but can be assisted by strain or by co-precipitation on pre-existing particles, such as TiN. In this way it has been possible to produce strong refinement of intragranular polygonal ferrite. A more recent finding is that V(C,N) promotes microstructures of acicular ferrite. Since this is a structure that is known for excellent combination of strength and toughness, this gives promise for future developments in V-microalloying. Although it has been shown that VN precipitate sizes in the range 20-80nm are required to gain the full effect of grain refinement of intraganular polygonal ferrite, it is also known that V-N microalloying may generate significant grain refinement under conditions when the VN particles should be smaller than 20nm. Hence, it appears that VN can be an effective ferrite nucleant in a larger range of sizes.

4. PRECIPITATION IN FERRITE

As regards strengthening, the effective vanadium carbonitrides are those formed in ferrite during the latest passage through the austenite-ferrite transformation. At equilibrium, the circumstances are such that a certain small portion of the vanadium in microalloyed steel should precipitate in austenite, especially if the contents of vanadium and nitrogen are high. However, the kinetics of V(C,N) formation in austenite are sluggish and for processing at finishing temperatures higher than 1000^{o}C and for normal steel compositions virtually all vanadium will remain in solid solution and be available for precipitation in ferrite. Some solute vanadium may be forfeited during controlled rolling as a result of strain-induced V(C,N) precipitation, or by the formation of alloyed (Ti,V)N particles during casting and reheating of Ti-V-microalloyed steels, as discussed in Section 3.

However, compared to the other microalloying elements vanadium has a higher solubility and therefore remains in solution to a much larger extent during processing in the austenite range. Accordingly, in steels where especially efficient precipitation strengthening is wanted, vanadium is the preferred choice. Furthermore, experience from steelworks shows that the strengthening effect of VN is very consistent and reliable.

Precipitation of V-carbonitrides can occur randomly in ferrite in the wake of the migrating austenite-ferrite (γ/α) boundary – general precipitation – or by interphase precipitation characterised by the development of sheets of particles parallel to the γ/α-interface, formed repeatedly with regular spacing. Many investigations have shown that for compositions typical of structural steels the general precipitation takes place at lower temperatures, typically below 700^{o}C, and the interphase precipitation at higher temperatures.

It is now a well established fact, demonstrated in several electron microscopy studies, that V(C,N) particles are also formed inside the pearlitic ferrite (4.1). Because of the lower transformation temperatures of pearlite this type of precipitation is usually finer. Both interphase and general precipitation have been observed. Vanadium carbonitrides are sometimes observed in a fibrous morphology when cooling is slow or on holding at high temperature in the γ/α range. The typical feature of this mode of precipitation is that the fibres are perpendicular to the γ/α interface. Furthermore it occurs sparsely and is never a dominant microstructure. In view of the sparse occurrence of the fibrous mode of V(C,N) precipitation in the steels considered here we will not deal with it further in the present paper.

4.1 Interphase precipitation

Interphase precipitation has been observed in steels containing strong carbide or nitride forming elements such as V, Nb, Ti, Mo, Cr, W and combinations of them (4.2-4.12). Figure 4.1 shows the typical morphology of interphase precipitation of V(C,N) in microalloyed 0.12%V steels with varying N and C contents (4.13). As can be seen, this microstructure consists of parallel sheets densely populated with V(C,N) particles. The sheets appear with a rather regular spacing. The morphology of the growing ferrite/interphase precipitate front was clarified already in the early work of Honeycombe and coworkers by careful electron microscopy (4.4, 4.5).

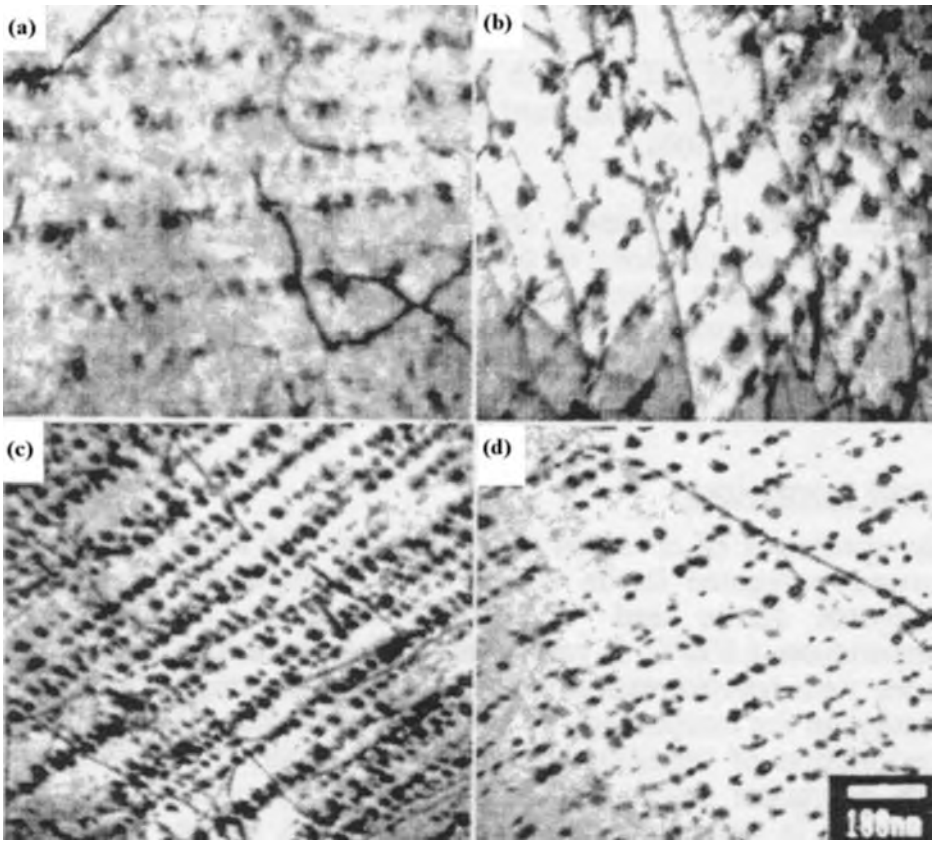

Fig. 4.1 Electron micrographs illustrating the effect of N in 0.10%C-0.13%V steels on the spacing of the interphase rows and the density of V(C,N) precipitates after isothermal transformation at 750℃ for 500 s, (a) 0.0051%N (b)0.0082%N (c) 0.0257%N (d) 0.0095%N, 0.04%C (4.13).

They demonstrated that the advancing front is stepped like a staircase, as shown schematically in Fig. 4.2. The ferrite growth occurs entirely by lateral migration of ledges (risers in the staircase) while the nucleation and initial growth of the precipitates take place in the stationary horizontal γ/α-interfaces (treads of the staircase). Originally, it was suggested these interfaces normally are semi-coherent $\{111\}_\gamma/\{110\}_\alpha$ facets, but today it is known that they can also be curved and incoherent (4.6 4.10).

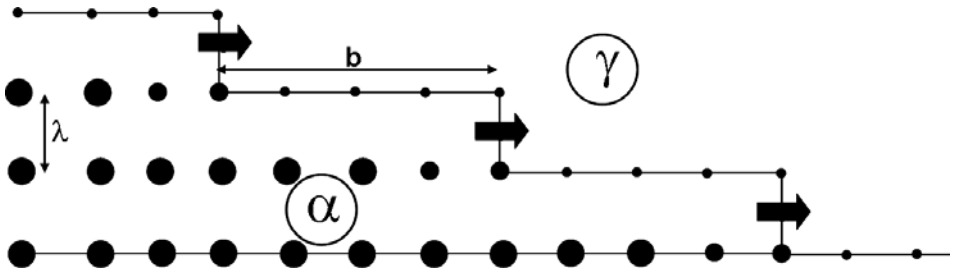

Fig.4.2 Schematic drawing showing the advancement of the ferrite/interphase precipitation by ledge migration along the particle sheets and the repetitive formation of new ledges and particle sheets.

At high transformation temperatures, ~800^{o}C, for typical compositions of V-microalloyed structural steels, the interphase precipitation consists of irregularly spaced, and often curved

sheets of V(C,N)-particles. With decreasing temperatures the incidence of curved rows of precipitates diminishes and the dominant mode is regularly spaced, planar sheets of particles, Fig. 4.1. Below about 700°C the interphase precipitation is commonly found to be incomplete, and random V(C,N) precipitation from supersaturated ferrite after the γ/α-transformation takes over progressively with decreasing temperature.

A characteristic feature of interphase precipitation is that it becomes more refined at lower temperatures, as confirmed by many investigations (3.2, 4.13). This is demonstrated for the inter-sheet spacing in 0.10%C-0.12%V steels in Fig.4.3a. The inter-particle spacing within the sheets of precipitation and the precipitate size also decrease with temperature. Figures 4.1 and 4.3b show that the inter-sheet spacing is considerably affected by the nitrogen content. As is evident, this is diminished to almost one third at 750°C on increasing the nitrogen content from 0.005 to 0.026%.

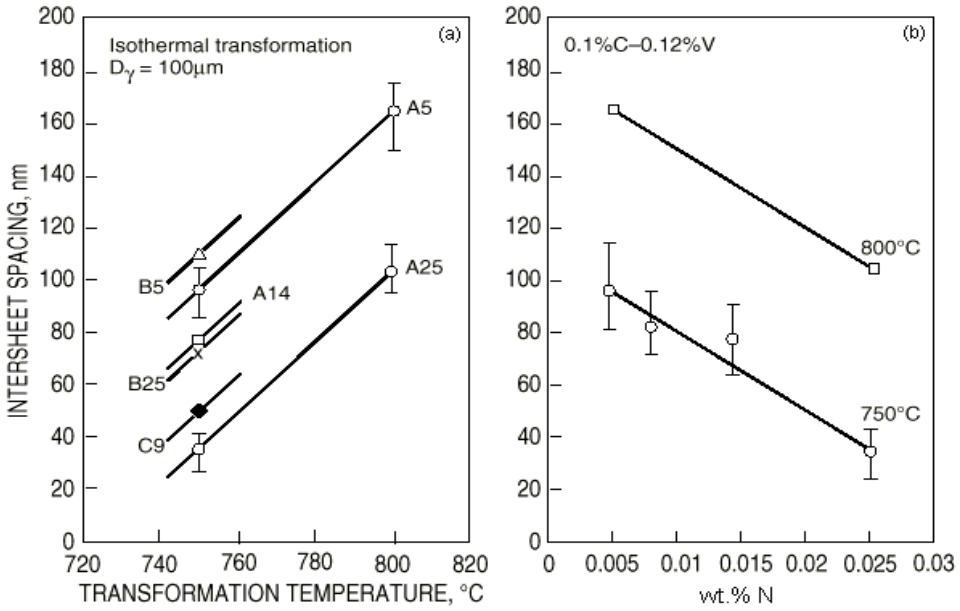

Fig. 4.3 The effect of transformation temperature (a) and N-content (b) on inter-sheet spacing of V(C,N) interphase precipitation, B5 0.10%C-0.12%V-0.0056%N, A5 0.10%C-0.12%V-0.0051%N, A14 0.10%C-0.12%V-0.014%N, B25 0.10%C-0.06%V-0.025%N, C9 0.04%C-0.12%V-0.0095%N, A25 0.10%C-0.12%V-0.026%N (4.13).

V(C,N), which has an fcc structure, forms in ferrite as semi-coherent discs with the orientation relationship, $(001)_\alpha$ // $(001)_{V(C,N)}$, $(110)_\alpha$ // $(100)_{V(C,N)}$, first established by Baker and Nutting (4.14). The discs are parallel to $(110)_\alpha$. Many electron microscopy studies have shown that V(C,N) in interphase precipitation exhibits locally a single variant out of the three possible ones having the B-N orientation relationship (4.15). Two alternative explanations have been given for this crystallographic selection (4.16-4.18). In cases where the ferrite and the austenite into which it grows are related by the Kurdjumov-Sachs relationship, $(111)_\gamma$ // $(110)_\alpha$, the variant will be chosen that makes the close packed planes of all three phases parallel. This choice should minimise the free energy for nucleus formation. In cases without a specific crystallographic γ/α-relationship, as for incoherent interfaces, it is suggested that the variant is chosen that puts the disc plane as close as possible to the γ/α-boundary plane, thereby again minimising the free energy. In both these cases we realise that the selection of a

unique variant of the B-N orientation relationship is a further confirmation of the nucleation of the interphase particles in the γ/α-boundary.

An essential characteristic of the V(C,N) precipitation in these types of steels is the considerable variation of the different modes of precipitation within the same sample, and indeed within the same grain. This has been observed in many investigations, but has been emphasised in particular by Smith and Dunne (4.15). Not only is there a variation of the different modes of interphase precipitation but, as these authors have found, general precipitation occurs both at low and high temperatures and is commonly formed jointly with interphase precipitation inside the same ferrite grain. They even observed general precipitation, as confirmed by the occurrence of all three Baker-Nutting crystallographic variants of V(C,N), at a transformation temperature as high as 820°C. The explanation they offered for this apparent anomaly is that the first-formed ferrite may grow too rapidly for interphase precipitation to occur, leaving the ferrite supersaturated for general precipitation subsequently (4.15).

4.2 The mechanism of interphase precipitation

There seems to be a general acceptance of the staircase morphology of the advancing ferrite/interphase precipitate front as described above and shown in Fig. 4.2 (4.4 - 4.8, 4.10). What is not included in this picture is the mechanism of creating new ´treads and risers in the staircase´. The present authors consider that such new steps are formed on the top step somewhat behind the moving ledge by bulging of the γ/α-interface where the precipitates are sufficiently thinly spaced. The bulge bows out and the two new ledges so formed move sideways on top of the underlying sheet of particles. In the remaining top part of the released bulge, new precipitates will form when it has moved a critical distance corresponding to the inter-sheet spacing. Hence, a new sheet is formed and the process repeats itself. Referring to Fig. 4.2, the spacing between such bulges will be the same as the length of the tread, *b*.

In this context it is interesting to note that measurements of the lengths of the treads in the staircase morphology, Fig.4.2, have recently been made for a wide range of inter-sheet spacings, λ (4.8). A strong linear correlation was found between those two variables showing that the ledge spacing is about four times longer than the row spacing. This means also that there will be a simple linear relationship between the overall ferrite growth rate, *v,* and the ledge velocity, v^L

$$v = v^L(\lambda/b) \qquad (4.1)$$

In a general sense this is a logical result since both λ and *b* are expressions of precipitate density and should be expected to vary proportionally as different parameters affecting the precipitation are changed. The main draw back with the process as described so far is that it cannot account for the observed, consistent dependence of the inter-sheet spacing with temperature and steel composition, e.g. V, N and C.

The formation and growth of the ferrite/precipitate morphology just described was given a quantitative description by Lagneborg and Zajac (4.7). Fig. 4.4 illustrates how they conceived the events in interphase precipitation from the completion of one precipitate sheet, through the local bulging of the γ/α-interface at a point where the precipitates are thinly spaced, and its further advance to the position where a new row of particles can be nucleated. This is followed by the lateral spread of the new row of precipitation by motion of two γ/α-interface super-ledges along the lower row of particles. In this temperature regime the austenite-ferrite transformation is controlled by carbon diffusion in austenite while maintaining local

equilibrium at the interface. As the bow bulges out between two V(C,N) precipitates V will flow from the advancing γ/α-interface to the growing precipitates in the first row. With increasing diffusion distance, the V concentration in the interface will grow from a low value corresponding to the equilibrium concentration between V(C,N) and ferrite, $c_V^{\alpha/VCN}$, to a concentration sufficiently high for V(C,N) to nucleate, c_V^{α/γ^*}.

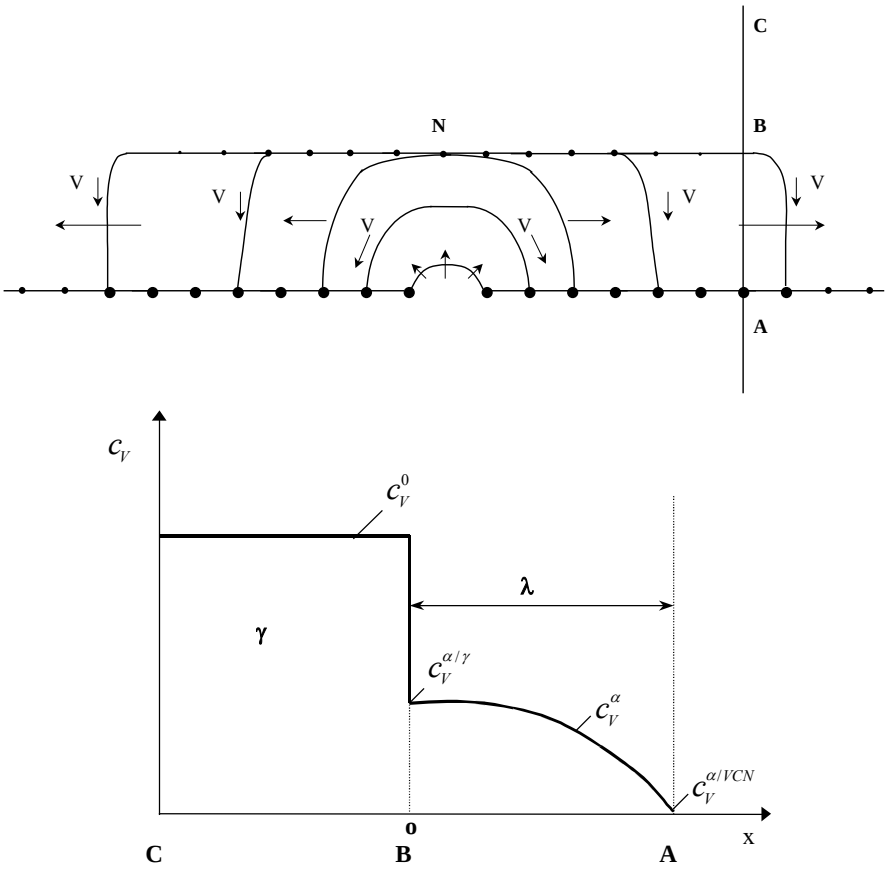

Fig. 4.4 Upper figure shows schematically how the γ/α-interface bows out, expands sideways and reaches eventually material with sufficient V for renewed precipitate nucleation to occur. The transfer of V by boundary diffusion to the lower precipitate row is indicated. The lower figure shows the V-content profile in a cross section (4.7).

From this description it follows that the rate of redistribution of V must match the rate of ferrite growth controlled by carbon diffusion. As a logical consequence of this, the model showed that volume diffusion of V was much too slow to account for the observed V(C,N) inter-sheet spacings (4.7). Hence, it was concluded that the redistribution of V occurs by much faster boundary diffusion in the advancing γ/α-interface. More specifically, and referring to the V concentration profile in Fig. 4.4, this means that the rates for the ledge migration and for the removal of V above the curved profile between points A and B and transfer to the lower precipitate row must at each instant match each other exactly. This type of boundary diffusion in a moving super-ledge has been solved analytically previously (4.19, 4.20). Adapting this analysis to the present case gives the following expression for the V gradient in the ledge, Fig. 4.4.

$$\frac{c_V^{\alpha} - c_V^0}{c_V^{\alpha/VCN} - c_V^0} = \frac{\cosh(x\sqrt{a}/2\lambda)}{\cosh(\sqrt{a}/2} \qquad (4.2)$$

where the meaning of the symbols c_V^{α}, c_V^0, $c_V^{\alpha/VCN}$, x and λ are given in Fig. 4.4, and

$$a = \frac{4v^L\lambda^2}{(D\delta)^{boundary}} \tag{4.3}$$

Here, v^L is the velocity of the γ/α-interface super-ledge and $(D\delta)^{boundary}$ is the diffusion coefficient for V in the interface. At $x = 0$ this expression generates the V-content of ferrite in the upper end of the super-ledge, $c_V^{\alpha/\gamma}$, and when this reaches the critical value for V(C,N) nucleation, c_V^{α/γ^*}, we get the following condition for the inter-sheet spacing.

$$\frac{c_V^0 - c_V^{\alpha/\gamma^*}}{c_V^0 - c_V^{\alpha/VCN}} = \frac{1}{\cosh\sqrt{a}/2} \tag{4.4}$$

For the calculation of c_V^{α/γ^*} reference is made to (4.7).

In accordance with the early observations of interphase precipitation of Honeycombe et al. the present model assumes that the V(C,N) precipitation occurs in semi-coherent $\{111\}_\gamma/\{110\}_\alpha$ interfaces (4.4, 4.5) , cf. Figs.4.2 and 4.4. This implies that, referring to the top drawing of Fig. 4.4, V boundary diffusion in the horizontal, semi-coherent interface is negligible compared to that in the incoherent ledge. Therefore we need only consider V diffusion in the ledge down to the lower precipitate sheet and not up to and into the top sheet, as described above. However, as mentioned previously interphase precipitation may also occur in incoherent λ/α interfaces. In that case V diffusion can obviously occur both to the lower and the top precipitate sheet. This mode of interphase precipitation has been analysed in detail (4.7, 4.21) and it was found that also in this case the inter-sheet spacing and its dependence on temperature and alloy contents is predicted by Eq.4.4.

A consequence of the model outlined above is that the V(C,N) precipitates nucleated in the tread will at this stage grow only marginally because here V can only be fed by slow volume diffusion into the tread-γ/α-interface. It is not until the next stage, when the ledge on top of the tread passes over the precipitates, that substantial quantities of V can be fed to the particles by fast V diffusion in the γ/α-interface of the moving ledge. This implies that the precipitates will only reach a size easily observed by electron microscopy in this second stage when the minute particles in the tread have been passed by the ledge. Indeed, this difference in precipitate size between these two stages can be observed in the electron micrographs of the early work of Honeycombe et al. (4.4, 4.5). In the drawing of Fig. 4.2 these differences in precipitate size have been indicated.

The calculated inter-sheet spacings as a function of temperature are shown in Figs. 4.5 and 4.6 for some V-microalloyed steels. The three curves in the graphs demonstrate also the dependencies on carbon content, Fig. 4.5, and vanadium content, Fig. 4.6, of the steels. The variation with N content is shown in Fig. 4.7. Experimental data are inserted in all three graphs. As can be seen, the agreement between observation and prediction is quite good, especially in view of the fact that the theory contains no adjustable parameters. One exception is the temperature dependence at low temperatures, Fig. 4.5, where the relative deviations between observed and calculated values are much larger when going from 750º to 700°C than from 800º to 750°C. As suggested in (4.7) this can be explained by the fact that local equilibrium in the moving γ/α-interface can no longer be maintained in this temperature range and the situation shifts to paraequilibrium with a constant V-content across the interface.

The declining inter-sheet spacings with decreasing temperatures indicate that the mechanism of interphase precipitation eventually breaks down somewhere below 700°C. According to the model the basic cause of this transition is that the γ/α-interface velocity becomes too fast relative to the V-diffusion for nucleation and growth of V(C,N) to take place in the moving interface. This will leave ferrite supersaturated with respect to V(C,N) and produce a general precipitation in ferrite after the passage of the γ/α-interface.

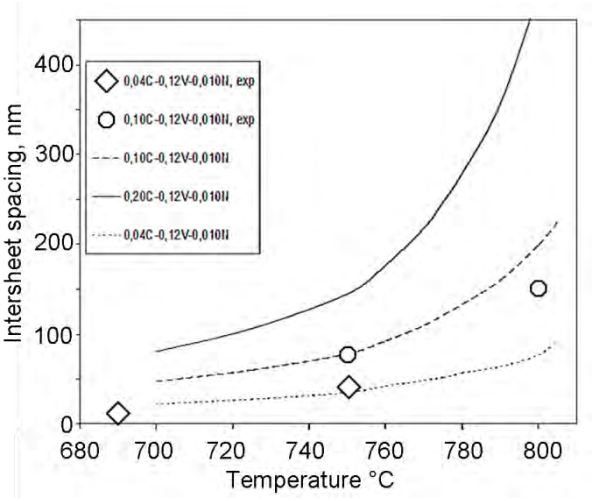

Fig.4.5 Calculated variation of the inter-sheet spacing with temperature for 0.12%V-0.010%N steels at three levels of C-content, 0.04, 0.10 and 0.20wt%. Experimental data from (4.13) are given for comparison.

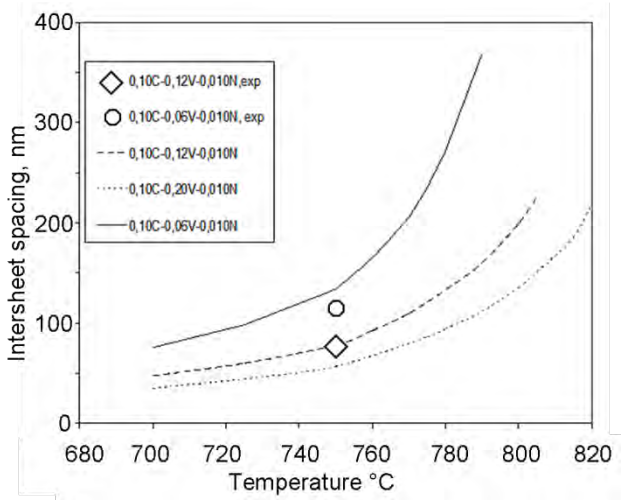

Fig. 4.6 Calculated variation of the inter-sheet spacing with temperature for 0.10%C-0.010%N steels at three levels of V-content, 0.06, 0.12 and 0.20 wt.% V. Experimental data (4.13) are given for comparison.

Similarly, the conditions for interface precipitation break down at high temperatures when $c_V^{\alpha/\gamma *}$ approaches c_V^0 and no nucleation of V(C,N) can occur in the moving γ/α-interface.

The observed and predicted effects of C, V and N contents on the inter-sheet spacing are readily understood from Eq. 4.4. The increased spacing with increasing C-content is caused by a coincident reduced growth rate of ferrite, *v* in Eq. 4.4. The effect of V can physically be considered to be a result of the fact that, at low V-levels, the interface must advance further to build up the necessary V-content for V(C,N) nucleation in the interface. The strong declining effect of small increases of N, Fig. 4.7, is due to the fact that the necessary chemical driving force for V(C,N) nucleation in the γ/α-interface is reached for a lower V-content as the N-content is increased, cf. Fig. 2.10.

An important feature of the model is that it explains the observation that interphase precipitation seldom occurs alone, but normally together with general precipitation, often within the same grain. This is simply results from the considerable variation of the ferrite growth rate as the transformation proceeds, high in the start and gradually declining which implies that the growth rate is too high at the transformation start and that interface precipitation only develops later. An estimate in reference (4.7) indicates that only about 40% of the volume should be occupied by well-defined interface precipitation in a 0.10%C-0.12%V steel annealed at 750°C.

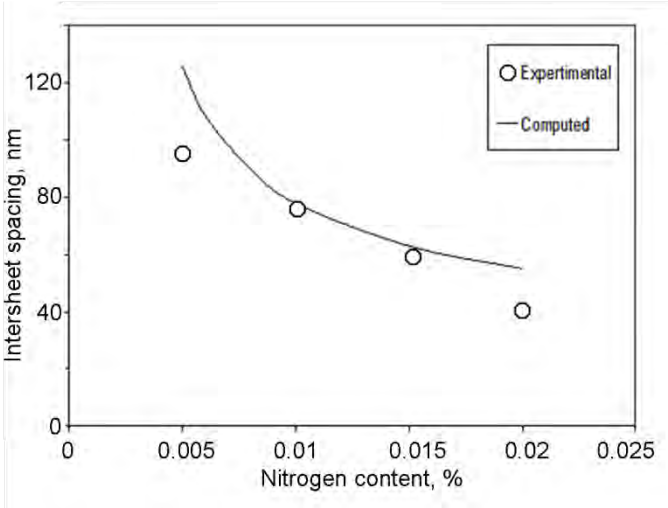

Fig.4.7 Comparison between computed and observed inter-sheet spacings in 0.10%C-0.12%V steels as a function of N content. Experimental data (4.13) are given for comparison.

The model presented above has recently been further developed by Okamoto and Ågren (4.8) by including the effects of solute drag on the ledge velocity. It was shown that this should have a pronounced effect for Nb-microalloying in slowing down the carbon diffusion controlled ledge velocity. Based on the fact that V has a negligible influence on recrystallisation by solute drag (3.27), cf. section 3.3, it seems likely that it should have only minor effect on the mobility of γ/α-interfaces.

4.3 General precipitation

For compositions typical of V-microalloyed steels, 0.10%C-0.10%V, general precipitation of V(C,N) occurs in a temperature range below about 700°C. As already discussed in the previous section this transition from interphase to general precipitation can be predicted by the solute-depletion model (4.7). We have also already seen that general precipitation may also occur locally above that temperature and have discussed how it should be understood.

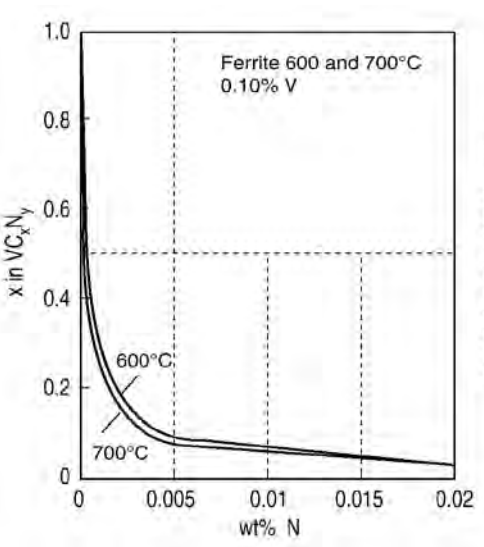

Fig. 4.8 Thermodynamic calculations of the variation in composition of VC_xN_y with content of N remaining in solution during precipitation in ferrite (4.22).

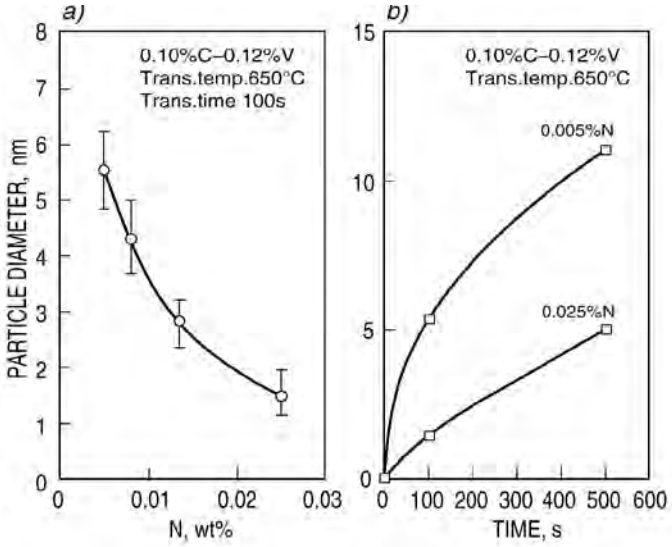

Fig. 4.9 Growth of V(C,N) precipitates after transformation at 650 °C (a) as a function of the N-content of the steel, and (b) as a function of holding time (4.13).

Experimentally it is well established that VN has a considerably lower solubility than VC, both in ferrite and austenite. The thermodynamic background to this is the much larger chemical driving force for formation of VN. This larger chemical driving force makes N-rich V(C,N) the preferred precipitation as long as there is sufficient nitrogen in the matrix, as has been demonstrated both by thermodynamic analysis (4.22) and by experiment (4.22, 4.23) in ferrite as well as in austenite. It is only when the nitrogen content falls below about 0.005% that the initial V(C,N) starts to increase its C-content, Fig.4.8.

A technically very important finding is that the precipitate size diminishes considerably with increasing nitrogen content in the steel, as is shown in Fig.4.9 (4.13). This is accompanied by a concurrent increase of precipitate density, although that is more difficult to measure quantitatively, Fig.4.10. These effects must be accounted for by an increased nucleation frequency as a result of the larger chemical driving force for precipitation of nitrogen-rich V(C,N). For the temperature and holding times in the experiments of Fig. 4.9 super saturation with respect to V(C,N) still remains. Therefore the observed difference in precipitate growth between high and low-N steels cannot be explained by differences in particle coalescence. Instead, it must be interpreted as resulting from the denser particle nucleation in the high-N material, thereby producing an earlier soft impingement of V-denuded zones and so slowing down the precipitate growth. This reasoning is substantiated by the computed curve for precipitate growth inserted in Fig. 4.11, where no allowance is made for impingement of solute depleted zones. Evidently, the computation can perfectly account for particle growth in the low-N steel with less dense precipitation, whereas in the high-N steel where we would expect effects of impingement, the growth is less than half of this. The size of the depleted zone corresponding to half the original solute content is double the size of a particle growing without impingement. According to the calculations in Fig.4.11 this gives a depleted zone with a diameter of 23 nm after an ageing time of 500 s at 650°C. Comparing this with the precipitate densities in the micrographs of Fig. 4.10 shows clearly that impingement of denuded zones has taken place long before 500 s ageing in the high N-steel, whereas it has hardly started in the low N steel.

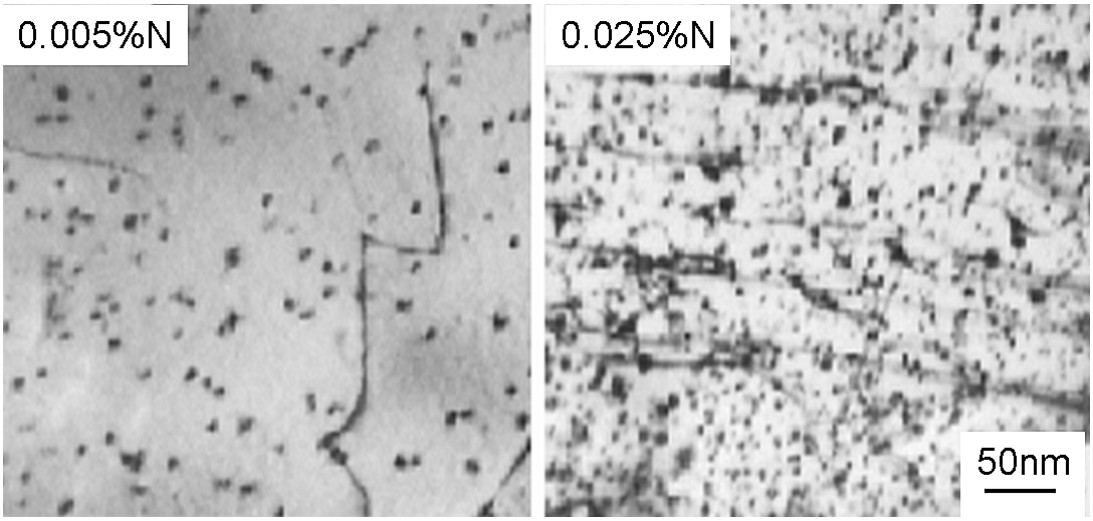

Fig. 4.10 Electron micrographs illustrating the effect of N-content on the density of V(C,N) precipitates during isothermal transformation at 650°C for 500s.

In numerous investigations of V-microalloyed steels it has been shown that the observed precipitation strengthening originates seemingly only from N-rich V(C,N), despite the fact

that there is abundant V to combine with the carbon dissolved in ferrite. The normal explanation of this behaviour has been that when the first formed N-rich precipitates have consumed practically all nitrogen, the chemical driving force for formation of C-rich V(C,N) is too small for profuse precipitation to occur and hence no added strength is observed. However, this issue is complex, and recently it has been shown that under certain conditions the C-content in the steel can add significantly to precipitation strengthening. This question will be treated in the following section.

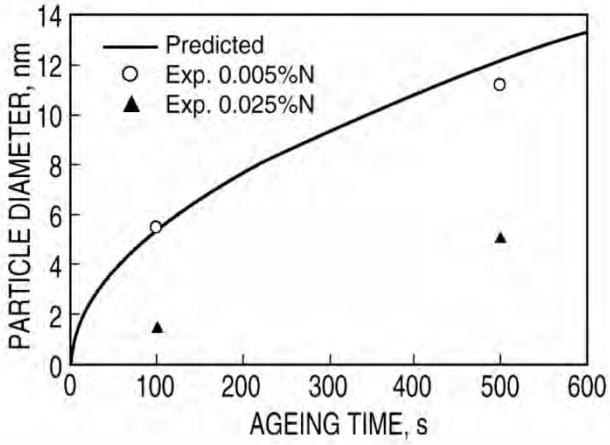

Fig. 4.11 Computation of V-diffusion controlled growth of V(C,N) at 650°C showing comparison with experimental values at two levels of N; no allowance is made for impingement between adjacent particles.

4.4 Effects of precipitation on strength

Since normal contents of vanadium in structural steels dissolve in austenite at relatively low temperatures, unlike the other microalloying elements, and so can contribute fully to precipitation strengthening when the steel is cooled into the α-range, V is usually the preferred element when precipitation strengthening is wanted. A modest addition of 0.10%V can bring about a strength increase beyond 250 MPa, and in special cases even up to 300 MPa. This was demonstrated in an early work by Roberts et al. (4.24) where the contribution of precipitation to yield strength level, ΔRp, was evaluated after subtracting other influences such as grain size etc., Figs. 4.12 and 4.13.

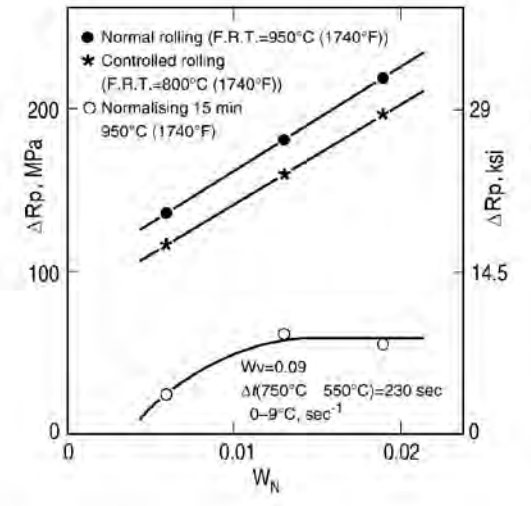

Fig. 4.12 Effect of processing method (lab. simulation) on the precipitation strengthening derived from V(C,N). Base steel composition: 0.12%C,0.35%Si-1.35%Mn-0.095%V,0.02%Al

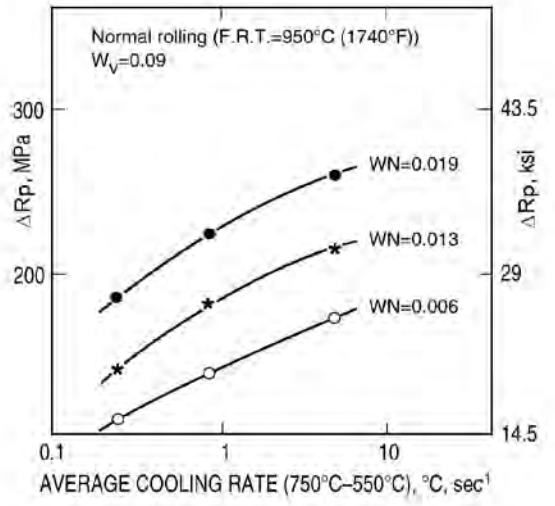

Fig. 4.13 Influence of cooling rate on the strength contribution from V(C,N) precipitates. Base composition as for Fig. 4.12 (4.24).

These graphs show another essential feature of V-steels, viz. that nitrogen in small contents adds significantly to precipitation strengthening. Similarly, enhanced cooling through the γ/α-transformation and afterwards augments the particle hardening, Fig. 4.12.The results show also that normalising at 950°C does not allow the V to go into solution completely and hence produces only modest strengthening.

In a number of subsequent investigations at the Swedish Institute for Metals Research (now Swerea KIMAB) (3.2, 4.24-4.27) the strengthening effects of V have been carefully examined in isothermally heat treated steels of varying V, N and C-contents. Fig.4.14 shows the influence of V, N and ageing temperature on precipitation strengthening. The technically very important effect of N on the strengthening of V-steels has sometimes been interpreted such that only VN forms as precipitates, and that the remaining V does not combine with C, possibly due to the larger solubility and lower chemical driving force for VC. However, this is a rather loose statement and is not an entirely correct description of the phenomenon.

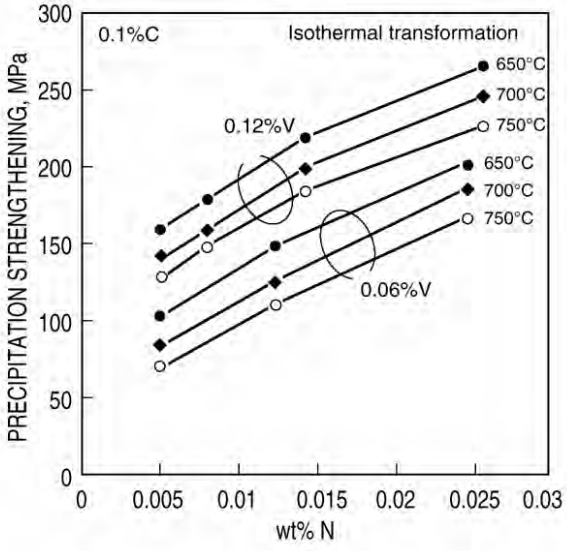

Fig. 4.14 Effect of N, V and transformation temperature on the precipitation strengthening in 0.1%C-V-N steels after isothermal ageing at different temperatures for 500s (3.2).

A physically more correct account would be as follows. In the present material with hard non-penetrable V(C,N) precipitates the particle strengthening occurs by the Orowan mechanism – bowing of dislocations between particles – and in that case the decisive parameter is the inter-particle spacing in the slip plane. In turn, that is determined by the density of the precipitates. This density is controlled by the nucleation frequency and the number of nuclei it creates until the supersaturation has diminished so that nucleation ceases. The essential parameter governing the variation in nucleation is the chemical driving force for V(C,N)-precipitation, and there we know that this varies relatively strongly with the N-content, as shown in Fig.2.10 (4.28). To put it simply, this is a consequence of the larger stability, or lower free energy, of VN than of VC. Hence, the larger driving force will cause a denser precipitation in the high-N steels than in the low-N steels. Electron microscopy has clearly confirmed this, as shown in Fig.4.10. When nearly all N has been consumed in the precipitation of N-rich V(C,N) the process can follow one of the following lines:

- in the case of continuous cooling, the temperature may have dropped sufficiently for V-diffusion to essentially cease, and therefore continued precipitation stops (in line with the traditional explanation stated above).
- the decomposition continues by co-precipitation of C-rich V(C,N) on previously formed N-rich V(C,N).
- if the carbon content in solution is sufficiently large (cf. below) the driving force may be large enough for continued nucleation, but now of C-rich V(C,N).

Experimental investigations (4.25-4.28) have demonstrated very clearly that the precipitation strengthening of V-steels increases significantly with the C-content of the steels. Plots of the observed strengthening ΔRp against the C-content, and for comparison also N-content, are given in Figs. 4.15(a) and (b) (4.27). These results show that carbon raises ΔRp by ~ 5.5MPa for every 0.01%C in the steel, whereas nitrogen raises it by ~ 6 MPa for every 0.001%N. This important effect of carbon had for a long time evaded notice, presumably due to an uncertainty in the procedure for evaluating the respective contributions of precipitation and of pearlite to the measured yield strength. This procedure was improved in the present case, and furthermore nano-hardness measurements were performed in order to unequivocally demonstrate the precipitation hardening inside the ferrite (4.25, 4.27, 4.28). The measured yield stress values are given in Figs. 4.15(c) and (d) (4.27) for the same steels and treatments as for the ΔRp values shown in (a) and (b). At a level of 0.12%V and enhanced content of N of 0.025% a yield strength of 560MPa could be reached at 0.10%C and 670MPa at 0.22%C. In all these cases the microstructures were fully ferritic-pearlitic.

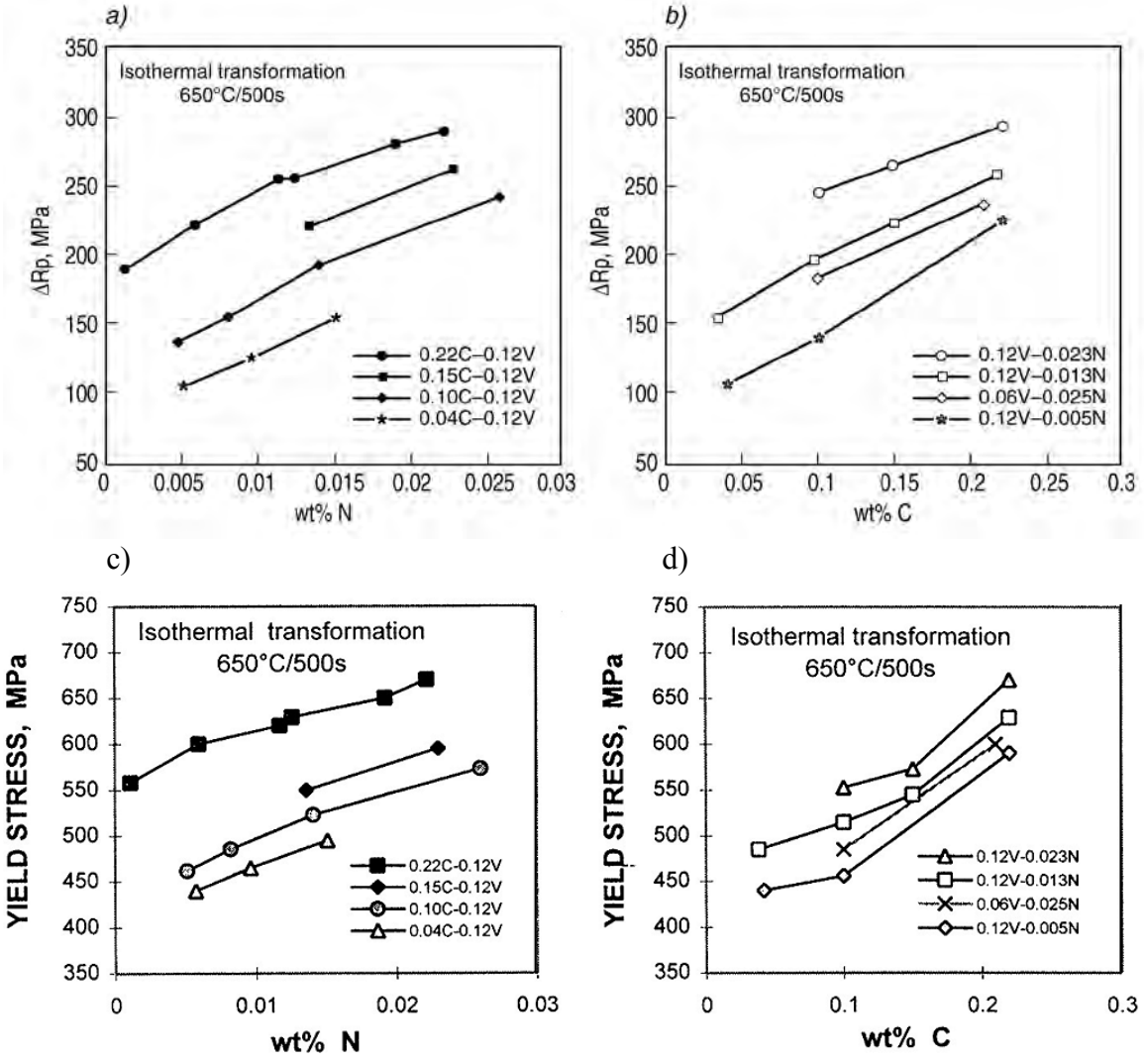

Fig. 4.15 Deduced values of precipitation strengthening, a) and b), and measured yield stresses, c) and d), for isothermally transformed V-steels (650℃/500s). (a) and (c) as a function of N-content; (b) and d) as a function of C-content (4.27).

That carbon *dissolved in ferrite* should contribute to precipitation strengthening is, of course, no surprise. As a matter of fact all the traditional graphs showing precipitation strengthening

as a function of nitrogen content exhibit a considerable residual strength when the curves are extrapolated to a N-content of zero, cf. Figs. 4.12 and 4.14. The strong effect of the *total carbon content*, however, is at first sight puzzling, as the C-content of ferrite is controlled by either of the phase equilibria, α/γ or α/cementite. The key to understanding the influence of the total C-content is as follows.

- The considerable difference in solubility of carbon in ferrite between the α/γ and α/cementite equilibria below A_1, shown in Fig.4.16. The solubility at 600°C is 5 times larger in α/γ than in α/cementite. The austenite phase also acts as a reservoir of carbon, which can flow into the ferrite and maintain its high saturation even when precipitation of V(C,N) is occurring.
- The fact that the total C-content affects the kinetics of the transformation from γ to α and eventually to α+cementite. The essential point here is that increased carbon contents displace the pearlite formation to longer times, Fig. 4.17 (3.41, 4.28). The implication of this is that a larger chemical driving force for V(C,N) precipitation will remain longer and hence promote profuse nucleation. It should also be recognised that the shift to lower C-content in ferrite, and therefore lower driving force, as a result of the cementite formation occurs very quickly, in less than a second for typical microstructures, because of the fast diffusion of carbon in ferrite.

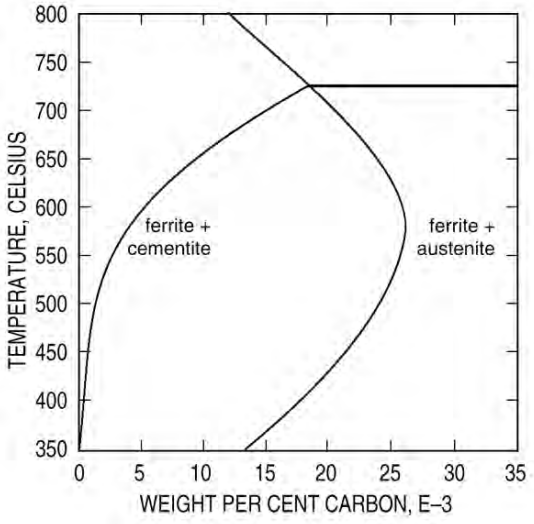

Fig. 4.16 Solvus lines for C in ferrite calculated using ThermoCalc for equilibrium with cementite and austenite, respectively (4.26).

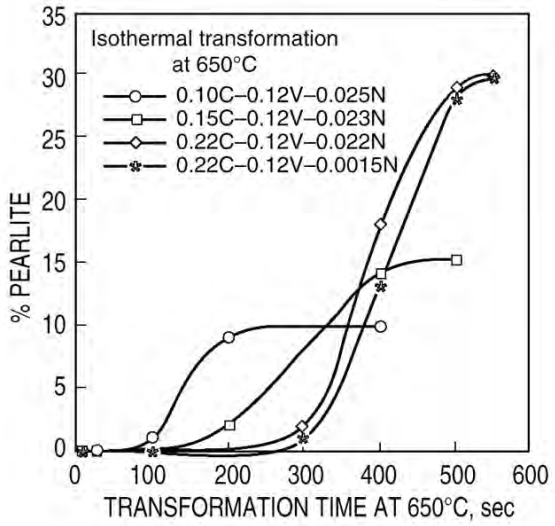

Fig. 4.17 Pearlite start time during isothermal transformation at 650°C for V-N steels with C-contents varying between 0.10 and 0.22% (3.41).

Hence, this chain of inter-relations leads with increasing total carbon content to gradually longer dwell times during which nucleation occurs under the high chemical driving force. Consequently, we can expect denser V(C,N) precipitation as the C-content of the steel is raised. This is very clearly demonstrated by the electron micrographs in Figs. 4.18.

It may also be noted at this point that the symbiotic effects of N and C come to especial advantage in long products such as ships' profiles and reinforcing bar which normally have higher C-contents (0.2% – 0.3%C) than in strip and plate products and which typically also have higher N-contents, in the vicinity of 0.01%N, being made from electric arc furnace steel. Precipitation strengthening by V(C,N) plays a very valuable role in increasing strength of these as will be discussed further in Sections 6 and 7.

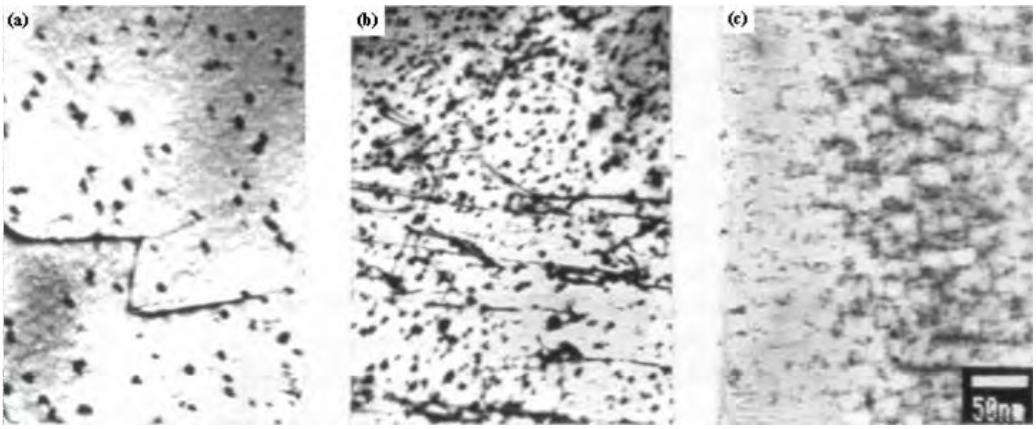

Fig. 4.18 Electron micrographs showing V(C,N) precipitation after isothermal transformation at 650°C in 0,12%V-0.013%N steels with different C-contents; (a) 0.04% C, (b) 0.10% C and (c) 0.22% C (4.27).

It is known that the precipitation strengthening of Ti-V steels is notably smaller than for V-steels with the same V-content. This is evident from Fig. 4.19 (4.26). It is readily shown that the reduction of effective N and V due to formation of (Ti,V)N in the austenite cannot alone account for the substantial reduction in strengthening (by ~ 100MPa) of the 0.22%C-0.12%V-Ti compared with the 0.22%C-0.12%V steel. It seems likely that the remaining part can be explained by the faster γ/α-transformation and hence earlier pearlite formation in the Ti-V steel as compared to the V steel (4.26, 3.40). As described above this will withdraw dissolved C in ferrite and therefore reduce precipitation strengthening from VC.

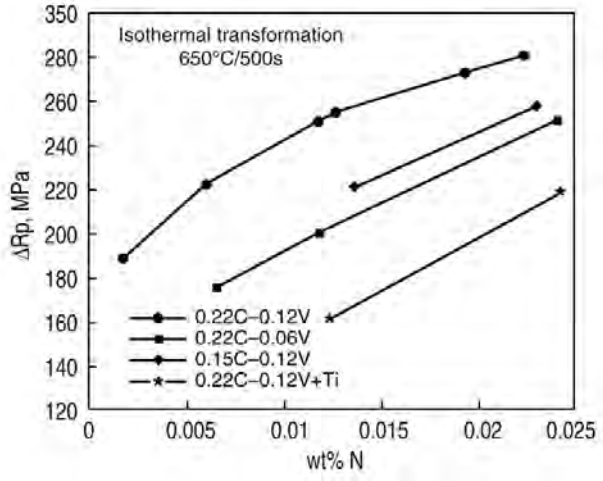

Fig. 4.19 Deduced values of precipitation strengthening in steels isothermally transformed at 650°C (4.26).

In the endeavour for higher strengths of hot strip structural steels the interest has lately been drawn to bainitic steels, see Section 7. In a recent development of such steels the basic idea was to make use of very fine precipitation of V-carbonitrides formed in the bainite to enhance the strength of a low carbon steel, 0.04%C (4.30). Yield strength levels of 750 - 800MPa were reached for V-N microalloyed steels when coiled at 450°C and below, which equals the strength of the virgin bainite for a corresponding V-free steel rapidly cooled to room temperature. Analysis of the strength components of this type of steel showed that strain hardening from the very dense dislocation substructure of the bainite contributes about 400MPa and that the effect of any V(C,N) precipitation formed during coiling is almost entirely limited to preventing recovery of this substructure. The effect of true precipitation

strengthening is only marginal. The reason for this is that the hardening derived from the dislocation substructure and the precipitates can be considered as the strength of two dispersions of point obstacles - strong dislocation nodes and hard particles - where dislocation bypassing occurs by the Orowan mechanism. In such a case the total strength is given by the sum of the squares of the component strengths when operating separately according to

$$\sigma^2 = (\sigma_1)^2 + (\sigma_2)^2 \qquad (4.5)$$

The implication of this is that the two components contribute less to the total strength than when acting alone, and in particular the smaller one - here the precipitation strengthening - contributes much less.

4.5 Summary of chapter

- Precipitation strengthening in microalloyed steels benefits from the γ/α-transformation because the chemical driving force for precipitation of microalloy carbonitrides increases suddenly and strongly as γ is transformed to α - also reflected in their widely different solubilities in the two phases - thereby giving rise to profuse precipitation in the ferrite. Vanadium-microalloyed steels are particularly suited for generating precipitation strengthening because of their ability to dissolve large quantities of V-carbonitrides at relatively modest temperatures in the γ-range due to the larger solubility as compared to other microalloy carbonitrides. This again creates conditions for a high driving force and therefore dense precipitation.
- At low supersaturations for V-carbonitride precipitation, corresponding to temperatures between A_3 and A_1 and slow cooling, nature takes advantage of easier nucleation in interfaces and carbonitrides are formed repeatedly in the moving γ/α-boundary, so called *interphase precipitation*. On lowering the temperature the interface will gain speed relative to the rate of precipitation, implying that the boundary escapes the precipitates, leaving supersaturated ferrite in its wake for subsequent *general precipitation* to occur behind the migrating γ/α-boundary. For compositions typical of microalloyed structural steels, general precipitation takes place below about 700°C and interphase precipitation at higher temperatures. However, there is a considerable variation of the different modes of precipitation. Thus, general precipitation is commonly also found at high temperatures, jointly with interphase precipitation.
- A model for interphase precipitation with predictive capacity is presented. In an austenite/ferrite boundary pinned by a sheet of interphase precipitates, local breakaway occurs where the particles are thinly spaced. The bulge so formed migrates both sideways and normal to the boundary. The ledges moving along the pinned boundary will provide V to the precipitates by fast boundary diffusion in the ledge. Simultaneously as the bulge moves into the austenite the V-content of ferrite facing the boundary will gradually rise and at a critical content, new V(C,N) will nucleate at the front of the bulge, so forming a new precipitate sheet. The implication of the process described is that the rate of redistribution of V from the front, through the ledge and to the particles in the first sheet must exactly match the rate of the moving ledge which is C-diffusion controlled. This situation has been analysed and solved analytically. The model exhibits good agreement with observed values of inter-sheet spacing, with its temperature dependence and transition from interphase to general precipitation, as well as with its dependence on C, V and N contents.

- Experiments show clearly that the V(C,N)-precipitation becomes denser and the particles finer with increasing N-content. This originates from the fact that the chemical driving force for this reaction increases as more N is dissolved in ferrite and therefore increases the nucleation rate. The larger particle density causes an earlier depletion of V in the surrounding ferrite resulting in a slower growth of the precipitates.
- V(C,N)-precipitation generates considerable strengthening at moderate additions of V; a V-content of 0.10% engenders in steels with 0.010%N, typical of EAF steels, precipitation strengthening up to 250MPa. Enhanced cooling through the γ/α-transformation and in the ferrite range is effective for increasing strength, particularly at high N-contents.
- In steels with hard and for dislocations non-penetrable particles such as V(C,N) the one microstructural parameter determining the precipitation strengthening is the interparticle spacing. Therefore to obtain the largest possible strengthening the nucleation rate of V(C,N), which determines the density of the precipitate population, should be maximised. The strong effect of N in precipitation strengthening of V-microalloyed steels, amounting to ~6MPa per 0.001% N, is due to its ability to enhance V(C,N)-nucleation.
- It has been shown that the first V(C,N) to be formed is N-rich. It is only until almost all N has been consumed that the C-content of the carbonitride rises. To benefit from continued precipitation strengthening of C-rich V(C,N) beyond this point implies that there must be sufficient C in solution and chemical driving force for new V(C,N)-nucleation to occur. It is demonstrated that such a situation is at hand when the ferrite C-content is controlled by the γ/α- rather than the α/cementite-equilibrium; in the former case the ferrite C-content is 5 times larger than in the latter at 600°C.
- Recent studies have demonstrated that the precipitation strengthening in V microalloyed steels increases significantly with the total C-content of the steel, an effect previously not recognised, ΔR_p ~5.5MPa per 0.1% C. This is explained by the fact that the C-content of the steel delays the pearlite formation and thereby maintains the higher content of C dissolved in ferrite corresponding to the γ/α- equilibrium for a longer time, cf. previous paragraph.

5. CAST STRUCTURES

5.1 Microstructural features

Much less attention has been devoted to the microstructures of as-cast slabs than those of rolled products for obvious reasons. On the one hand, sampling of these thick gauges (typically 220mm) is troublesome and on the other hand their influence on final properties is often only indirect. Nevertheless, some knowledge of these structures is necessary, especially in connection with down-stream processing such as hot rolling. Broadly, the as-cast structures contain two types of features; those which are persistent and may directly affect the final properties and others which are modified beyond recognition during subsequent stages of the manufacturing process. Among the persistent features can be listed inclusion morphology, TiN dispersion and segregations which can lead to banded structures and inhomogeneous dispersions of microalloy carbonitrides. Transient microstructures include grain structures and microalloy precipitates in the form of eutectics or other coarse carbonitrides, which may be refined by recrystallisation or dissolved by diffusional processes.

In fact, the distinction between such persistent and transient features is not always clear cut. For example, when comparing conventional slab casting and reheating prior to rolling with thin slab casting and direct hot rolling it is advisable to consider more carefully the influence of as-cast structures. The absence of the $\gamma-\alpha-\gamma$ phase transformation prior to rolling and the smaller total reduction may mean that the initial grain structure still has some influence on the final grain size. Similarly, the lower temperature and shorter holding time before rolling may not be sufficient to dissolve eutectic alloy carbides, with implications for precipitation strengthening in the final product. Few systematic studies on thin slab structures have so far been reported so it is not possible to draw clear conclusions but it is probably wise to assume at least some differences from the behaviour in traditional processing.

Continuously cast slabs of structural steels usually show evidence of columnar solidification near to the surfaces with equiaxed structure towards the centre. However, this is often not apparent in the final ferrite+pearlite or bainite microstructure due to the sequence of transformations $\delta-\gamma-\alpha$ on cooling. Figure 5.1 is taken from Bruce (5.1) on 220mm thick cast slabs of a V-Ti-microalloyed steel (0.13%C, 1.46%Mn, 0.042%V, 0.01%Ti).

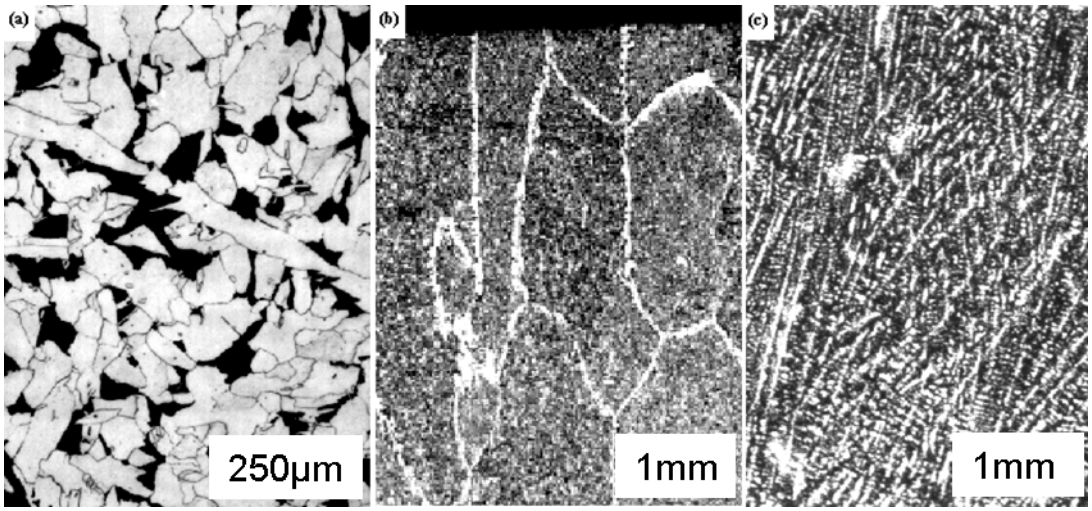

(a) (b) (c)

Fig. 5.1 Optical micrographs of as-cast HSLA steel slab. (a) grain structure, (b) prior austenite grain boundaries, and (c) dendritic structure of the original δ-ferrite.

At higher magnification the microstructure is a relatively uniform mixture of ferrite and pearlite (Fig. 5.1(a)) but low magnification (Fig.5.1(b)) reveals the prior austenite grain boundaries decorated by continuous networks of ferrite. In this sub-surface region the austenite grains are seen to be columnar with a thickness of about 1mm and are several millimetres in length. The original dendritic structure of this steel was revealed by a heat treatment involving austenitising at 950ºC followed by slow cooling to 770ºC, water quenching and tempering at 400ºC. After etching in nital the dendrites appear as light coloured ferrite in a background of darker tempered martensite (Fig 5.1(c)). It is apparent here that the as-cast δ-ferrite grains were considerably larger than the subsequent austenite in this case. There are indications that titanium additions can assist this austenite refinement or alternatively hinder grain growth in the newly transformed austenite (5.1). On the other hand, giant austenite grains centimetres in diameter may also occur in such microallyed steel, especially near to corners. These give the appearance of secondary recrystallisation or of a critical strain recrystallisation phenomenon arising from bending, thermal effects or, possibly from strains caused by the peritectic reaction.

Vanadium in cast slabs of microalloyed steel is found in carbonitride particles that may adopt at least three types of morphology. Fine scale precipitates around 100nm in diameter are thought to arise during cooling through the low temperature austenite range (Fig.5.2(a)). In steels containing also Nb these may occur as mixed (V,Nb)(C,N) phases. These sorts of particles are often seen in rows, having nucleated along the austenite grain boundaries. Steels alloyed with both V and Ti, Zajac et al. (5.2), contain large 'dendritic' particles with arms extending in three mutually perpendicular directions (Fig. 5.2(b)). At the centres of these crosses can be found cuboidal TiN particles on to which the arms of almost pure VN have grown. Their size indicates that diffusion must have occurred over relatively long distances and accordingly that these structures formed at higher temperatures in the austenitic range, when the solubility limit was exceeded during slab cooling, nucleating on the pre-existing TiN precipitates. The third type of V(C,N) phase which has been found in cast slabs is much coarser still and appears to be a eutectic product similar to the NbC eutectic phases that have been reported by Priestner and coworkers (e.g. 5.3, 5.4) in solidified niobium microalloyed steels. Occurrence of such products in these steels is attributed to microsegregation which leads to enrichment of the alloy elements within the liquid phase so that solidification terminates with a eutectic reaction in inter-dendritic regions An example of such a phase in a cast slab structure (0.09%C, 1.41%Mn, 0.013%N, 0.08%V, 0.01%Ti) is shown in Fig. 5.2(c).

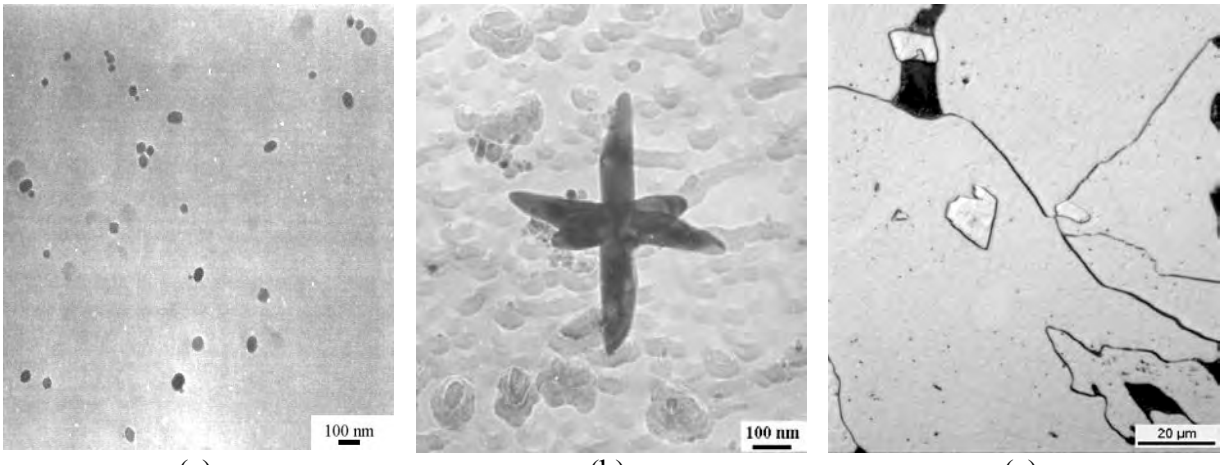

(a) (b) (c)

Fig. 5.2 V(C,N) phases precipitated in as-cast HSLA steel slab. (a) and (b) replicas in TEM, and (c) optical micrograph from unpublished work at Swerea KIMAB.

The vanadium-rich carbonitride phases normally dissolve during the prolonged high temperature reheating of slabs before hot rolling in conventional processing. Even the coarse eutectic phases are seldom apparent in final rolled products. It can be supposed that the microalloy addition is therefore made available for precipitation strengthening as intended. For direct rolling of thin slabs, both the holding time and temperature prior to hot rolling are less and it is possible that some of the coarse particles remain with detriment to the final properties. This seems to be the case for some Nb-microalloyed steels (5.4); as yet, the situation with regard to V-steels has not been clarified to our knowledge.

5.2 Ductility during casting

Probably the most important practical consequence of the structure and chemistry in as-cast steels is how these affect ductility of the slabs when the strand is bent and unbent at high temperature in the production process. Crowther has provided an excellent summary (5.5) of mechanisms involved in this 'transverse cracking' and the effect that different alloy and impurity elements have on it. It is well known that a trough in ductility exists over a certain range of temperature where surface cracking of the strand is likely to occur and that the problem is exacerbated in microalloyed as compared to plain C-Mn steels. The low ductility region usually lies in the range 700ºC-1000ºC but the most critical factor is the upper temperature at which ductility deteriorates since bending of the slab, which is cooling continuously, must be complete before any part of it (face, edge or corner) falls below this temperature.

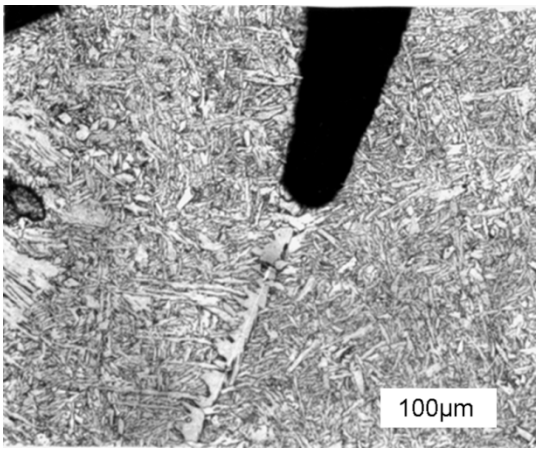

Fig. 5.3 Example of cracking along a prior austenite grain boundary in a cast slab of Ti-V-microalloyed steel.

The normal appearance of these cracks is that they follow prior austenite grain boundaries as shown by the example of a corner crack in a slab of Ti-V-microalloyed steel in Fig.5.3 from Bruce (5.1). In this case, the ferrite films delineating the original austenite grain boundary have formed after the cracking took place. The cracking along austenite grain boundaries at high temperature and rather low rates of deformation is an example of typical creep rupture behaviour which is known (5.6) to become more serious at large grain sizes as in the case of these cast products. As the grain boundaries act as softer material than the grain interiors, deformation and sliding concentrate at these, leading to void initiation at triple junctions or second phase particles lying in the boundaries. Microalloyed steels have been postulated to be sensitive to such cracking for several reasons (5.7, 5.8) namely:

- Void initiation at coarse carbonitride particles located on austenite grain boundaries
- Hardening of the grain interiors by fine scale carbonitride precipitation
- Inhibition of dynamic recrystallisation by precipitation on deformation substructures thus preventing relaxation of stresses built up at grain boundaries.

An additional effect in steels comes into play when the temperature falls below Ar_3 and ferrite starts to form, commencing along the austenite grain boundaries. At a given temperature the strength of ferrite is only about 60% that of austenite so the tendency for deformation to concentrate to the boundary regions becomes magnified with rapid localised rupture as a consequence. Only when the structure becomes mainly ferritic at lower temperatures can the deformation become more uniformly spread and ductility be restored.

A number of investigations have been reported comparing the high temperature ductility behaviour of different types of steels. These have mostly made use of tensile testing or in some cases bending to simulate more closely the steelworks situation. The most reliable data come from tests where the steel is melted and solidified and then cooled directly to the testing temperature but in some cases a very high prior austenitisation temperature was used to achieve coarse grain structures having the microalloying elements in solid solution. Results of four sets of hot tensile tests are compared in Fig. 5.4, all using different ranges of steel chemistry. Reduction in cross-sectional area at failure was the measure of ductility. Figure 5.4(a) is from Mintz and Abushosha (5.9) for samples pre-heated at 1330ºC while Fig. 5.4(b) refers to solidified samples (5.10) as does Fig. 5.4(c) from the work of Karjalainen et al. (5.11). An alternative measure of hot ductility in Fig. 5.4(d) is the length of the largest crack in 50mm thick slabs bent at various temperatures after casting, from Crowther et al. (5.12).

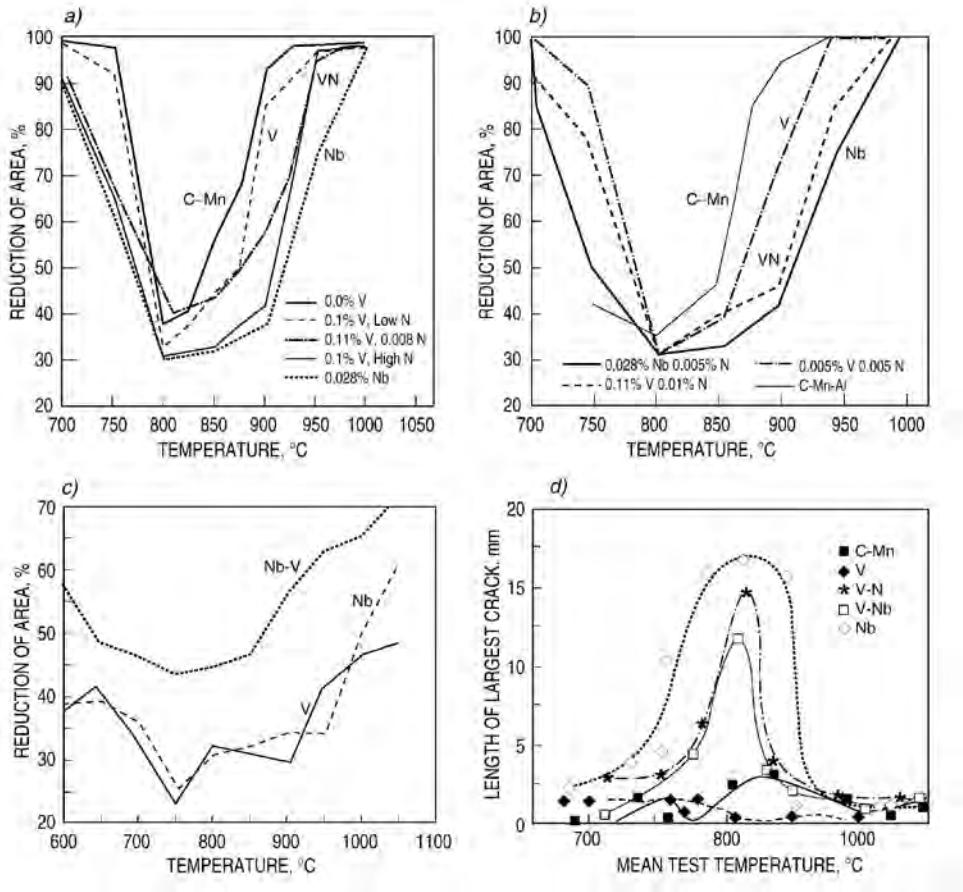

Fig. 5.4 Comparative hot ductility data for steels from various literature sources.(a)-(d) references (5.9-5.12) respectively.

These various results are not easy to compare in absolute terms of deformation or temperature that can have been affected by the particular conditions of cooling or strain rates that were

applied. However, they show a fairly consistent trend when different steel compositions are compared in each case. Plain C-Mn steels show the least sensitivity to cracking, both in terms of the depth of the ductility trough and the range of temperature over which it exists. The most susceptible steels are those microalloyed with Nb and this appears to be particularly true when the upper temperature of the embrittlement range is considered. As mentioned above, this is the most relevant parameter for steelworks practice. Vanadium microalloyed steels show an intermediate behaviour between the plain and the Nb steels. It is seen that higher nitrogen contents in the V-steels extend the low ductility trough, especially towards the higher temperatures. According to Mintz and Abushosha (5.9), the hot ductility of V-steels are superior to Nb-microalloyed ones provided that the V and N levels in the steel expressed in weight % are such that $[V][N]<1.2x10^{-3}$. A high N-content is generally deleterious to hot ductility (5.5), probably because it promotes more precipitation of AlN, VN or NbN and at higher temperatures. In the case of V-N-microalloyed steels the VN particles may also promote earlier ferrite formation by the mechanism described in Section 3 and so contribute further to the reduction in ductility. A curious feature in some of these reports, however, is that the presence of V in Nb-microalloyed steels seems actually to improve the resistance to hot cracking even though the level of Nb remained the same.

Interpretation of the ductility trough results in Fig. 5.4 is not entirely straightforward. The cracking data of Crowther et al. (5.12) were considered to be partly a result of ferrite formation along austenite grain boundaries. This seems reasonable in view of the temperatures that were all below 900ºC. All the tensile tests show that loss of ductility commences at much higher temperatures, however. The effect of the microalloying elements is, of course, not due to a change in the Ar_3 temperature but must be associated with precipitation of carbonitride particles. This is fully compatible with the lower solubility of Nb than V in austenite such that precipitation of NbC occurs at higher temperatures.

The effect of precipitation can also be reconciled with the effect of nitrogen on the driving force for VN as discussed in Section 2. Nevertheless, full agreement concerning the mechanism of ductility loss still seems to be lacking. The idea that dynamic recrystallisation is inhibited by Nb is in qualitative agreement with many observations on hot working and could indeed be true for the hot tensile test conditions. However, the strains involved in these tests are much larger than those in the real steelworks situation. Dynamic recrystallisation would not normally be expected for the strains of less than 1% which occur in practice. Strengthening of the austenite grain interiors by precipitated particles which in turn raises loading on the grain boundaries is suggested by some test results and the same effect may possibly become magnified when softer grain boundary ferrite develops. Fine precipitates are expected to have a greater strengthening effect than coarse ones so would be more deleterious. In one study (5.12), the beneficial effect of V-additions to the hot ductility of Nb-microalloyed steels was seen to be associated with an increase in size of the precipitated particles. Vanadium also appears to inhibit precipitation of detrimental fine NbTi(C,N) which contributes further to its beneficial influence in Nb-microalloyed steels (5.13).

5.3 Thin slab (CSP) conditions

The rapid growth of CSP technology during the last two decades raises new questions about the structures and properties relevant to thin slabs. An extensive review has recently been presented by Rodriguez-Ibabe (5.14) who noted that some 15% of the whole World's strip production, already in 2007, was manufactured in this way.

The higher casting speeds in thin slab casting appear to place further demands upon the hot ductility of microalloyed steels. As a consequence of this, carbon contents in the peritectic range, ~0.07-0.17%, are avoided. Furthermore, it has been demonstrated that Nb-microalloying deteriorates the surface quality of hot rolled strips because of surface microcracking during thin slab casting (5.15). V-microalloying even when combined with an enhanced N-content is capable of remedying these problems. First the loss in strength by reducing the C-content below 0.07% can be satisfactory compensated by proper V/N microalloying. Furthermore the hot cracking during casting in Nb-steels leading to impaired surfaces can be considerably reduced in V-steels (5.10, 5.13).

The as-cast structures of thin (50mm) slabs of V-Nb microalloyed steel (0.06%C, 1.49%Mn,0.11%V, 0.017%Nb) have been examined by Siwecki (5.15). The columnar as-cast structure was almost continuous except for a layer of finer equiaxed grains at the surface (Fig. 5.5(a)). Also here, the austenite grain boundaries were visible at low magnification decorated by ferrite films (Fig. 5.5(b)). The austenite grains tended to be columnar except close to the surface and were somewhat smaller than those in the CC slab in (5.1).

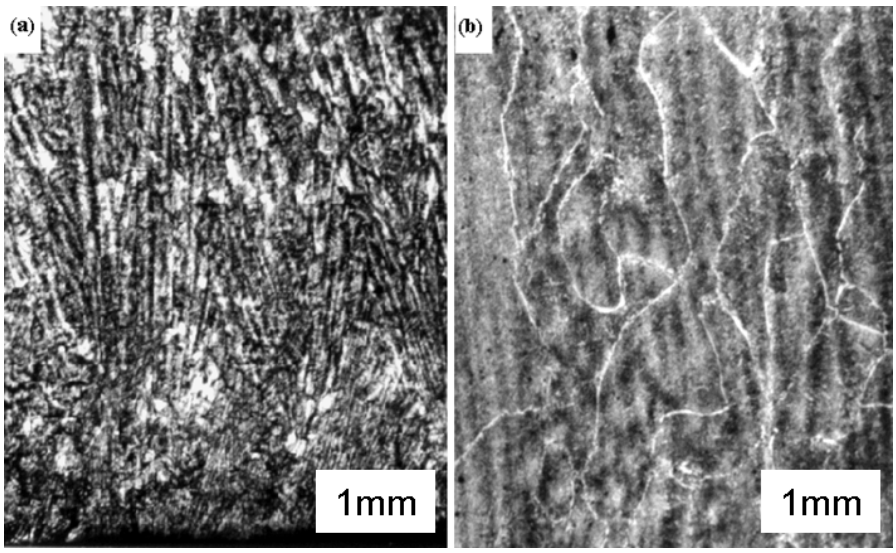

(a) (b)

Fig. 5.5 Optical micrographs of as-cast thin (50mm) slab showing (a) original dendrite structure, and (b) prior austenite grains.

Knowledge of the austenite grain sizes in thin slabs is important since these are charged directly into the equalisation furnace without the possibility of structural refinement that is permitted by the phase transformations in conventional slab processing. Also, the total reduction during subsequent rolling is less and the possibility for grain refinement is accordingly more restricted. Results from large-scale laboratory simulations of thin slab casting with various controlled cooling rates were reported by Mitchell et al. (5.17) for steels with 0.06%C, 1.5%Mn, 0.45%Si with different V- and N-levels. Austenite grain sizes from these experiments together with some from simulations of slabs of different thicknesses are shown in Fig. 5.6. These show finer austenite grain structures with increasing cooling rate or decreasing slab thickness as might be expected. However, there is a considerable discrepancy in magnitude between these and values reported from industrial CSP production reported by Rodriguez-Ibabe (5.14). Most mean grain sizes in Fig. 5.6 are less than 500μm while the industrial samples had average sizes around 1200μm with the largest grains extending up to 2500μm both near the slab surfaces and in the centre. The commercially produced 50mm slab structure in Fig. 5.5 also contained similarly large austenite grains. This may indicate that the

actual conditions during continuous teeming under industrial conditions are not easily achieved even in large scale laboratory trials.

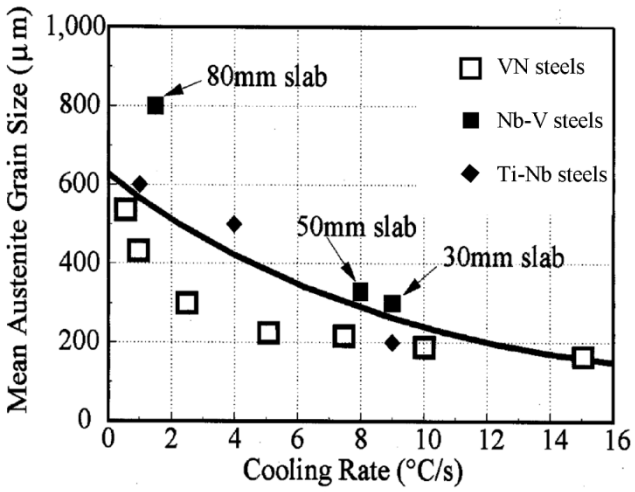

Fig, 5.6 Mean austenite grain sizes in casting experiments with different applied cooling rates (5.17).

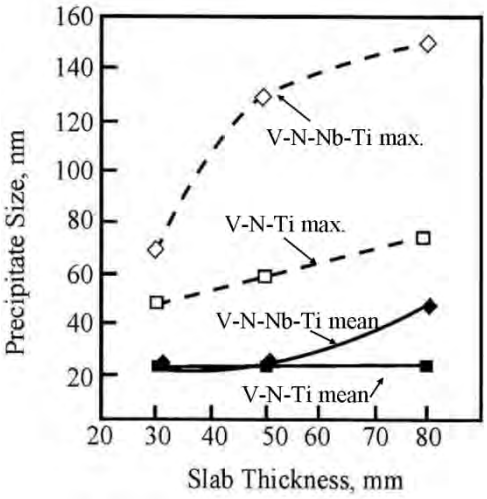

Fig. 5.7 Sizes of (V,Ti,Nb)(C,N) particles in two microalloyed steels as a function of the as-cast slab thicknesses (5.17).

The varying cooling rates in slabs of different thicknesses affect not only the grain structures but also the size of second phase particles precipitated in the austenite. Figure 5.7 shows average and largest particle sizes for two microalloyed steels from the same report as above (5.17). Faster cooling in thinner slabs reduces the size of (V,Ti,Nb)(C,N) precipitates which may be expected to have some influence on the final grain sizes after hot rolling due to their greater Zener pinning effect on grain growth.

5.4 Summary of chapter

- Grain structures in as-cast steels are not strongly dependent on the presence of V as a microalloying element. Vanadium exists in carbonitride particles having a wide range of sizes as a result of precipitation in different temperature ranges during solidification.
- The reheating treatment of slabs prior to conventional hot rolling is normally adequate to ensure that V is re-dissolved and is available to provide precipitation strengthening in the final rolled products. In the case of direct hot rolled thin slabs, the normal temperatures in the equalisation furnace usually ensure that all V remains in solid solution.
- The tendency for hot cracking of cast slabs is more severe in Nb-microalloy steels than in V-steels. High N-levels increase the susceptibility for hot cracking. Addition of V to Nb-steel appears to have a beneficial effect associated with coarsening of the (Nb,V)(C,N) particles in the cast material.
- Direct rolling of thin slabs means that grain refinement by $\gamma-\alpha-\gamma$ phase transformation cannot take place. The austenite grains may be very large prior to hot rolling in this case. There appears to be some uncertainty as to the true size of austenite grains in this situation.

6. PRINCIPLES AND PRACTICE OF THERMO-MECHANICAL CONTROLLED PROCESSING, TMCP

6.1 General principles

Processing of steel can be viewed as a generic sequence of temperature, times and deformations from the original as-cast solid to the final product which may be plate, strip, bar, section, pipe or forging. Throughout this sequence, the microstructure is progressively modified and the aim of TMCP is to achieve optimum mechanical properties for the material in its final shape. The microstructural development depends on the creation of dislocation substructures followed by recovery, recrystallization, grain growth, phase transformation and the precipitation of second phases, most notably the microalloy carbonitrides. Figure 6.1 shows schematically the various stages of the process together with the associated changes in microstructure.

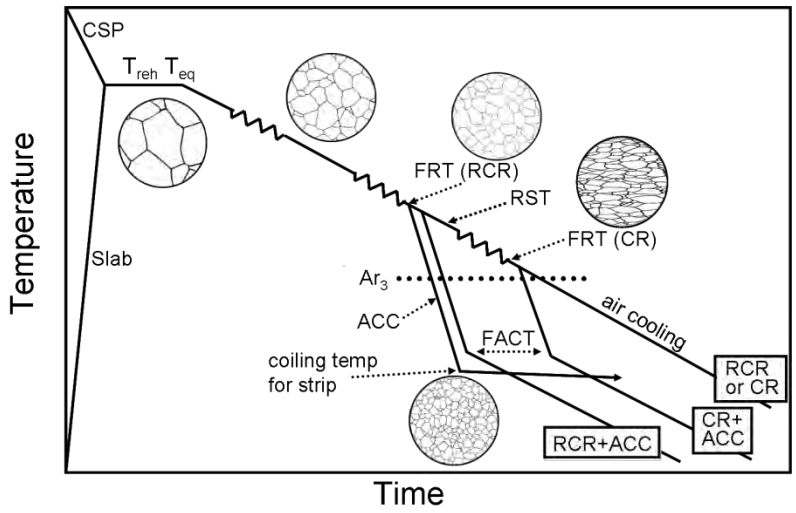

Fig. 6.1
Schematic representation of various thermo-mechanical controlled processes (TMCP) in steel production

In traditional production from continuously cast steel, the slabs are reheated prior to rolling whereas in the newer thin slab processes the solidified strand goes directly to an equilibrating tunnel furnace followed by rolling, which gives a considerable saving in energy. Different hot rolling processes also result in significant variations in the deformation-time schedules of the finishing stage which must be taken into account when aiming to control the microstructures. In strip rolling, the steel passes through a series of rolls in tandem. These are close together so the inter-pass times are short and they become progressively shorter, a result of the band accelerating as its thickness reduces. By contrast, plate and long products are usually reversibly rolled so the inter-pass times are much longer and these increase as the product becomes longer after each pass. A similar but more extreme situation arises in strip rolling in Steckel mills where the band is coiled up on either side of the reversing mill with much longer inter-pass times that also increase with the rolling reduction as the band becomes longer. These practical circumstances impact upon the microstructural development of the steel in terms of its recovery, recrystallisation and the precipitation of second phases

Good combinations of strength, fracture toughness and weldability can be obtained for V-microalloyed HSLA steels in the as hot rolled condition by careful choice of thermo-mechanical controlled processes (TMCP) (6.1-6.13). The improvement in properties of plates, long products, strips and forgings is associated with different strengthening mechanisms of which the most important is grain refinement whereby strength and toughness are both improved at the same time. In order to obtain optimum ferrite refinement, it is necessary to

maximise the area of austenite grain boundary per unit volume at the on-set of phase transformation (6.8, 6.9). This may be achieved either by low temperature controlled rolling (CR) or by recrystallisation controlled rolling (RCR) when the finish rolling temperature is relatively high (see Fig. 6.1).

The aim of (RCR) is to make use of grain refinement by repeated recrystallisation of austenite. The fine austenite structure is retained during inter-pass delays and during cooling down to Ar_3 by a suitable dispersion of second phase particles, usually TiN. This, together with accelerated cooling (ACC), leads subsequently to a minimisation of the ferrite grain size after transformation. The concept of RCR is attractive in that it is a relatively uncomplicated and high productivity process and can be applied on conventional mills. This procedure is intrinsically more economical than controlled rolling (CR) at low finish rolling temperatures (lower than the recrystallisation stop temperature, RST) and also lends itself well for use in mills which are not sufficiently strong for low temperature controlled rolling practice and for rolling of long products with their inherently high finishing temperatures.

Vanadium and niobium play significantly different roles during TMCP that derive from the differences in solubility of their carbonitrides in austenite, as discussed in Section 3. Niobium, both in the form of solute and precipitates, hinders recrystallization and facilitates deformed 'pancake' grain structures during low temperature rolling, leading to very effective grain refinement during the transformation to ferrite. Relatively little of the Nb then remains in solid solution so that precipitation makes only a modest contribution to the strength after CR processing. Vanadium has a greater solubility in austenite and the temperature of final rolling is usually higher in this case so that almost all the V is retained for effective strengthening by precipitation in the ferrite. Grain refinement is essential here since, without it, the toughness would deteriorate as a result of the precipitation hardening effect.

Accelerated controlled cooling after hot rolling alters the microstructure from ferrite-pearlite to fine-grained ferrite-bainite and, consequently, increases the strength with little detriment to the low temperature toughness. Hot strip is cooled rapidly after rolling along the run-out table but the band is then coiled tightly so that subsequent cooling becomes very slow. In this case, the coiling temperature becomes a most important parameter controlling the ferritic microstructure and the precipitation of microalloy precipitates. While precipitation strengthening of Nb(C,N) or V(C,N) is enhanced by accelerated cooling; the deleterious effect of this on impact toughness is counteracted by the improved grain refinement. Proper processing of microalloyed HSLA steel aims to combine grain refinement with an effective utilisation of the strengthening potential of the microadditions. This is best achieved if the process schedule is designed to give rapid cooling through the γ to α range to provide the finest possible ferrite grain size, followed immediately by a delay or much slower cooling in order to precipitate out the V(C,N) as fully as possible. In strip rolling, this is obtained almost ideally by the combination of water-cooling on the run-out table followed by coiling at a temperature around 550º - 600Cº. This situation is less easy to manage for other steel products but, nevertheless, may be considered as a good principle to aim for.

Another key to success with TMCP-processing lies in defining rolling schedules combining a maximum degree of microstructural refinement with acceptably low rolling loads, good shape control and high productivity. In this context, computer models for calculation of microstructure development and precipitate evolution during hot rolling (6.14-6.17) are invaluable for design of rolling schedules.

6.2 Microstructure development during TMCP rolling

Knowledge of the microstructure development during hot rolling is very important for optimising rolling schedules with the aim of improving properties of TMCP steels. The optimisation of rolling schedules for TMCP-processing by recrystallisation hot rolling requires detailed knowledge concerning the coupling between rolling schedules (reduction, temperature and pause time) and development of microstructure. With intelligent design of the rolling schedules it is possible to obtain a very fine and uniform austenite microstructure. Computer models for calculation of microstructure evolution during hot rolling have proved to be extremely useful for optimising rolling schedules, following the lead of Sellars and Whiteman (6.18). The computer model MICDEL, developed at the Swedish Institute for Metals Research, has been applied to many different steel compositions and permits comparison to be made of the effect of various material and process parameters (6.14-6.16). The model is based on the concept that the resulting structure is dependent on the static recrystallisation, static recovery and grain growth of austenite. The static recrystallisation kinetics and recrystallized austenite grain size are influenced strongly by: strain, strain rate, temperature and pre-existing grain size as well as the steel chemistry. Grain growth of austenite following static recrystallisation is described in accordance with Hilbert's theory, where the normal growth rate of spherical grains with radius R is dependent on the average grain size, the inhibition caused by second phase particles (Zener parameter), the specific grain boundary energy and mobility of the grain boundaries.

Figure 6.2 shows examples of predicted microstructure evolution during realistic full-scale hot rolling of 0.01%Ti-V-N and 0.01%Ti-V-Nb steels having different levels of vanadium, niobium and nitrogen, when subjected to the same rolling schedule (6.15). The data refer to rolling of 25 mm plate in 11 passes, starting from 1100°C. The initial grain sizes after reheating were taken to be 20 μm for both 0.01%Ti-V-N steels and 55μm for the Ti-V-Nb steel. For the lower alloyed steel, 0.04%V, 0.01%N, 0.01%Ti, the effect of abnormal grain coarsening is demonstrated by using an initial grain size of 500 μm.

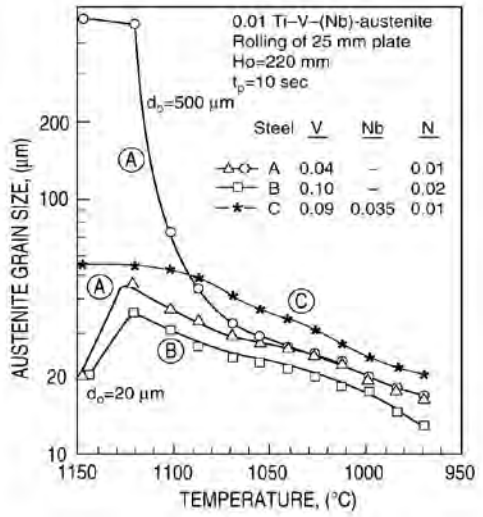

Fig. 6.2 Development of austenite microstructure for Ti-V-(Nb)-N-steels during simulation of industrial hot rolling of plates with different microalloy contents (6.15).

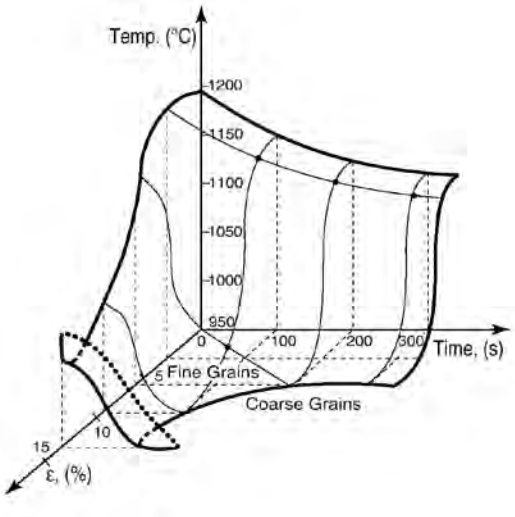

Fig. 6.3 Processing window for avoiding coarse grained austenite structures in Ti-V-N steel after the final sizing pass. The surface in ε-T-t space separates the original fine structure from coarse grains created by recrystallisation or grain growth (6.19).

As evident from Fig. 6.2 the steel with high vanadium and nitrogen is characterised by the most effective microstructural refinement. The microstructure evolution routine has also been used to compute austenite microstructure development during strip rolling of 0.08V-0.018N or similar HSLA steels (6.17), which have been processed by RCR in one of the mini-mills of NUCOR Steel. A general observation is that the grain size existing after slab reheating has almost no effect on the final austenite grain size resulting from recrystallisation rolling, so long as the rolling schedule involves more than 3 or 4 passes. After large reductions, recrystallisation takes place via copious nucleation of new grains and refinement of the structure can be achieved.

The nucleation of recrystallisation decreases strongly as the level of strain is reduced, and hence small rolling reductions at high temperatures can cause abnormally large recrystallized grains. This is most serious at the end of the hot rolling sequence when a small `sizing` pass, applied for control of thickness or shape, may destroy the fine-grained austenite structure created by RCR processing. A study of sizing passes on the final microstructure of Ti-V-N-steel (6.19) shows that undesirable coarse grain structures can be expected (Fig. 6.3). No grain coarsening was observed following a strain of 3% for any of the combinations of holding time and temperature. Figure 6.3 demonstrates the result in ε-T-t space where a surface is defined which separates the safe working region for the final processing from that region where undesirable coarse grain structures can be expected (arbitrarily defined at an austenite grain size of 30 μm). Coarsening of the austenite can occur as a result of grain growth at high temperatures or, at lower temperatures, from the 'critical strain anneal' phenomenon. With small reductions in final sizing passes, nucleation of new grains takes place only infrequently at a few favoured sites followed by extensive growth. Instead of refinement, this process leads to a mixture of recovered pre-existing grains of approximately 10 μm size together with some very much coarser grains. Holding time at temperature is also important for microstructure coarsening and a practical conclusion of this is that accelerated cooling, applied rapidly after the final pass, can be of real benefit in reducing the danger of structure coarsening.

6.3 Mechanical properties and microstructure of TMCP material

The mechanical properties and the final microstructure of V-(Ti-Nb)-microalloyed steels are dependent on the following process parameters:

- reheating temperature (T_{reh})
- rolling schedules: reduction (Red), inter-pass times and finish rolling temperature (FRT)
- cooling parameters: accelerated cooling rate (ACC)
- temperature for finish of accelerated cooling (FACT)
- steel chemistry.

The slab reheating temperature can have a significant influence on the strength, toughness and microstructure of microalloyed steel in the as thermo-mechanical controlled processed condition. A low slab reheating temperature gives finer austenite grains and may refine the final microstructure of the materials, as a consequence, improving the low temperature toughness for steels. This is mainly attributed to the more profuse fine precipitation remaining after low temperature reheating which more effectively resists grain growth of austenite. However, the yield stress and tensile strength decrease because lower reheating temperature reduces the amount of dissolved vanadium (or niobium) in the austenite and accordingly also the potential for precipitation hardening after cooling. For Ti-V-N microalloyed steels it was found that a reduction in reheating temperature from 1250º to 1100ºC reduced the yield stress

by about 40MPa while at the same time decreasing the ductile-brittle transition temperature by about 15ºC (6.5).

Rolling schedules, the finish-rolling temperature and deformation in the final pass are TMCP-parameters affecting strength and toughness. Effects of the finish rolling temperature on the microstructure and mechanical properties for various microalloyed steels are summarised in Fig. 6.4 using data from various sources (6.1, 6.4, 6.8, 6.9). Fig. 6.4 shows that the very best combinations of low temperature toughness and tensile strength are obtained in Ti-V-(Nb)-N steels for finish rolling temperatures close to Ar_3 (i.e. conventional CR practice). However, an almost equally good combination of strength and toughness is obtained for a FRT of 950ºC by recrystallisation controlled rolling of V-N-steel. These observations are in agreement with the results reported by Chilton and Roberts (6.20) for V-N steels showing that FRT has only a limited effect on the mechanical properties, especially when precipitates such as TiN are present to restrict austenite grain growth.

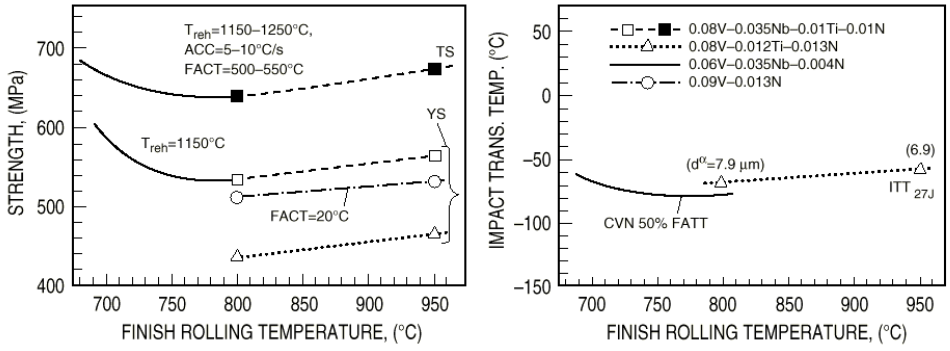

Fig. 6.4 Effect of finish rolling temperature (FRT) on the strength, impact toughness and ferrite grain size of Ti-V-(Nb)-N steel (6.9).

On-line accelerated cooling (ACC) processes after hot rolling, from recrystallized or non-recrystallized austenite are very important because the cooling rate and the finish ACC temperature have a strong influence on the final microstructure and mechanical properties (6.9). The effect of cooling rate and finish cooling temperature on the final microstructure, yield strength and toughness of Ti-V-(Nb)-N-steels after RCR are illustrated in Fig. 6.5. It is apparent that the final microstructure and mechanical properties are greatly influenced by cooling rate. The yield stress of the Ti-V-(Nb)-N-steels rises with faster cooling, although the variation of strength with cooling rate is smaller at higher rates than lower (<7^{o}C/s). At very high cooling rates (15^{o}C/s) the austenite transforms to a ferrite/bainite microstructure. The final ferrite grain size depends only weakly on the finish accelerated cooling temperature (FACT) in the range of 400-600^{o}C although the second phase becomes bainite when FACT is below 500^{o}C. Yield strength, on the other hand, does depend on the finish accelerated cooling temperature and improves with decreasing FACT down to 500^{o}C or even lower. The highest yield stress was observed in the 0.09%V microalloyed steel (without Ti), RCR processed followed by ACC to room temperature as shown in Fig. 6.5.

The appearance of bainite in the structure of Ti-V-N and Ti-V-Nb-steels changes the dependence of yield strength on FACT. The conventional yield stress (0.2% proof stress) is reduced when the FACT falls below 600ºC since sharp yielding does not occur in the presence of bainite, although the tensile strength continues to rise.

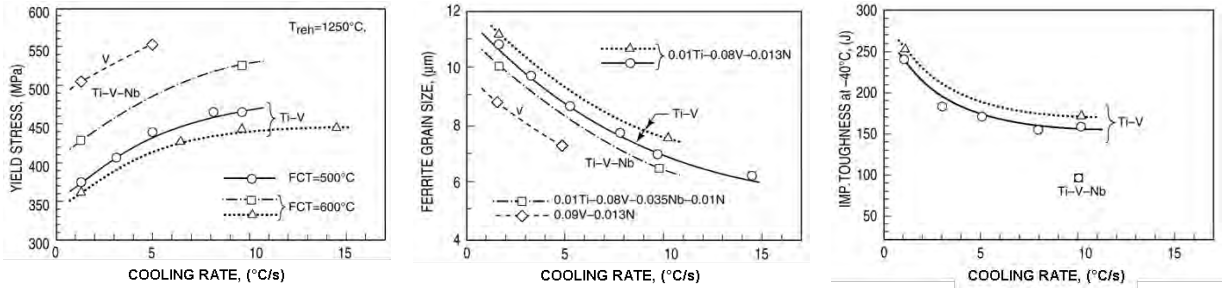

Fig. 6.5 Effect of cooling rate from a finish-rolling temperature of 1030°C to finish-cooling temperature (FCT) on the ferrite grain size, yield stress and toughness of Ti-V-(Nb)-N steels. The final reduction was 25% in all cases (6.9).

Impact transition temperatures of RCR+ACC material increase as the cooling rate becomes higher, despite the fact that the ferrite grain size decreases. This is a result of the precipitation strengthening of V(C,N) or (V,Nb) (C,N) and at low FACTs the increasing volume fraction of bainite in the microstructure. Cooling rate is a principal factor influencing the size distribution of precipitates. A greater proportion of smaller particles and reduced particle spacing were observed when the cooling rate was increased (6.5), so producing more efficient precipitation strengthening. Cooling rates subsequent to RCR (during $\gamma \rightarrow \alpha$ transformation) should be, in principle, restricted to a maximum 10-12°C/s and the finish accelerated cooling temperature should not be lower than 500°C if the formation of martensite is to be avoided. However, direct quenching (DQ) and tempering (T) processes can also be utilised in the production of heavy plates of high strength steels.

6.4 Effect of nitrogen content

The positive effect of higher nitrogen content on the yield strength, notch toughness and weldability of V-microalloyed steel was reported during the 1960s by Melloy (6.21). Siwecki et al. (6.1) have also shown that nitrogen in V-microalloyed steel is conducive to improved grain refinement and raised yield stress (see Fig. 6.6). As shown in this figure, the cooling rate is an important parameter affecting yield stress and microstructure. However, the process conditions of final rolling temperature do not strongly affect the yield stress. Heavy plate (40mm thick), thin plate (10mm) or 10mm bar (with cooling rates of 0.24, 0.088 and 5 ºC/s respectively) can be processed by controlled rolling or RCR of V-steel with attractive strength properties only weakly dependent on FRT as can be readily deduced from Fig. 6.6.

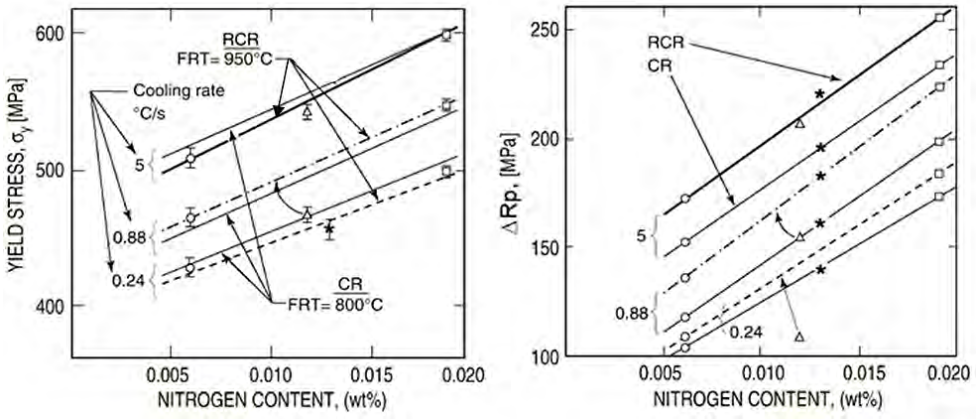

Fig. 6.6 Dependence of yield stress and precipitation strengthening on nitrogen level in 0.09%V steel with 0.12%C and 1.35%Mn for the various processing methods and cooling rates (6.1).

Higher temperature RCR rolling provides a greater precipitation strengthening effect, while the low temperature CR processing gives a finer grained structure although with less precipitation strengthening and these two effects almost cancel one another.

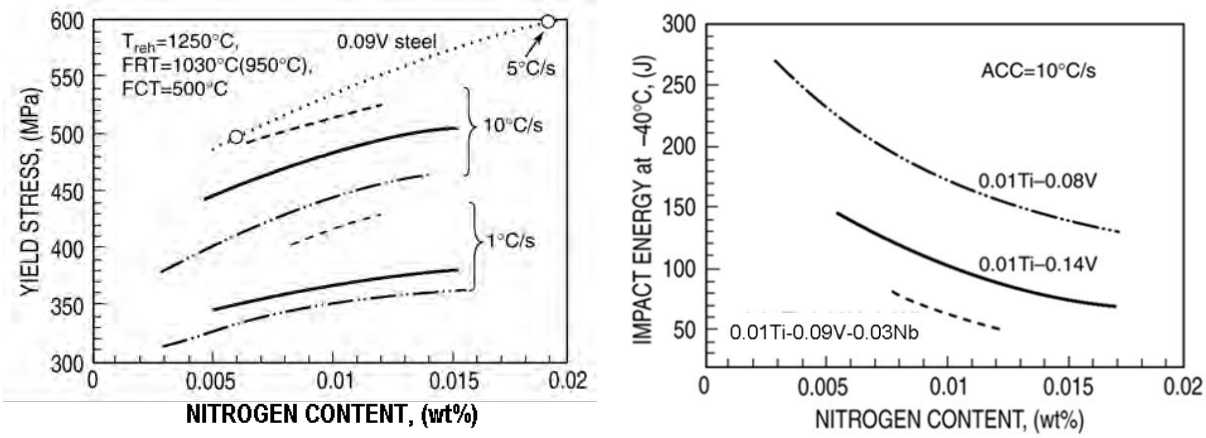

Fig. 6.7. The effect of nitrogen, vanadium (niobium) and cooling rate on the yield stress and impact toughness of Ti-V-(Nb)-N-steels after RCR processing (6.8).

Nitrogen's effect in connection with recrystallisation controlled rolling and accelerated cooling is also demonstrated in Fig. 6.7. Material with higher N-content is significantly stronger than that with low N processed in the same manner although with some sacrifice of toughness. It may be seen that the strengthening potential of vanadium can be effectively utilised only at higher levels of nitrogen and that increased cooling rate has a profound effect especially at these higher levels. For one thing, ferrite grain sizes of low nitrogen steel are significantly larger than those of the higher N steel, especially for slow cooling rates. In particular, with Ti-microalloyed steels, the effectiveness of nitrogen in the low temperature controlled rolled condition is much smaller than in the RCR and ACC condition, (6.5, 6.8). For low N steel with titanium (0.01%Ti, 0.08%V, 0.003%N), the yield stress after low temperature CR was found to be almost identical with that following RCR+ACC processing since almost no precipitation of VN in austenite could take place. However, for higher N steel (0.013%N) the yield stress was ~50MPa less after the CR treatment, which is attributed to the loss of precipitation hardening due to premature formation of coarse VN particles in austenite.

Some results illustrating the effect of processing method by recrystallisation hot rolling, controlled rolling and normalising (the processes were followed by air cooling at 0.9^{o}C/s) on the precipitation strengthening contribution to yield strength, ΔRp, for V-N steels are presented in Fig. 4.12 (6.1). For RCR steels, ΔRp increases linearly with nitrogen content. For normalised material, however, the precipitation hardening contribution to yield stress saturates at high nitrogen levels because of the increasing amount of V(C,N) remaining undissolved at the normalising temperature. Fig. 6.6 also demonstrates that ΔRp is lower after processing by CR with FRT=800^{o}C than after RCR with FRT=950^{o}C. This difference in ΔRp can be reconciled with the loss of precipitation hardening potential when deformation-induced precipitation of V(C, N) accompanies rolling at low finishing temperatures.

6.5 Summary of chapter

- The aim of TMCP processing of V-microalloyed steels is to combine the greatest degree of grain refinement through control of the austenite grain structure and its transformation to ferrite with the maximum amount of particle hardening of the ferrite through precipitation of V(C,N).
- To maximise strength, it is important that vanadium remains in solution in the austenite prior to cooling and transformation. For this reason it is desirable to maintain the finishing temperature of deformation above 900ºC.
- Vanadium microalloying does not lend itself to controlled rolling in the non-recrystallising range (CR) so grain refinement is best achieved by repeated recrystallization of the austenite (RCR processing). Pass schedules and can be designed to give the best grain refining effect through application of computer programs such as MICDEL.
- Small additions of Ti effectively inhibit grain growth after austenite recrystallization due to Zener pinning by TiN particles. This makes a valuable contribution to strength and toughness after RCR rolling.
- Critical ranges of small deformation must be avoided in the final passes to prevent coarse grain formation in the austenite at that stage in the process.
- Further structure refinement is possible when RCR is combined with accelerated cooling (ACC) at rates up to 10ºC/s, so that coarser ferrite-pearlite structures are replaced by fine ferrite-bainite ones in the final product which enhances both strength and toughness.
- Processing by RCR+ACC not only provides excellent mechanical properties but also reduces mill loading because of the higher finish rolling temperature and also provides a quicker production route than low temperature controlled rolling.
- Nitrogen is an essential microalloying element in conjunction with vanadium, contributing both refinement of the ferrite grain structure and more effective precipitation hardening by V(C,N).

7 APPLICATIONS OF TMCP PRACTICE

Results relating to production of plate, strip, long products, pipe and forgings using TMCP practices are presented in the following sub-sections. Where possible the data are derived from full-scale industrial production. In some cases these are supplemented with results from laboratory or pilot line investigations.

7.1 Heavy plates

A thorough study of processing and properties of heavy plates of V-Ti-microalloyed steel having two levels of nitrogen was reported by Zajac et al. (6.5). These steels contained 0.09%C, 1.4%Mn, 0.08%V and 0.01%Ti with either 0.003%N or 0.013%N. Samples taken from industrial cast slabs were first investigated in laboratory examinations to determine various optimal conditions for hot rolling and cooling. The slabs were then hot rolled in full-scale and the resulting microstructures and mechanical properties were thoroughly investigated. Three different processing routes were used in these trials as summarised in Table 7.1. Recrystallisation controlled rolling was used in two cases with pass schedules designed to give best refinement of the austenite grain structure and having small additions of titanium to limit grain growth with precipitates of TiN. One of these variants was air cooled after rolling (RCR) while the other was given accelerated cooling (RCR+ACC). A third variant was rolled to lower temperatures to apply conventional controlled rolling (CR), finishing with a deformed austenite microstructure.

Table 7.1 Process parameters for full-scale production of heavy plates

Process	Treh (^oC)	FRT (^oC)	No. of passes	Time (min)	Thickness (mm)	Cooling rate (deg.C/s)	FCT (^oC)
RCR	1250	1050	10	3 min.	25	0.4	-
RCR+ACC	1250	1050	10	3 min.	25	7	600
CR	1250	800	13	8 min.	20	0.5	-

Mechanical properties of the as hot rolled plates of 0.01%Ti-0.08%V-0.013%N steel are summarised in Fig. 7.1. Toughness is in all cases excellent (ITT_{40J} <-80^{o}C) but best for the CR treatment because of the very fine ferrite grain size and smaller precipitation hardening contribution.

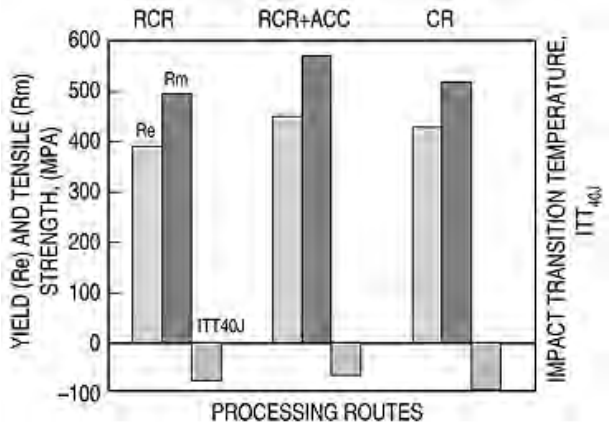

Fig. 7.1 The mechanical properties of the commercially processed 0.01Ti-0.08V-0.013N steel plates with different process routes (6.5).

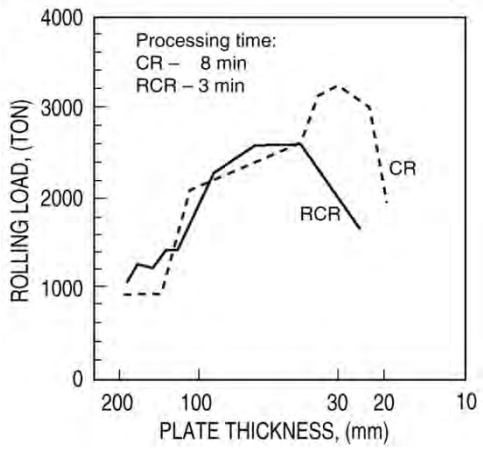

Fig. 7.2 Comparison of observed rolling loads during RCR and CR rolling of Ti-V-N-steel (6.8).

The finest grain structure is obtained from the CR route and this should be capable of some further refinement with application of accelerated cooling. However, despite the finer grain size of the CR plates these have slightly lower strength than the RCR+ACC ones as a result of premature precipitation of VN in austenite during the final low temperature CR-rolling passes.

Important advantages of the RCR process are its high productivity and lower mill loading as compared to CR. The measured rolling loads for the two types of processing when rolling identical plates are compared in Fig. 7.2. It is evident that the maximum loads are ~ 25% higher for the CR process due to the lower temperatures and the accumulated deformation below the recrystallisation stop temperature. The longer time necessary for CR is mainly due to the delay for cooling from 1100°C to 920°C which took place at the 40mm gauge but partly also due to the greater number of finishing passes. For these reasons, RCR processing offers intrinsically higher productivity than does CR for a given plate product, while at the same time making more efficient use of the microalloying additions for precipitation strengthening.

Optical micrographs of the final grain structures are presented in Fig. 7.3. Clear effects of cooling rate on ferrite grain size are evident as are the effects of rolling practice and nitrogen level.

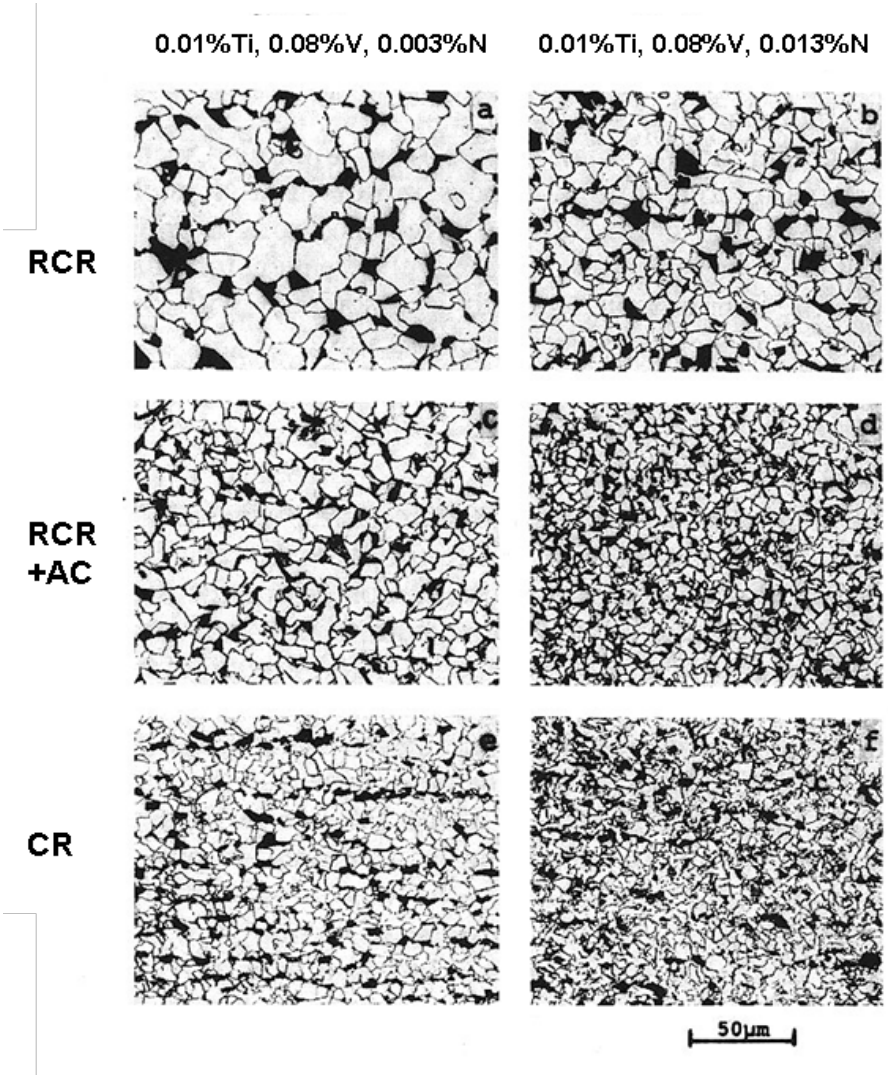

Fig. 7.3 Optical micrographs of plates of V-Ti-N-microalloyed steels produced in full scale using different process routes (6.5)

The grain refining effect of nitrogen is believed to derive mainly from its role in the phase transformation, cf. Section 3, but probably also from a finer dispersion of TiN particles that more effectively restrict austenite grain growth following deformation and recrystallization.

Very similar results to these reported by Zajac et al. have been obtained by Lee et al. (6.7) on a 0.015Ti, 0.08V-steel with a base composition: 0.09C, 0.3Si, 1.5Mn, 0.005N. The mechanical properties of the 12 mm thick plate manufactured at Pohang, processed by RCR followed by ACC with the following parameters: Treh=1250°C, FRT=950°C, ACC=5°/s and FACT=550°C, were Re=~360 MPa, Rm=490 MPa and CVN-40°C=300 J.

RCR + ACC was applied by Rautaruukki Oy for heavy plate production. Tamminen (6.10) reported that good mechanical properties of Ti microalloyed steels were obtained. Moreover, flatness as well as residual stress levels of these plates was better than those produced by CR practice.

More recent investigations have examined the effect of V-N-microalloying to even thicker plates, up to 60 and even 70mm in thickness. Yang et al. (7.1) and Sun et al. (7.2) at Baoshan both confirm the positive influence of increased nitrogen contents in the region of 0.01% which is beneficial both for increased strength and improved toughness. Even after strain ageing treatments there was no detrimental effect of the higher nitrogen contents according to (7.1).

Changes in the mechanical properties of heavy plates of Ti-V and Ti-V-Nb steels processed by low temperature controlled rolling have also been studied. The results in Fig. 7.4 demonstrate that the yield strength of CR-processed steels increases with decreasing the FRT from 840°C to ~730ºC. Above about 850ºC, the yield stress is expected to increase with rising temperature as more V is available for precipitation strengthening in ferrite. However, at these lower temperatures this influence seems to be counteracted by a more extreme grain refining effect. Strength and toughness depend not only on FRT but also on the plate thickness and cooling rate. As shown in Fig. 7.4, the strength increases with decreasing plate thickness, whereas the toughness decreases at the same time.

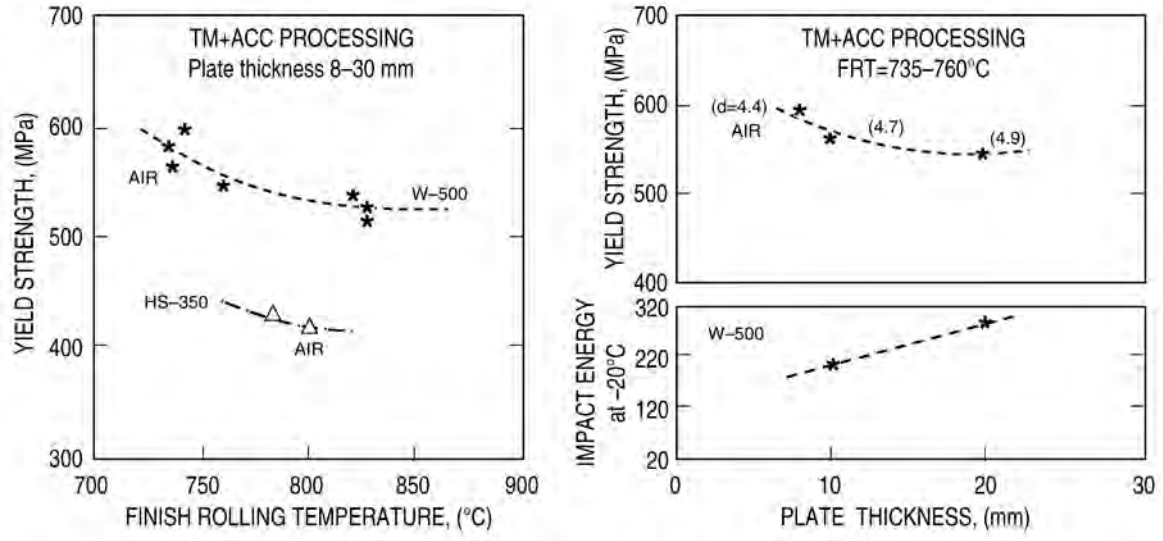

Fig. 7.4 Mechanical properties and ferrite grain size of the commercially CR-processed 0.01Ti, 0.04V (HS-350) and 0.01Ti, 0.085V, 0.04Nb (W-500) steels as a function of: (a) FRT and (b)-plate thickness (6.11).

7.2 Strip rolling

The principal difference between the steels which are intended for strip and plate products lies in the usually lower carbon contents (≤0.08%C) of the former steels. Since the processing of strip necessitates relatively low finishing temperatures (usually ≤900°C), the CR processing route together with appropriate microalloying should lend itself well for obtaining improved mechanical properties. Water cooling for obtaining high strength steel following hot rolling was first introduced on strip mills about 35 years ago. A maximum refinement of ferrite microstructure was achieved by increase of cooling rate after hot rolling. High cooling rates suppress the start temperature for $\gamma \rightarrow \alpha$ transformation and increase the rate of ferrite nucleation. However, recrystallization of the austenite is also possible with only small changes in final rolling conditions. For example, Kovac et al. (7.3) claimed to have achieved RCR conditions in hot rolled strip of Ti-V microalloyed steel using a FRT of 930°C followed by laminar cooling. A yield strength of 550 MPa was achieved, for 8-10mm thick strips, along with a 35J transition temperature at –40°C.

The rolling parameters and the thickness of strips are important for refinement of austenite contributing to ferrite grain size strengthening, whereas nitrogen content shows a very strong effect on yield stress due to precipitation strengthening (see Fig. 7.5) and some further ferrite grain refinement (Fig.3.13).

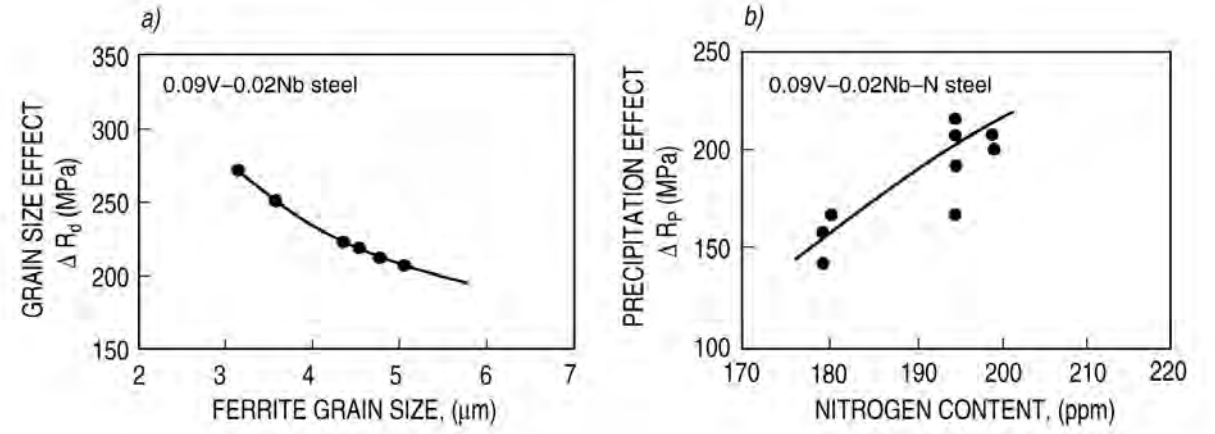

Fig. 7.5 Strengthening effect of (a) ferrite grain size and (b) nitrogen content to the yield stress of the commercially processed HSLA strip steels microalloyed with V and Nb.

In fact, the conditions in strip rolling are almost ideally suited to the use of V-microalloying provided that the final rolling temperature is not too low. The vanadium is maintained almost entirely in solution in the austenite while rapid water cooling gives a high degree of refinement of the ferrite which is followed by very slow cooling in the coil where there is adequate time for complete precipitation of V(C,N) for strengthening. The combined desires of a fine grained ferrite structure together with maximal precipitation hardening are achievable. An important process parameter then becomes the coiling temperature and Grozier et al. (7.4) showed that for steels containing 0.12%V there is a broad optimum in the range 550º to 600ºC for the best strength properties, Fig.7.6. Above this temperature range, the precipitates are too large for best effect and below it the precipitation in incomplete due to the slow diffusion. These results confirm the powerful effect of nitrogen on strengthening of V-microalloyed steels also in strip products.

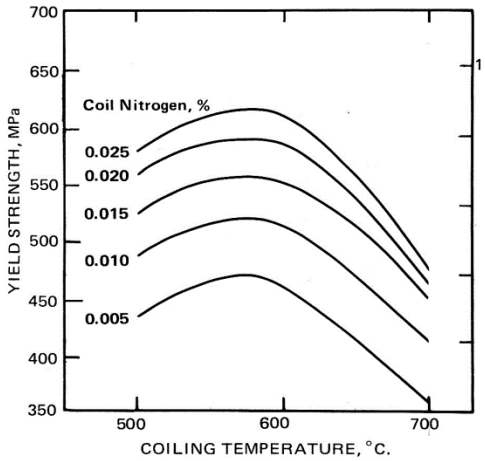

Fig. 7.6 Effect of coiling temperature on yield stress for strips containing 0.12%V and various N-levels (7.4)

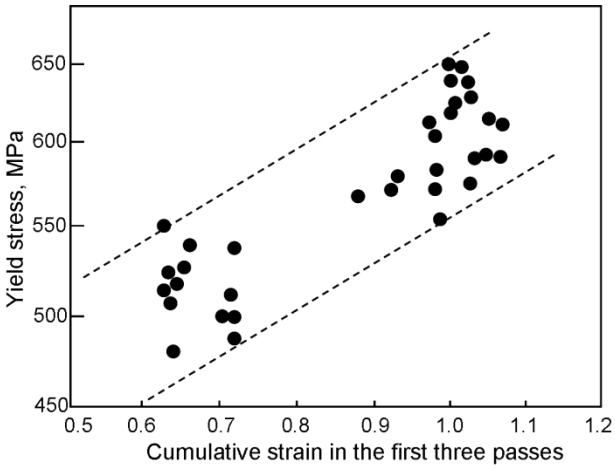

Fig. 7.7 Effect of total strain during the first three rolling passes of 65mm thin slabs on yield strength in the final product (7.5)

Vanadium microalloying is well suited for steels processed from thin slabs by CSP processes as the typical temperatures for slabs in the equalising tunnel furnace prior to hot rolling are around 1100ºC. Accordingly, the vanadium is fully dissolved in the austenite and available to provide precipitation strengthening in the final ferrite, provided that the finish rolling temperature is high enough to avoid strain-induced precipitation taking place in austenite. Since the initial grains are not refined by phase transformations, as in the case of conventional slabs that are cooled and reheated, the starting austenite structures will be coarser and the total reductions during rolling are more limited. This may have some effect on the optimum pass schedule for hot rolling. Conventionally, heavy reductions are wanted in the finishing passes to provide the best grain refinement. However, work at Gallatin steel (7.5) showed that their 80mm CSP slabs had best strength when heavy reductions were applied in the first 3 passes (of total 6) as shown in Fig.7.7. The steels contained 0.12-0.13%V, 0.019-0.022%N and also had small additions of Mo. The author explained that the cumulative strain in the early passes was desirable for bringing about repeated recrystallization to break down the initially coarse grains. It is also probable that heavy deformations in the finishing passes when the strip is cooler tend to cause strain induced precipitation which reduces the strengthening potential of the V(C,N).

The results of microstructure and strength properties of V-Nb-N strip steels processed via direct charging of thin slab (50mm) showed that a yield strength of ~600MPa and elongation of 24% were obtained for 3.5-6.0 mm strips with hot rolling finishing at 900ºC and coiling at a temperature of ~600ºC (7.6).

Crowther (7.7) reported the results of a study on high strength V-microalloyed strip steels produced by thin slab casting but reheated prior to rolling. It was found that a higher reheating temperature of 1200ºC produced the highest strengths with FRT ~850^{o}C followed by cooling at ~18^{o}C/s and coiling at ~600ºC. The effect of slab thickness on the mechanical properties of strip was also studied. Results of the yield strength vs. slab thickness for a number of microalloyed steel combinations (Ti-V-Nb-N) are shown in Fig. 7.8(a). As can be seen, the Ti-free steels exceed comfortably a yield strength of 550MPa for the studied slab thickness although the Ti containing steels failed to meet this strength level in some cases. With increasing slab thickness some reductions in precipitation and grain size strengthening were observed which tended to decrease the yield stress but contributed to improved Charpy toughness.

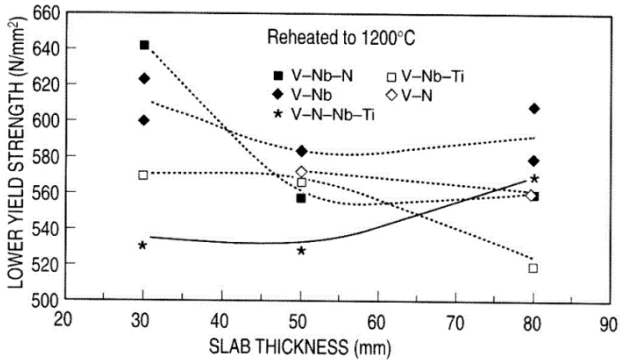

Fig.7.8(a) Effect of steel chemistry and slab thickness on lower yield strength (7.7).

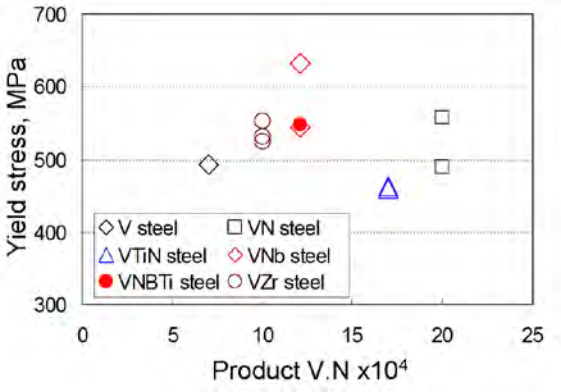

Fig. 7.8(b) Yield stresses for simulated CSP strips for microalloyed steels (7.8)

A subsequent project by Crowther, Li and co-workers (7.8-7.10) investigated similar steels but with a closer simulation of CSP practice. The 50mm laboratory cast slabs were directly equilibrated at temperatures from 1050º to 1200ºC prior to hot rolling with FRT of ~860ºC and simulated coiling at 600ºC. Unfortunately, the finish cooling temperature varied rather widely and this factor had a marked influence on the final properties. In industrial production, the finish cooling temperature is the same as the coiling temperature so many of these results must be treated with reserve. Selected values of yield stress where the finish cooling temperature lay in the range 550º to 600ºC, i.e. within 50 degrees of the coiling temperature, are shown in Fig.7.8(b) as a function of the product of V and N contents. The deleterious effect of Ti on strength of V-N steel is seen here but also only a weak effect of N-alloying and the strength levels are generally lower than those in Fig. 7.8(a). Although it is difficult to draw firm conclusions, this seems to indicate that the initial coarse grain structures in CSP processes may bring about some loss in strength as compared to conventional slab practice. It may be noted that the best properties shown in Fig. 7.7 were for relatively rich V- and N-contents, and they relied on control over the hot rolling schedule.

Production experience shows that it is difficult to raise yield stresses in strip steels much above 600MPa through traditional HSLA technology with grain refinement and precipitation hardening. The alternative approach for reaching higher strength is through transformation hardening with bainitic or martensitic microstructures. Low carbon martensites are becoming increasingly important but for useful ductility in combination with high strength there is a strong interest in bainitic low carbon steel strip. A recent laboratory investigation at Swerea KIMAB showed that yield strength in excess of 700MPa could be achieved in simulated 8mm thick strip corresponding to a cooling rate ~30ºC/s. An upper limit of 0.05%C was set to ensure good weldability, with alloy elements 1.5%Mn, 1.0%Cr and 0.25%Mo based on bainite hardenability criteria. Comparison was made of steels with and without an addition of 0.08%V (4.30). Figure 7.9 compares yield stresses for two comparable steels after simulation of strip rolling with controlled cooling to room temperature and with coiling at different temperatures. In addition, the directly cooled steels were subjected to tempering at 600ºC.

After direct cooling to room temperature there is no difference in strength between the steels with and without the V-addition. Thus, vanadium is not affecting the nature of the transformation to bainite. However, after coiling at both 500ºC and 400ºC, which implies long holding time at these higher temperatures because of the very slow cooling rate, the V-free steel is significantly softer. Evidently, strength is lost due to recovery of the dislocation structure but this is much less when vanadium is present in the steel. The same is confirmed

by the samples that were cooled directly to room temperature and subsequently tempered at 600ºC. The V-free steel lost almost 300MPa in strength after tempering while the V-microalloyed steel lost only 30MPa. A great benefit of V in this case is that the steel becomes insensitive to the actual coiling temperature, a parameter that is difficult to control in the run-out table at these low temperatures.

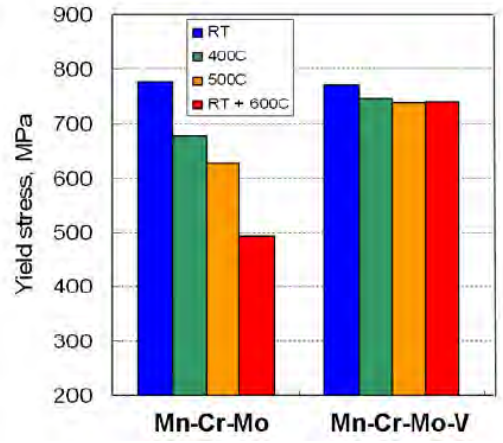

Fig.7.9 Yield stresses for bainitic steels with and without 0.08%V after simulated strip rolling and cooling 7.11).

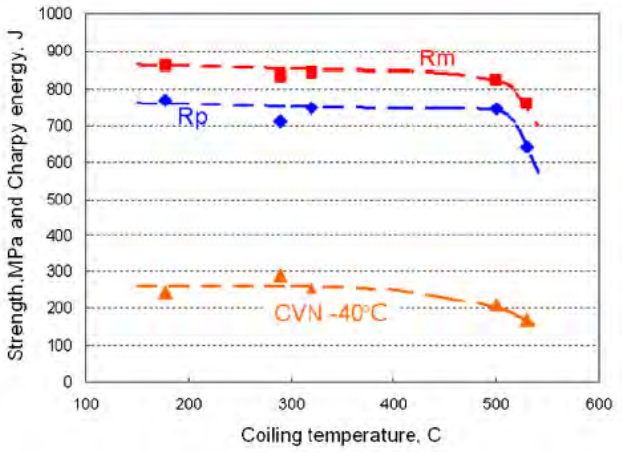

Fig.7.10 Strength and toughness of Mn-Cr-M- V bainitic strip steels after coiling at different temperatures (7.11).

The laboratory simulations of bainitic strip steels have been followed by full-scale production trials at the SSAB steel plant in Sweden (7.11). Results for yield and tensile stresses confirm that the strength and also the Charpy toughness, Fig.7.10, are virtually independent of the coiling temperature up to about 500ºC and fulfil the 700MPa target. Total elongation values from tensile tests were >13% and bendability was excellent with R/t ratios less than 1.6. The requirement for good weldability was also confirmed with excellent toughness in simulated HAZ conditions thanks to the low carbon contents of ~0.04%.

7.3 Long products

Long products comprise bars and sections, of which the latter includes a variety of shapes such as beams, angles, tubes, etc. Typical for these steel products is that they, compared to plate and strip steels, are rolled at higher temperatures. Bar steels, such as construction rebars, rolled in continuous mills have normally finishing temperatures of about 1050°C. For steel products rolled in reversing mils, such as heavy beams, finishing temperatures are lower, extending to 950º - 920°C. The relatively high finishing temperatures and good opportunities for controlled cooling after finishing makes vanadium the natural and best choice for microalloying when added strength is demanded. Furthermore, a large proportion of long product material is made through EAF processing which typically has a higher N-content than for BOF steels and which serves to further enhance the effectiveness of V-microalloying.

Bar steels, especially in thicker gauges, are frequently shaped by forging or machining and heat treated before ending as final product. This implies that the as-rolled properties are not used and have no direct influence on the mechanical behaviour in the final product. Hence, in these cases the properties that are possible to reach by advanced TMCP and microalloying have normally limited value.

Steels for construction rebar include gauges up to Φ30mm, sometimes Φ40mm, and this is a finished product where the as rolled properties are directly employed in constructions. Due to

the development of infrastructure in Asia, especially China, the production of rebar has grown to about 130Mton/year in China (2010), which is approximately 9% of the global steel production and about 20% of China´s (7.12, 7.13). Traditionally, carbon contents up to about 0.40% were used in rebar steels to generate sufficient strength, but the introduction of more welding in the reinforcement of constructions has required lower carbon equivalents in the steels. Modern rebar steels contain therefore only about 0.16-0.22%C. The concomitant loss in strength can be compensated, either by microalloying or by in-line heat treatment after finish rolling (7.12-7.15). The latter method, known as Tempcore or Thermex, is based upon a quick quench of the running bar after the last rolling stand, thereby creating a martensitic surface of the bar that will self-temper by the heat flow from the bar interior (7.14). This process has become the dominant method to produce high strength rebar in Europe. In the rest of the world, V-microalloying has become the preferred technique for high strength rebar. Beside the need to compensate for the loss in strength from reduced carbon levels, there is a general and strong endeavour for higher strength of rebar because of resulting savings of weight and costs. Furthermore, since rebars in the concrete elements of constructions are subjected to pure tension or compression in most cases, an increase of rebar strength generates the same reduction in weight in relative terms, and hence is very effective.

The rolling schedule with high finishing temperature and fast air cooling of rather slender rebars presents suitable conditions for effective precipitation strengthening with V-microalloying. The solubilities for both VC and VN ascertain that all V remain dissolved in austenite down to finish rolling for normal levels of V, N and C and can hence be fully used for effective precipitation strengthening during cooling. The possibilities to further enhance this strengthening by arranging for accelerated cooling are also good in many mills. Nb-microalloying is less suited for strengthening of rebars. With C-contents of 0.2%, Nb(C,N) will not even dissolve fully at reheating temperatures of 1200°C. Furthermore, the high finish rolling temperature for rebars is incompatible with the fine grain strengthening with Nb requiring low temperature rolling.

The role of N for enhancing precipitation strengthening in V-steels has been discussed in some detail in Section 4. In the development of high strength rebar this effect has become a vital part (7.12-7.14). Figure 7.11 shows that the yield strength of a 0.11%V steel increases by almost 120MPa, from 440 to 560MPa, by doubling the N-content from 85ppm to180ppm (7.12). This effect can, of course, equally well be applied for reducing the V-content at a maintained level of strength, thereby saving alloying costs. Accelerated cooling after finish rolling increases precipitation strengthening significantly.

In Fig. 7.12 the effects of V-content, added N and fast cooling are demonstrated for rebars (7.12). As has been shown previously in Figs. 6.5 and 6.6, the effect of N is raised substantially with increasing cooling rate. Another feature of V-N-microalloying is that the higher level of N leaves much less V in solid solution and hence drives the precipitation closer to completion (7.12). This is due to the much denser dispersion of V(C,N) precipitates, as explained in Section 4.3. In addition, the higher C-content of about 0.2%, as compared to flat products, will augment precipitation of C-rich V(C,N) according to the mechanism described in Section 4.4 and so adds further strength to the steel.

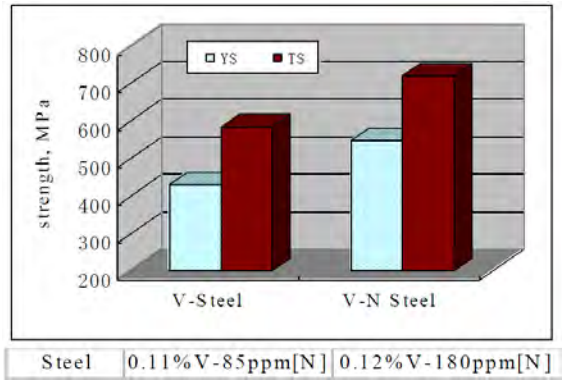

Fig. 7.11 Effect of N-content on the strength of rebar steels (7.12.)

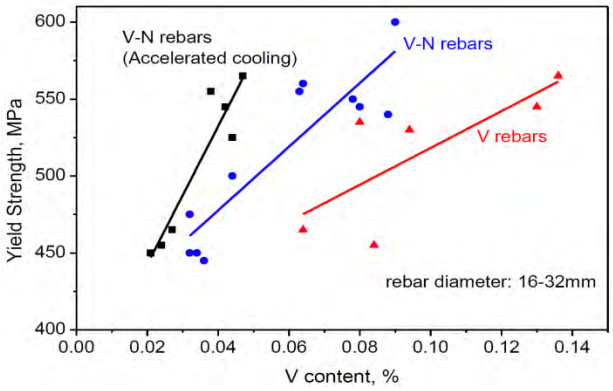

Fig. 7.12 *Effect of V-content, raised N- content and accelerated cooling on strength of rebars (7.12)*

Attempts have been made to apply the procedures of TMCP for plate to bar steel (7.16, 7.17). Two steels with a composition of 0.18%C, 1.5%Mn, 0.35%Si, 0.08%V and 0.012%N, one with 0.01%Ti and one without Ti, were studied. The practice of recrystallisation controlled rolling was adopted with cooling rates between 3 and 8°C/s through the austenite/ferrite transformation; for air cooling this corresponds to bar diameters between approximately 24 and 9mm. For a finish rolling temperature of 900°C the yield stress and impact transition temperature, ITT(20J), were found to be 600MPa and -30°C, respectively, at a cooling rate of 3°C/s and 670MPa and -20°C at 8°C/s with no significant difference between the two steels. By applying accelerated cooling, similar properties can be achieved for thicker dimensions than those given above. The microstructure contained, beside polygonal ferrite and pearlite, varying amounts of bainite/acicular ferrite, significantly more in the V-Ti steel than in the V steel and more at higher cooling rates. In the present case this variation in the amount of bainite/acicular ferrite does not appear to affect the mechanical properties, because these were similar for both steels despite a considerable difference in fraction of bainite/acicular ferrite, 95% in the V-Ti steel and 50% in the V steel.

The new method for ferrite grain refinement by intragranular nucleation on VN precipitates, described in section 3.4, was investigated for application on heavy beams (UPN160) in a large European project (3.34). Industrial trials were run in the Italian steel plant, Riva Acciaio Sellero. The finish rolling temperature was chosen as low as possible, 950-920°C, and the first part of the subsequent cooling was delayed by placing an insulating blanket after the last rolling stand, in order to promote strain-induced nucleation of VN precipitates and provide time for them to grow to into effective ferrite nucleants. The experimental materials were EAF steels and based on the standard grade Fe430 with 0.16%C, 0.75%Mn and 0.20%Si with additions of 0.11%V and a somewhat raised N-content of 0.013%. In one steel 0.01% Ti was also added. In this way the ferrite grain size was decreased from 15µm to 10µm and the yield strength was raised by about 130MPa as a result of both grain refinement and precipitation strengthening. The impact toughness was good down to -20°C.

While the higher levels of carbon in long products as compared to plate and strip steels are beneficial for their strength, there is an accompanying loss of toughness, both in the base steel and in HAZ regions after welding. Figure 7.13 shows a comparison of results for steels having typical carbon contents for plates and long products respectively. It can be seen that at the same strength level, the impact transition temperature is nearly 70 degrees higher for the long

product steels having higher carbon contents. This must be principally due to the higher content of pearlite which is well known to have a deleterious influence on the toughness.

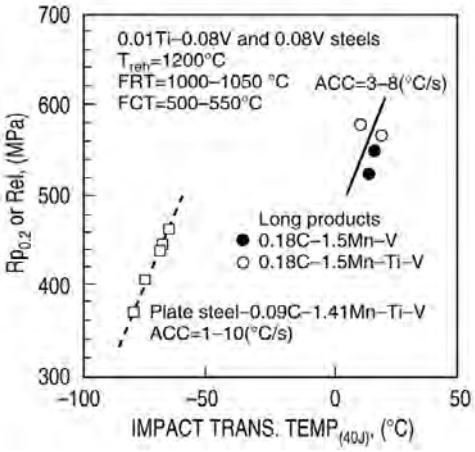

Fig. 7.13 Effect of carbon content in Ti-V- and V- microalloyed steels on the strength and toughness of specimens processed in similar manners (7.17).

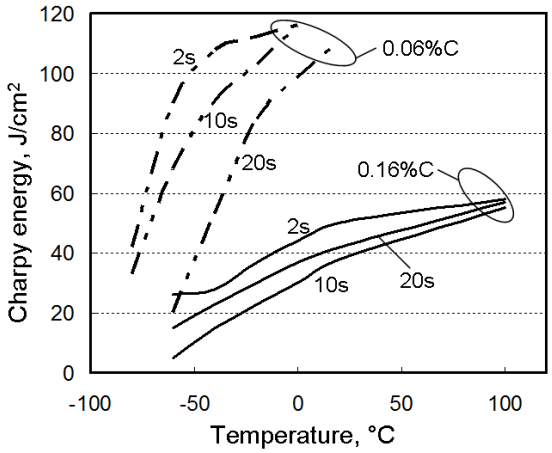

Fig. 7.14 Charpy energies for simulated HAZ structures in steel plate (0.06%C) and section (0.16%C) for different cooling times $\Delta t_{8/5}$ equal to 2, 10 and 20s (7.18).

A similar trend is also evident in the case of toughness in high temperature heat affect zone structures resulting from welding (7.18). Figure 7.14 compares results for plate having 0.06%C, 0.9%Mn, 0.078%V and 0.014%N with a section steel containing 0.016%C, 1.1%Mn, 0.055%V and 0.010%N. The 0.16%C section steel shows considerably higher 40J impact transition temperatures for all three welding conditions than the 0.06%C plate steel and furthermore, the upper shelf energy is substantially reduced. It is to be noted, though, that the slower rise in impact toughness with temperature with the high C-content, Fig. 7.14, affects the difference between the impact transition temperatures of the steels with the two C-levels in Fig. 7.13 considerably, depending upon which Charpy energy is chosen for the comparison. The results of Fig. 7.14 indicate that the curve of the 0.18%C steel would approach the 0.09%C steel, Fig. 7.13, with up to about 50°C if a Charpy energy of 20J (a level often considered sufficient, cf. above) had been chosen.

7.4 Seamless pipe

The manufacture of carbon steel seamless pipe or tube consists of three principal stages: (i) piercing at ~1230°C followed by hot rolling down to 1100-1020°C, (ii) transfer to furnace for intermediate reheating, and (iii) sizing in a stretch-reduction-diameter process at 930-830°C. This processing cycle is able to provide material with adequate strength properties but cannot always guarantee good transversal toughness at low temperatures. This problem is directly related to the coarse austenite grain structures formed at the high temperature necessary during piercing and hot rolling. The resulting coarse ferritic microstructure as well as occurrence of coarse bainite may in turn give inadequate toughness. To remedy this problem it has become normal practice in such cases to introduce an in-line normalising process at the intermediate stage, to produce a refined microstructure and improved toughness.

Vanadium microalloying has been applied in steels for seamless tube, primarily to enhance their strength by V(C,N) precipitation (7.19, 7.20). However, during the last decade the possibility of refining the ferritic microstructure by nucleation of ferrite on VN particles in the

austenite has attracted considerable interest, see Section 3.4. The effect of N-content on the ferrite-pearlite microstructure and the mechanical properties was studied in 0.30%C, 1.5%Mn, 0.10%V steels subjected to laboratory simulation of the seamless tube process, including in-line normalising (7.19). Provided the intermediate cooling temperature, stage (ii) above, was sufficiently low to ensure complete transformation, it was found that on increasing the N-content from 0.005% to 0.021% the ferrite grain refinement was effective enough to raise both yield stress and impact toughness significantly, Fig. 7.15. An optimum N-content appears to be about 0.015%. The main conclusion of this work is that a dense population of ferrite grains is formed as a result of their nucleation on V(C,N) particles in austenite which have formed during the intermediate cooling-reheating cycle.

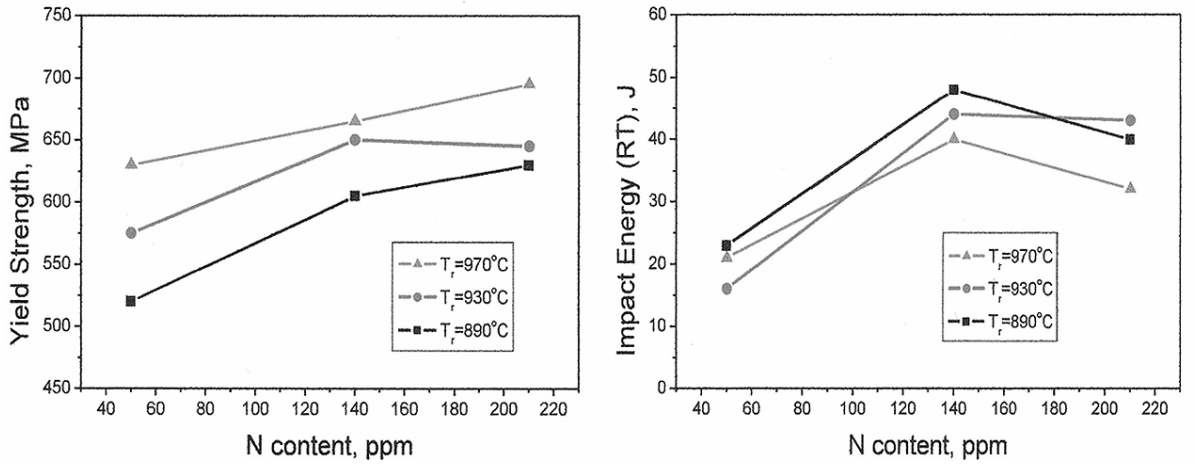

Fig. 7.15 Yield strength and impact energy of 0.20%C-1.5%Mn-0.10%V steel with varying contents of N subjected to simulated seamless tube processing. T_r is the intermediate reheating temperature (7.19).

However, in-line normalising has its drawbacks. Firstly it reduces the productivity. Secondly, if the austenite is not completely transformed during normalising, high carbon islands may form and deteriorate the final microstructure. To overcome these difficulties an alternative approach to ferrite grain refinement through intra-granular formation on V(C,N) precipitates has been proposed and investigated (3.39). This route is based on eliminating the deep cooling/ reheating cycle in the in-line normalising and instead utilising the transfer/heating time between hot rolling and sizing for precipitation of V(C,N) in austenite to act as nucleants for ferrite in the subsequent cooling. The transfer time depends quite strongly on the final tube size and can typically vary from about 80seconds up to 13minutes. It is known that precursors of fine TiN formed already during continuous casting of the steel can stimulate V(C,N) to form at higher temperatures with shorter times by co-precipitation on the TiN particles, cf. section 3.4. This concept was tried with the aim of enhancing intra-granular ferrite nucleation during processing with short transfer times and/or sizing at higher temperatures (3.39).

The process described is schematically demonstrated in a temperature-time diagram, Fig. 7.16. The ferrite grain refinements achieved are collected and displayed in Fig. 7.17. As can be seen, intra-granular nucleation provided an additional refinement about 2.5 times larger than that from austenite grain boundaries in plain C-Mn steels. The formation of active V(C,N) particles in austenite for subsequent ferrite nucleation will critically depend on the temperature-time profile between hot rolling and sizing, and in particular the sizing temperature. This is clearly seen in Fig. 7.17, showing the ferrite grain sizes for two V-N steels with 0.017 and 0.020%N and a V-Ti-N steel with 0.017%N and for various sizing temperatures. When the sizing is performed at high temperatures relative to the C-curve for

V(C,N) precipitation, Fig. 7.16, then V(C,N) precipitates are not able to fully develop in the centre of austenite grains in the two V-N steels, leading to a mixed microstructure with Widmannstätten ferrite and bainite. It is to be noted that merely a shallow cooling/reheating cycle down to 800°C renders all three steels insensitive to formation of these undesirable ferrite microstructures, Fig. 7.18. With Ti-microalloying, bainitic components in the microstructure can be completely prevented at all sizing temperatures.

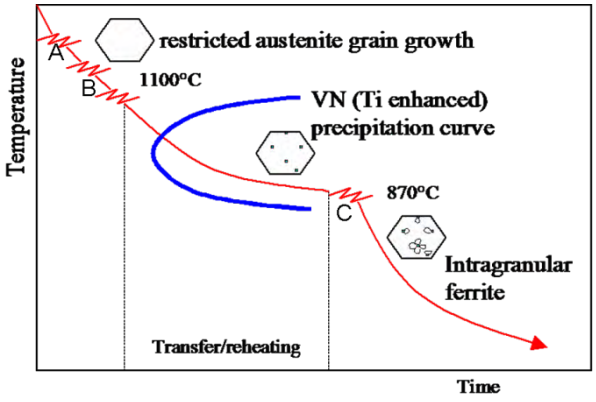

Fig. 7.16 Schematic temperature-time cycle for seamless tube processing, with the piercing (A), hot rolling(B) and sizing(C) steps inserted, together with the C-curve for Ti-enhanced V(C,N) precipitation(3.39).

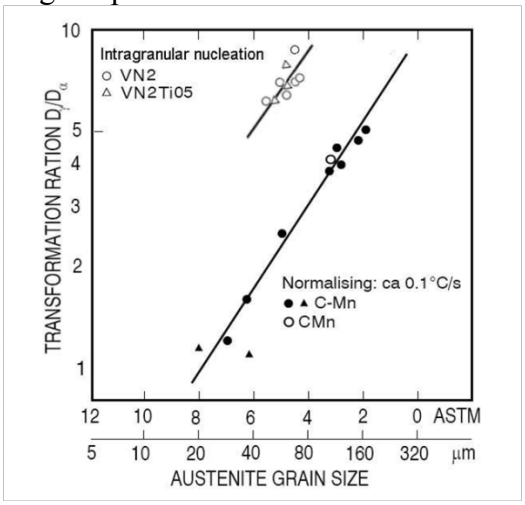

Fig. 7.17 The D_γ/D_α transformation ratio for intra-granular nucleation on VN (3.39)

The effect of transfer time is shown in Fig. 7.19 for the same three steels. For a long transfer time of 13minutes, full grain refinement was reached in all steels, whereas for the short times of 80 seconds, this was only achieved in the V-Ti steel. It can therefore be concluded that Ti is an indispensable addition to V-N steels for providing a robust microalloying that is insensitive to variations in transfer time and sizing temperature. In summary, it appears that the proposed concept for seamless tube processing for V-N and V-Ti-N microalloyed steels is able to eliminate in-line normalising while maintaining similar grain refinement as for normalising.

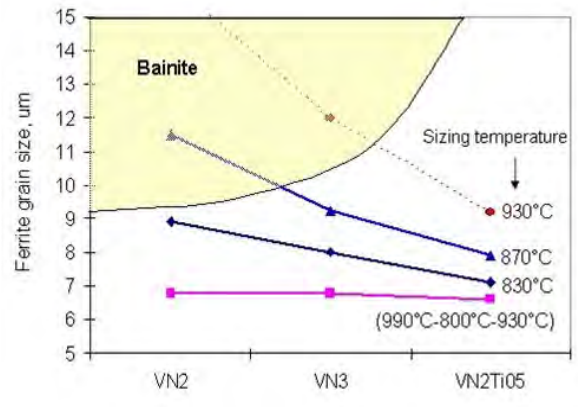

Fig. 7.18 The effect of sizing temperature on ferrite grain size for V-N and V-Ti-N steels (3.39).

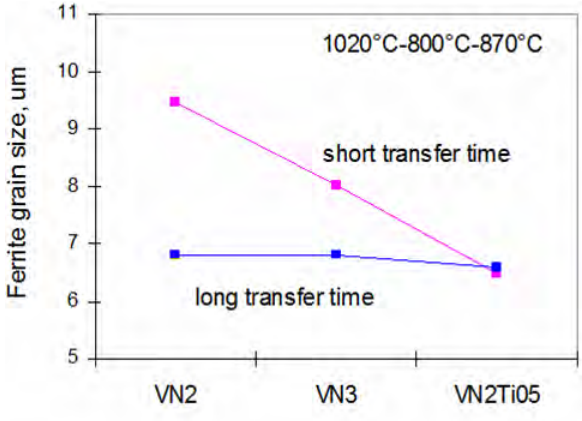

Fig. 7.19 Ferrite grain sizes for V-N steels with 0.017 and 0.20%N (VN2 and VN3 and a V-Ti-N steel processed with long and short transfer times (3.39).

7.5 Forgings

Traditionally high strength forgings are made of quenched and tempered (Q-T) steels alloyed to generate a martensitic microstructure for the full dimension of the part after quenching. These steels require several treatments after hot forging, viz. quenching, tempering, straightening and stress relieving. Moreover, the costs for the machining to the final shape and tolerance are particularly high for martensitic hardened steels.

The development of high strength ferrite-pearlite vanadium-microalloyed steels has aroused considerable interest for applications in forgings during recent decades. Strength properties equivalent to those of quenched and tempered steels can be reached directly after hot forging by adopting controlled air or forced air cooling (7.21-7.24). In this way one can escape the heat treatments and straightening operation of Q-T steels completely.

In forging, the reheating temperature, the forging temperature range and reductions are largely governed by the material flow necessary to reach the final shape of components, often having complex geometries. As a consequence there are fewer free processing variables for controlling microstructure and properties as compared to hot rolling. The V-microalloyed steels can, however, be processed by conventional forging practices with a minimum of process adjustments. The key process parameter is the cooling rate following the forging and in particular through the transformation range. A soaking temperature of 1150-1250°C is recommended to ensure full solution of all initial V(C,N) precipitates and realise the full strengthening potential of added V. The stacking/binning temperature after forging should be kept lower than about 600°C to ascertain complete transformation and precipitation strengthening.

Microalloying with vanadium is an efficient method for strengthening medium-carbon (0.30-0.50% C) ferrite-pearlite steels (7.21-7.23). From electron microscopy it has long been known that this occurs by fine nitrogen-rich vanadium-carbonitrides in the polygonal ferrite as well as in the ferrite-lamellae of pearlite. The precipitation in the polygonal ferrite occurs often as interphase precipitation. The temperature dependence of the solubility of V-carbonitrides makes dissolution possible at convenient temperatures and thereby gives potential for a considerable precipitation strengthening. Vanadium-microalloying is therefore commonly preferred to other microalloying additions in these types of steels. The effect of V- and N-additions for precipitation strengthening of these steels is clearly demonstrated in Fig. 7.20 (7.21)**.** These data have been normalized to 0.3%Si, 80% pearlite and 20mm section size. All steels contained 0.7%Mn and were austenitised at 1200-1250°C. According to these results, 5 parts per weight of N are equivalent to one part of V. Enhanced cooling is an efficient method to increase precipitation strengthening. Raising the cooling rate from 1°C/s to 4° C/s increases the tensile strength of a 0.4C, 1.2Mn, 0.10V steel by 120 MPa (7.21, 7.22).

The fatigue resistance of V-microalloyed steels has been studied quite extensively and has recently been summarised in a review by Li and Milbourn (7.24). Comparative fatigue tests on both smooth and notched specimens and on actual automotive components have shown that the fatigue strength of the V-microalloyed steels are comparable to and sometimes even higher than that of QT steels of the same hardness. An example from these investigations is shown in Fig. 7.21.

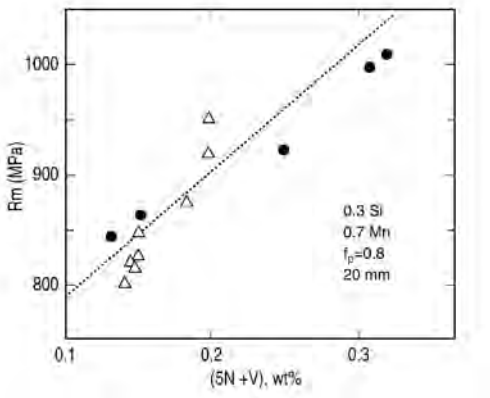

Fig. 7.20 Effect of precipitation strengthening by V and N on tensile strength. (7.21).

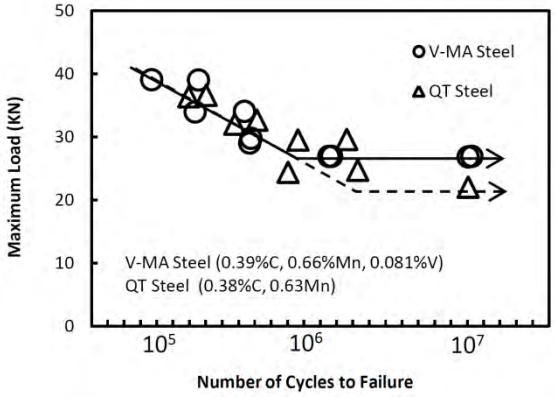

Fig.7.21 Fatigue strength of connecting rods for a V-microalloyed steel and a Q-T steel (7.24)

Machining often represents the largest cost component for a forged part. The vanadium microalloyed steels offer here a clear competitive advantage since it is well recognised that their machinability (based on tool life, cutting force and surface/integrity quality) is superior when compared to that of QT steels of the same hardness (7.24). Figure 7.22 shows a comparison of the machinability, expressed as tool life, between a V-microalloyed steel, (30MNV56), and two QT steels, AISI1045 and 5140, as functions of cutting speed and feeding rate. The two QT steels have nearly the same machinability but, as can be seen, the vanadium steel is clearly better than the QT steels in all cases.

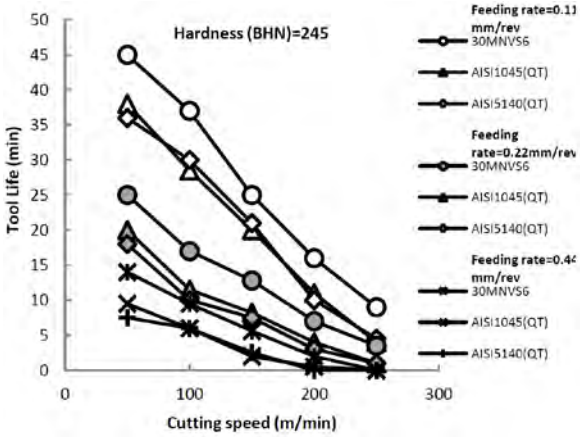

Fig. 7.22 Tool life for different cutting speeds and feed rates for a V-microalloyed steel and two Q-T steels(7.24).

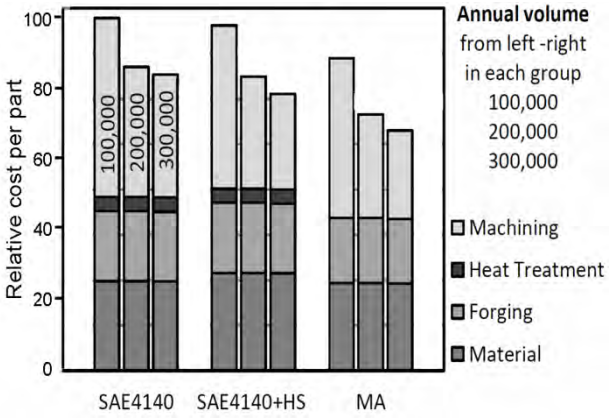

Fig 7.23 Relative costs for six cylinder crankshafts made of a V-microalloyed steel (MA) and two Q-T steels (one with high sulphur, HS) (7.26).

Although other properties are equivalent to or better than those of Q-T steels, the toughness of the microalloyed ferrite-pearlite steels is clearly inferior. Still the toughness is adequate for many advanced applications that are not subjected to severe impact loading. Such examples are automotive parts subjected to cyclic loading, such as connecting rods and crankshafts. However, to expand the use of these steels improvement of their toughness may be vital. By microalloying with Ti or alternatively raising the Al-content somewhat above normal levels and with close control of N it is possible to reduce the austenite grain size to below 50μm after reheating. This refines the final ferrite-pearlite microstructure and thereby increases toughness. By combining this approach with a reduction in the C-content and an increase in

the Mn-content to dilute the pearlite with respect to cementite, it has been possible to double the Charpy impact toughness of the standard V-microalloyed steel while maintaining the strength level (7.21, 7.22). Improving the toughness through grain refinement by promoting ferrite nucleation on N-rich V(C,N) co-precipitated on MnS inclusions has also been reported (7.25).

Vanadium-microalloyed forging steels have become increasingly popular in automotive applications, such as crankshafts, connecting rods, steering knuckles, axle beams and tension rods. Compared to traditional Q-T steels, the use of V-microalloyed forgings results in significant cost savings by elimination of a number of processing steps as well as through improved machinability and increased productivity. Figure 7.23 shows the cost of a six cylinder crankshaft, split into its costs for material, forging, heat treatment and machining, at three production levels for a V-forging steel, MA, and two QT steels, SAE4140 and SAE4140+HS(high sulphur) (7.26). The dominant role of machining cost is evident. Noteworthy in this context is that the machining cost for the V-forging steel is about 28% lower than the SAE4140 grade and 8% lower than the SAE4140 +HS.

By alloying with Mn, Cr and Mo, bainitic microstructures can be formed in air cooled forgings. Vanadium microalloying should be an efficient means of retaining the strength of the virgin bainite and also adding further strength by precipitation strengthening. This concept has found some applications, such as crank shafts and diesel injection components (7.24). However, several problems have been addressed to these types of steels. One is that they commonly contain considerable amounts of retained austenite, resulting in a low yield stress and probably poor fatigue resistance (7.27). Although this type of steels could be an area for new future applications of V-microalloying, it appears that this will require a good deal of further development work. Also, in view of the extensive alloying required to produce bainite in rather thick forgings during air cooling, it needs to be proven whether this route is, economically and property-wise, a better choice than that of traditional Q-T steels.

7.6 Summary of chapter

- Recrystallisation controlled rolling (RCR) followed by accelerated cooling (ACC) lends itself well to plate, long products as well as strip production of V-(Nb)-Ti microalloyed steels.
- All products discussed here benefit from N-microalloying together with vanadium. Grain refinement during the austenite to ferrite transformation is improved and strength is further raised by denser precipitation of V(C,N) particles. The ferrite grain refinement means that toughness is little impaired, or not at all, by the increase in strength due to precipitation.
- Strip rolling provides an ideal situation for V-N-microalloying since rapid cooling in the transformation range is combined with near-isothermal conditions in the coil for precipitation of V(C,N). Optimal coiling temperatures lie in the range 550-600ºC.
- High strength bainitic strip steel has recently been developed using V-microalloying. In this case, V acts to inhibit recovery of the dislocation structures and the associated loss of strength after coiling This also leads to the practical benefit that the mechanical properties become rather insensitive to the actual coiling temperature which is not easy to control below ~500ºC under steelworks conditions.
- Long products such as rebars and sections are well suited for V-N-microalloying. These necessitate higher rolling temperatures where RCR conditions favour structure refinement.

Furthermore, the higher C-contents as compared to plate and strip steels enhance the precipitation hardening potential of the V(C,N) particles.

- Seamless pipe production also demands hot deformation at relatively high temperatures in the austenite range. By application of Ti-microalloying it is possible to provide TiN particles that act as pre-cursors for VN precipitation and which subsequently act as nucleants for ferrite formation on cooling. Toughness is then improved by the grain refinement and by avoidance of harder phases such as bainite. Processing time can also be reduced without impairing the mechanical properties of the pipes.
- For many forgings, V-N-microalloying makes a competitive alternative to quench and tempering (QT). Strength and fatigue behaviour are equal or better although with some sacrifice in toughness. Furthermore, the better machinability of microalloyed steel in combination with its more direct process route means that these forgings are more economical to manufacture than corresponding QT products.

8. WELDABILITY

In recent decades, the need for structural steels having satisfactory low-temperature heat affected zone (HAZ) toughness has resulted in a general reduction in the carbon, sulphur and nitrogen contents (below 40 ppm N), often together with micro-additions of Ti and/or Ca. However, such low nitrogen contents are costly and also troublesome to achieve in practice, and are not conducive to strength in steels microalloyed with vanadium. Many features of various microalloyed steels have been studied at the Swerea KIMAB (previously the Swedish Institute for Metals Research) and particular attention has been paid to the important role of the microalloying elements V, Ti, Nb as well as N in the HSLA steels and their effects on properties of weldments (8.1-8.6). Mechanical behaviour and, in particular, toughness of heat affected zones (HAZs) is dominated by steel composition. The influence of prior processing which is vital to the properties of the base material is largely eliminated in the HAZ due to grain growth and particle dissolution at these high temperatures.

Three main problem areas can be identified when considering the toughness and fracture of HAZ structures and these have been reviewed for V-microalloyed structural steels by Hart (8.7). They are (i) the existence of hard zones with the associated risk of hydrogen cracking, (ii) the toughness of coarse grained heat affected zones (CG HAZ) close to the fusion line, especially in the case of single pass welds and (iii) toughness of these CG HAZ when they have been exposed to reheating into the inter-critical temperature range (IC CG HAZ) in successive welding passes.

8.1 HAZ hardenability and hydrogen cracking

Rapid cooling of regions adjacent to welds generally leads to local increase in hardness with the possible existence of martensite. Such hard zones in conjunction with tensile stresses and dissolved hydrogen can lead to the risk of delayed fracture and even spontaneous fracture. To avoid this, it is common practice to specify a maximum hardness that must not be exceeded in the HAZ. Pre-heating or post-heating of the welds helps here by reducing the cooling rate and so forming softer transformation products. The carbon content of the steel is especially important since higher carbon levels both increase hardenability and, in particular, raise the hardness of the martensite. However, steels also have varying hardenability depending on their alloy composition and it is normal practice to define a carbon equivalent (CE) that takes these into account when assessing the risk for forming brittle zones. Two of the several equations that have been deduced from multiple regression analyses are the following:

$$CE = C + Mn/6 + (Cr+Mo+V)/5 + (Ni+Cu)/15$$

and

$$CET = C + (Mn+Mo)/10 + (Cr+Cu)/20 + Ni/40$$

The possible role of vanadium is not entirely clear; it is not included in the CET formula and in some other work has even been found to have a negative coefficient in the carbon equivalent (8.7). Even on the basis of the CE formula, the influence of V is marginal. Microalloyed steels very seldom have levels of V that exceed 0.1% which would equate to an increase in the carbon content of only 0.02%C so this should not represent any practical problem. The reason for the inconsistency in the analyses of carbon equivalent can probably be ascribed to the roles of V, Ti and N that were discussed in Section 3. In solid solution in austenite, vanadium at these levels has a finite, although modest, effect of raising the hardenability. However, the presence of V(C,N) particles with precursors of TiN enhances the

formation of both polygonal and acicular ferrite phases, giving an opposing and often stronger effect of reducing the hardness. Thus it is likely that the disparate observations may be due to relatively minor changes in steel chemistry with respect principally to Ti and N.

8.2 Structures and properties of coarse grained heat affected zone (CG HAZ)

Nitrogen levels in plain C-Mn steels show a strong correlation with the CG HAZ toughness where higher N-levels are clearly deleterious, showing a marked increase in the Charpy impact transition temperatures (8.8) which is reflected in maximum permitted contents in various steel specifications (e.g. 8.9). This has frequently been attributed to the presence of 'free nitrogen' although there appears to be no good explanation for this phenomenon. Nevertheless the presence of nitride-forming alloy elements Al, Ti, Nb and V can mitigate considerably the negative effect of N and this has been accepted by steel specifications which permit considerable relaxation of the limit for N in the presence of these alloy elements. This is especially significant in the case of vanadium since nitrogen is an essential addition for optimising strength in V-microalloyed steels.

An early classic work by Hannerz et al. (8.10) reported the Charpy impact transition temperatures (ITT) for simulated CG HAZs for steels with ranges of V and N contents as well as different cooling rates defined as $\Delta t_{8/5}$, the period of time between 800ºC and 500ºC, which is where the phase transformation takes place on cooling. These results are shown in Fig. 8.1. In this investigation it could be seen that small additions of V, up to ~0.1%, have no deleterious effect on the toughness of single pass HAZ structures. Indeed, there is a small lowering of the impact transition temperature initially. Higher V-contents than are normal in HSLA steels do raise the ITT dangerously especially with long cooling times that are associated with very high heat-input welding. Not readily apparent in Fig. 8.1 is the situation for slow cooling in combination with higher N-contents in typical HAZ steels where the V-content is less than 0.1%. In these circumstances there is a risk for loss of toughness which will be discussed below.

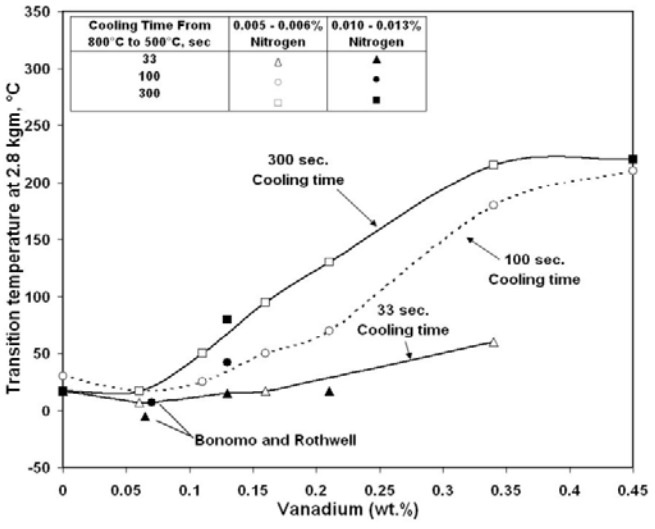

Fig. 8.1 Impact transition temperatures in simulated CG HAZs for steels having a wide range of V- and N-contents and with different cooling times $\Delta t_{8/5}$ to represent welds with different heat in-puts, (8.10).

The properties of CG HAZ structures can be related to two things which may be also inter-related. The first is the size of the austenite grains which generally is reflected in the coarseness of the resulting microstructure after cooling and the possible existence of hard phases. Large austenite grains are always detrimental to HAZ toughness. Steel composition and, to some extent, the prior processing conditions play a role here, as discussed in Sections

3.1 and 3.2. The second condition is the nature of the principal phases that form by transformation on cooling. These may consist of polygonal ferrite of various average grain sizes, bainite, acicular ferrite, pearlite or martensite. The prior austenite grain size is important here but so are other factors that impact upon the nucleation of ferrite as described in Section 3.4. The results of grain coarsening studies (8.1, 8.2) for various microalloyed steels are shown in Fig. 8.2 as the average austenite grain size after welding simulation at varying heating rates.

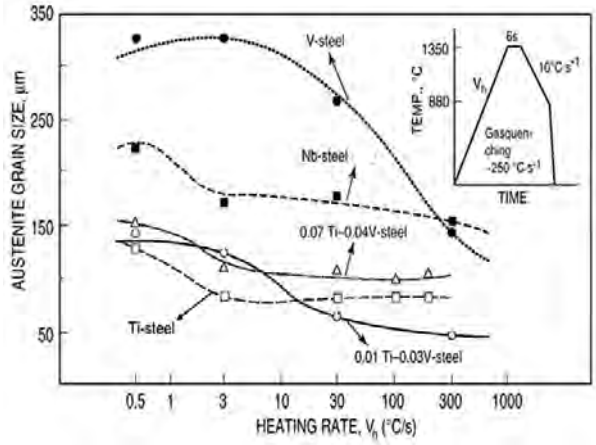

Fig. 8.2 Austenite grain size vs. heating rate for various HSLA-steels subjected to weld simulation (8.1).

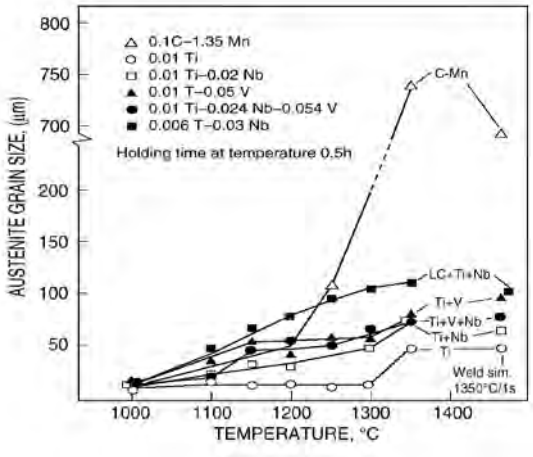

Fig. 8.3 Effect of peak temperature and steel chemistry on the austenite grain size for long and short holding times (8.2).

All steel compositions show a tendency for the austenite grain size to increase as the heating rate decreases. To some extent this is due to the longer periods of time spent at very high temperature but it is primarily a result of the rate of phase transformation to austenite on heating as discussed in Section 3.2. Large differences between the different micro-alloyed steels are apparent in Fig. 8.2. This reflects the effectiveness of the different remaining precipitate dispersions at high temperatures to impede austenite grain growth. The V-steel shows the largest austenite grain sizes for most conditions, although smaller than plain C-Mn steel (not shown). Grain coarsening is less in the case of the Nb-steel for which the carbonitrides are more stable but the most extreme case is the Ti steel where the grain size remains below 100µm for all but the very slowest heating rate since the particles of TiN are virtually insoluble in austenite. The advantage of introducing a small content of Ti in V-microalloyed steel to refine the austenite grain structure is seen very clearly here. As little as 0.01%Ti produces a dramatic effect. However, contents of Ti larger than about 0.02% give inferior behaviour due to coarser TiN particles. The higher Ti content decreases the TiN solubility and hence raises the primary precipitation of TiN during casting and results in coarser TiN precipitates.

The tendency for austenite grain growth at different temperatures demonstrating the effect of different microalloying elements is shown in Fig. 8.3 (8.2). These apply to different heating times where the condition most relevant to welding is shown on the extreme right hand side. It is seen there that the average austenite grain sizes of the Ti-bearing steels are ~6-15 times smaller than that of C-Mn steel after 30 minutes holding at 1350°C and at least 3 smaller in weld simulation. It can also be seen that the Ti-microalloyed steel has excellent resistance to grain growth for temperatures up to 1300°C. In the presence of V and/or Nb the grain coarsening resistance of the Ti-steel deteriorates somewhat but these are still far superior to the plain C-Mn steel.

The results of grain coarsening studies (8.3, 8.4) for commercial 0.01Ti-0.08V plates with low (0.003 % N) and high (0.013 % N) nitrogen contents show that extensive grain growth occurs just above 1250°C in the low N steel whereas the high nitrogen steel preserves its fine grained structure up to 1350°C. The combination of a small Ti addition together with a higher N-level can therefore make a useful contribution to the toughness in the HAZ adjacent to the fusion line.

8.3 Effect of nitrogen and welding parameters on HAZ toughness of V-steels

Experience over many years has shown that the microstructures and toughness of HAZs in V-microalloyed steels vary in a rather complex manner depending on the welding conditions and the steel chemistry, especially with regard to its N-content (8.1 – 8.6). Commercial 0.01Ti-0.08V-N steel plates 25mm thick with high (0.013% N) and low (0.003% N) nitrogen contents and processed by different routes (RCR, RCR+ACC and CR) have been investigated and compared in some detail. These were subjected to temperature cycles simulating the heat affected-zones during high, medium and low heat-input welding in order to investigate the influence of plate production processing route, nitrogen content and heat input on HAZ toughness and microstructure (8.3, 8.4). In addition, full scale welding trials were carried out on the same plates.

The Charpy impact toughness of these 0.01Ti-0.08V-N steels after thermal HAZ simulations are shown in Fig. 8.4(a), while the results of full-scale welding trials are shown in Fig. 8.4(b) for comparison. As seen here, there is virtually no effect of the previous TMCP parameters on the toughness of the coarse grained HAZ after welding. For the lower N-steel, the influence of cooling time, $\Delta t_{8/5}$, on toughness is rather little; the transition temperature rise by some 10ºC in the simulations with increasing cooling time. A similar but somewhat larger change is seen in the real welds as a function of heat input. The higher nitrogen steel is significantly different in that the impact transition temperature depends strongly on cooling time or heat input.

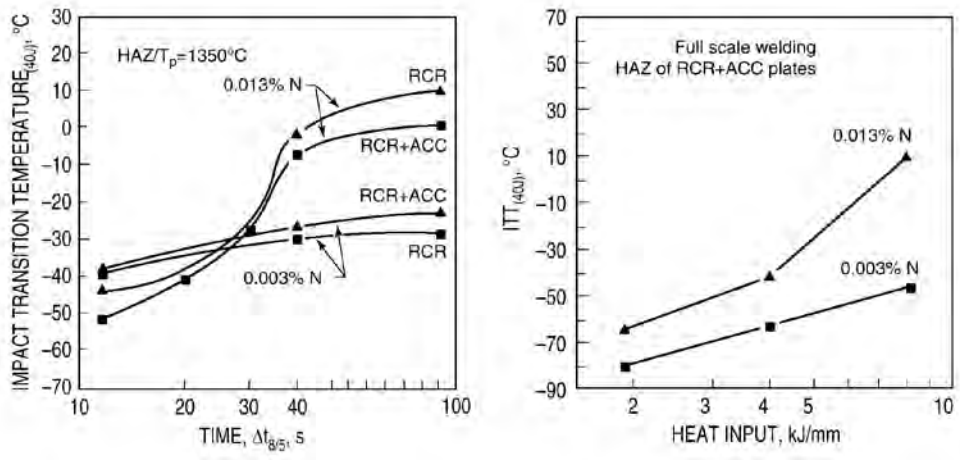

a) b)

Fig. 8.4 Charpy impact transition temperatures at 40J of: (a) simulated HAZs and (b) HAZ after full scale welding of low (0.003N) and high (0.013N) nitrogen 25mm plates with different heat inputs (8.3, 8.4).

As seen in Fig. 8.4, the toughness of the HAZ in V-N-microalloyed steels, as measured by their impact transition temperatures, improves with increasing cooling rates for $\Delta t_{8/5}$ times down to 12 seconds. There is presently interest in even faster cooling rates associated with

low energy processes such as laser (-hybrid), electron beam and pulsed arc welding processes. Further measurements (8.6) have been made on 5mm steel strip from CSP production having the composition 0.06%C, 0.9%Mn, 0.08%V and 0.014%N (not Ti-alloyed in this case). Weld simulations were carried out using a peak temperature of 1350ºC and with cooling times from 40s down to only 2s. Impact transition temperatures were determined as shown in Fig. 8.5. Since these were made on sub-size Charpy specimens the results are not strictly comparable with the previous ones but the trends should be reliable. In fact, the trend towards higher toughness with increasing cooling rate continues even to the fastest cooling condition.

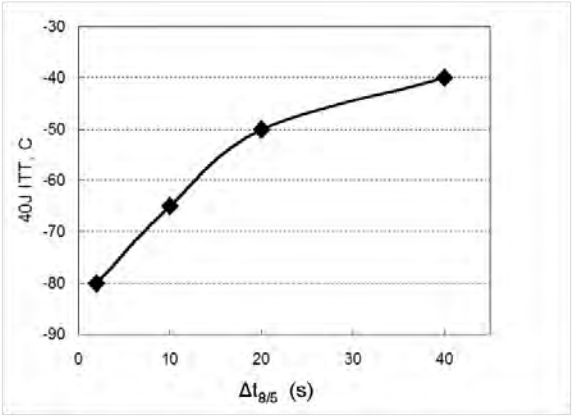

Fig.8.5 Variation of CG HAZ impact transition temperature for 0.08%V, 0.014%N steel after weld simulation with different cooling rates (8.6).

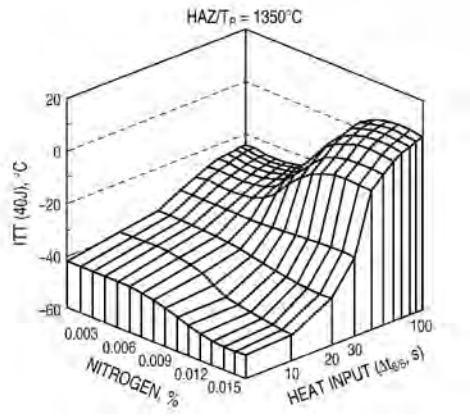

Fig. 8.6 Effect of heat input and nitrogen content on the HAZ impact transition temperature of RCR+ACC, 0.01 Ti-0.08 V plates (8.4).

The combined effect of heat input and N-content for V-Ti-N steels is summarised in Fig. 8.6. These results do not allow us to directly associate the low toughness after high energy welding with "free" nitrogen as has sometimes been suggested. On the contrary, the higher N steel (0.013 %N) exhibits the highest HAZ-toughness for the cooling time of <10s (low heat input). For this heat input (cooling condition $\Delta t_{8/5} \leq 30$s) one does not expect precipitation of VN in austenite during cooling to the transformation temperature and the amount of "free" nitrogen in ferrite should be higher than in the slower cooled specimens. With increasing cooling time, precipitation of V(C,N) should be more abundant reducing the amount of nitrogen in solid solution. However, it was these specimens which exhibited low toughness. Mitchell et al. (8.11) also drew the conclusion that free nitrogen was not principally responsible for variation in toughness of CG HAZ in their microalloyed steels. In Charpy tests, they found similar relationships to those above, where higher heat input raised the impact transition temperature for both V- and V-Nb-steels. However, an opposite trend was found in the case of CTOD tests where somewhat better toughness was associated with higher heat inputs.

Quite low impact toughness in the HAZ of 0.08%V, 0.05%Nb, 0.01%Ti steel was reported by Mitchell (8.11). This low toughness (40J at –5ºC) is probably not due to free nitrogen because the nitrogen level had almost the stoichiometric ratio to Ti, and should therefore have been entirely combined as TiN. However, some improvement in HAZ toughness (40J at -25°C for synthetic HAZ at $\Delta t_{8/5}$=50secs) was obtained by addition of 0.25%Mo to the V-Nb-Ti steel.

8.4 Toughness-microstructure relationships in the CG HAZ

Concerning the results in Figs. 8.4 - 8.6, the drastic changes in 40J ITT with varying of heat input /cooling time, it can be concluded that the notch toughness properties of coarse grained HAZ of the 0.01Ti-0.08V-N steels should be explained on the basis of their microstructures. Representative optical micrographs of the simulated HAZ microstructures are presented in Fig.8.7. The low nitrogen steel contains acicular phases at all cooling rates, although these become slightly coarser as the cooling time increases. A similar appearance is seen in the high nitrogen steel under fast cooling conditions. However, as $\Delta t_{8/5}$ increases, more and more, grain boundary ferrite becomes increasingly apparent. This coarse grained boundary ferrite in the HAZ is considered to make the most significant contribution to the overall low notch toughness properties. The grains are large, up to 100μm, and secondary cleavage cracks have been seen running through these grains, approximately along the prior austenite grain boundaries (8.3)

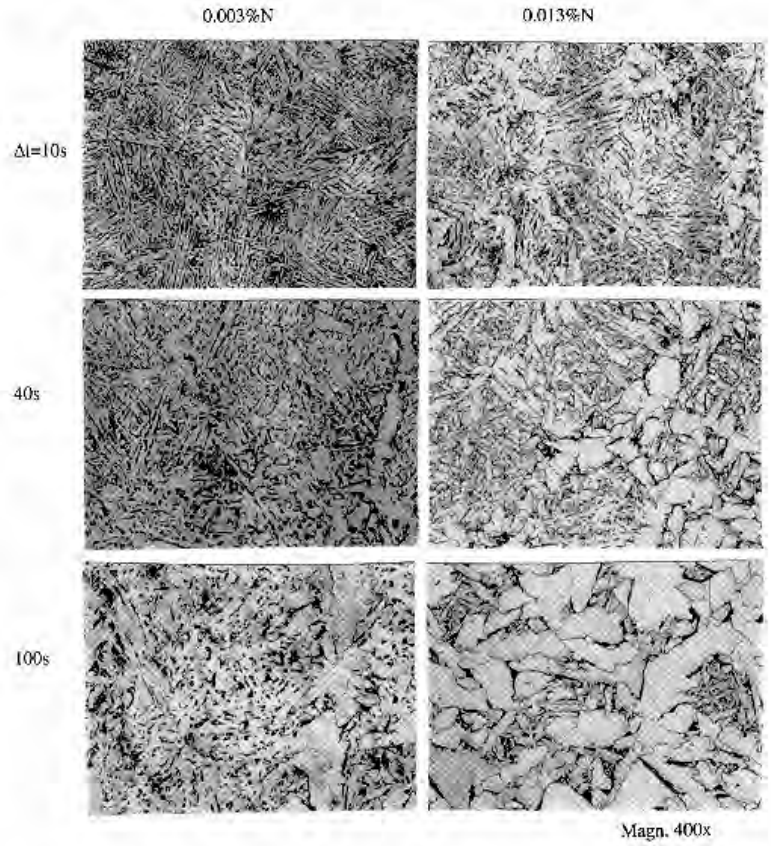

Fig. 8.7 Microstructure of HAZ of the Ti-V-N steels with low-0.003% and high-0.013% N contents after simulation at 1350°C and cooling with $\Delta t_{8/5}$=10s (a), 40s (b) and 100s (c) (8.4).

Quantitative analysis of these different structures has been carried out with the results shown in Fig. 8.8. These are presented with a terminology that has been used for weld microstructures but is not entirely satisfactory:

PG(G)	polygonal ferrite formed along prior austenite grain boundaries
PF(I)	polygonal ferrite formed inside prior austenite grains
P	pearlite
M	martensite
FS	fine ferrite with second phases

In particular, the description FS can embrace both upper bainite (in relatively large packets nucleated at austenite grain boundaries) which has poor toughness properties and acicular ferrite which is intra-granularly nucleated (as fine interspersed laths) and has good fracture resistance. Nevertheless, it is interesting to note that the observed structures here conform very well to the CCT results of Caballero et.al presented in Fig. 3.18. The presence of higher nitrogen shifts the transformation of grain boundary ferrite to higher temperatures, cf. section 3.4 and Fig.3.18. This implies that the austenite grain boundaries will be covered by such ferrite even at the high cooling rates in Fig.8.8 and will therefore prevent bainite formation and instead promote acicular ferrite in the grain interior, cf. discussion in section 3.4. For low nitrogen contents no grain boundary ferrite forms at high cooling rates, Fig. 8.8, thus promoting bainite with an inferior toughness than acicular ferrite. The drawback of these effects of V-N on microstructure is that for slow cooling the high transformation temperature results in coarse grain boundary ferrite, up to 100μm, with low impact toughness, Fig. 8.6.

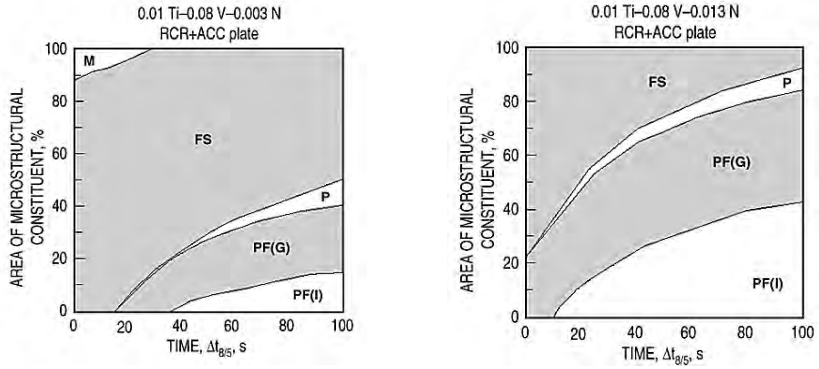

Fig. 8.8 Relation between volume fraction of microstructure constituents and heat input (cooling time $\Delta t_{8/5}$ from 1350°C) for Ti-V steel with low and high N-contents processed by RCR+AC (8.4) .

While the deterioration of CG HAZ toughness in V-N-microalloyed steels after high heat input welding can reasonably be ascribed to the occurrence of coarse grained polygonal ferrite, their excellent properties following rapid cooling are associated with intragranular nucleation of phases such as acicular ferrite. These must be related to the nature of the phase transformation from austenite to ferrite which is affected by the presence of V and N together in the steel. Such an effect is seen in dilatometer results where the transformation temperature is raised significantly in the presence of the higher nitrogen levels, Figs. 8.9 and 8.10.

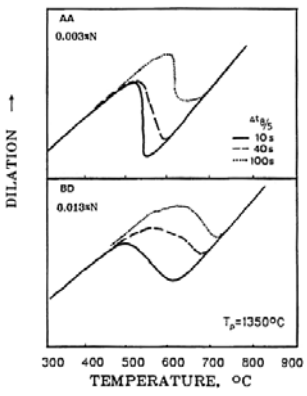

Fig. 8.9 Dilatation curves for cooling of V-microalloyed steels with low and high N-contents in weld simulation. (8.3)

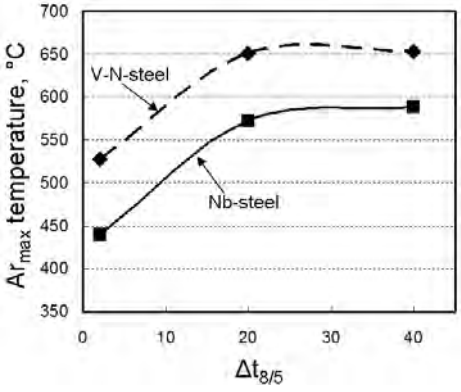

Fig. 8.10 Temperatures for the maximum rate of transformation after heating 2s at 1350°C and cooling at different rates for Nb- and V-N-microalloyed steels (8.6).

In Fig. 8.9 the two steels have 0.08%V with either 0.003%N or 0.013%N. Although nitrogen is an austenite stabilising element and so would be expected to lower the transformation temperature, the opposite effect is observed. Similarly, in Fig. 8.10, the Nb-microalloyed steel (D) having 0.07%C and 1.4%Mn, transforms at approximately 80 degrees lower temperature than the V-N-steel (A) with 0.06%C and 0.9%Mn. The difference in base composition cannot account for more than a 10 degree difference in theAe_3 temperature . Detailed examinations of the microstructures after fast cooling ($\Delta t_{8/5}$ of 2s) have been made using electron back-scattering diffraction (EBSD) which allows misorientations across lath and packet boundaries to be determined on a statistical basis (8.13). Selected results of these investigations are shown in Fig. 8.11.

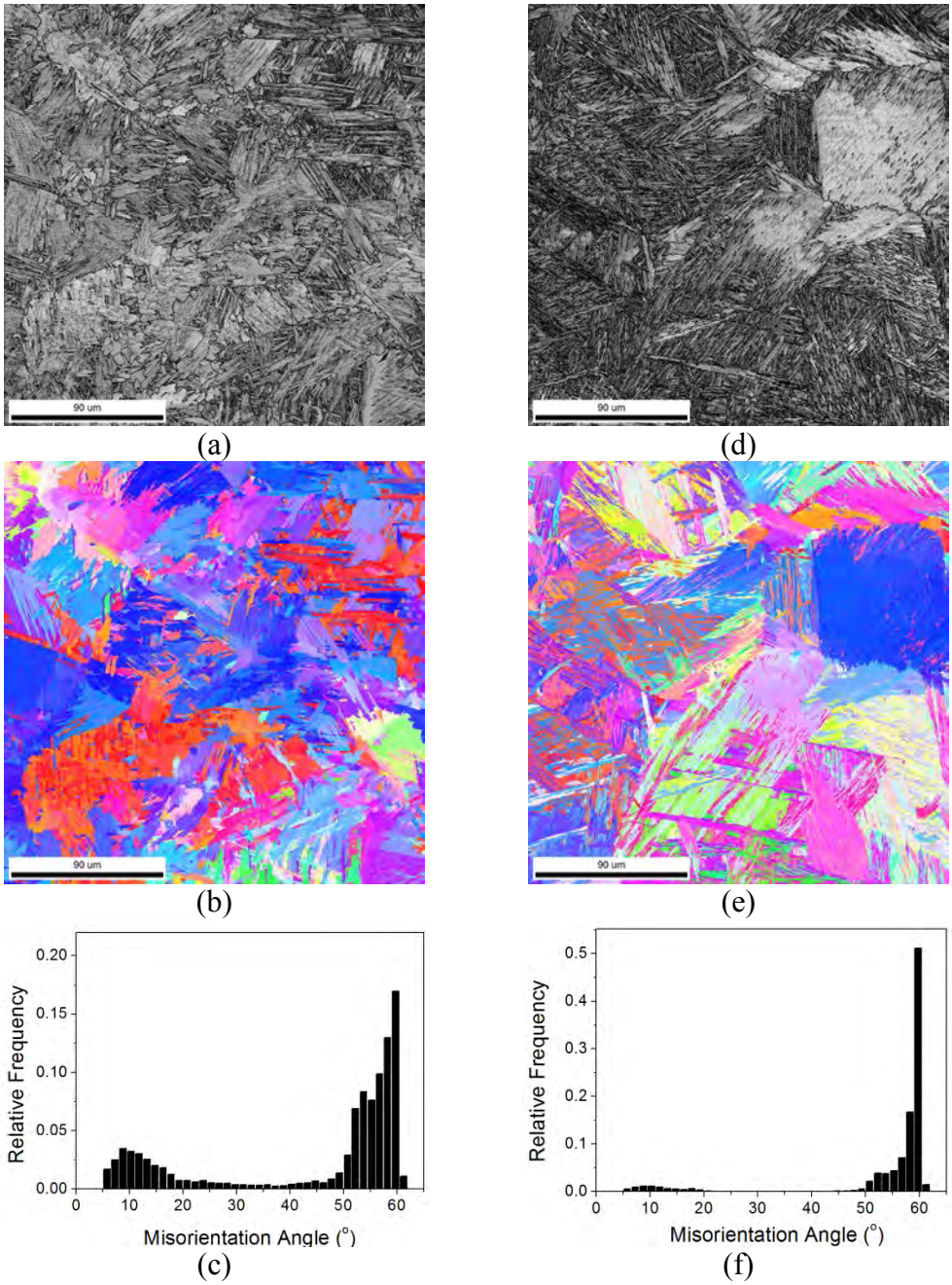

Fig. 8.11 Simulated HAZ structures for (a)–(c) V-N steel A and (d)–(f) Nb-steel D with cooling times $\Delta t_{8/5}$ of 2s. (a) & (d) band contrast images, (b) & (e) orientation (IPF) images, (c) & (f) boundary misorientation distributions (8.13)

In optical microscopy it is difficult to recognise differences between the acicular structures in steels A and D. However, the EBSD results show that the Nb-steel D has a very high frequency of lamellar twin-like boundaries with 60º misorientations whereas the V-N-steel A contains a wider spread of both low and high angle boundaries. Even at the fastest cooling rates, there is some formation of grain boundary ferrite in the V-N-steel, sufficient to prevent widespread formation of bainite, leading to mixtures of acicular ferrite and dispersed bainite. It is the distributions of boundary misorientations which define the effective grain sizes in these cases and are believed to account for the large differences in toughness (8.13). Although these microstructures do not appear precisely like the basket-weave pattern of classical acicular ferrite, they have similar grain boundary properties. These structures contribute to the FS phase recognised in optical microscopy and correlations can be found between the impact toughness and the volume fraction of FS as shown in Fig. 8.12. The Nb-steel with a fully bainitic structure under these cooling conditions has considerably inferior toughness with an ITT transition temperature of -20ºC as compared to -80ºC for the V-N-steel (8.6).

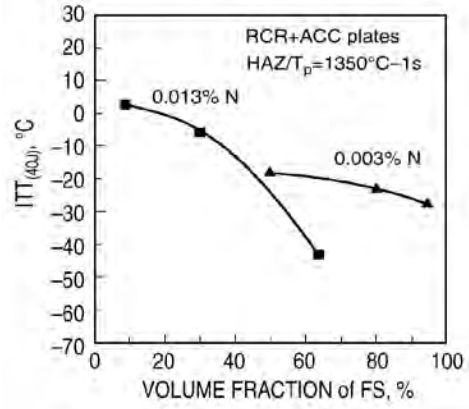

Fig. 8.12 Relationship between ITT_{40J} of HAZ and volume fraction of ferrite with second phase (FS).

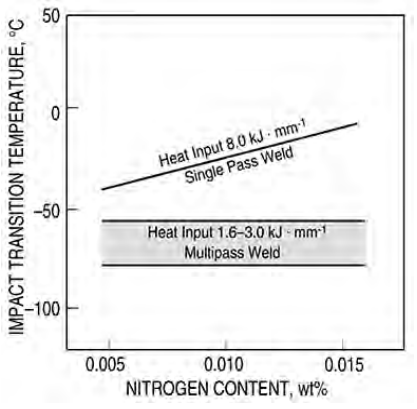

Fig. 8.13. Effect of N on toughness of heat affected zones of welded 0.1 % V steels (8.2).

In high heat input welding exceeding 10 kJ/mm, toughness becomes sometimes critical at the coarse grained HAZ due to formation of the upper bainite and associated martensite-austenite islands. The problem can be alleviated by deliberate addition of Ti (~0.015%) or various combinations of Ti, B, REM and Ca. Steels modified by these micro-additions show satisfactory HAZ toughness at -20^{o}C for the high input of 15 kJ/mm (8.3-8.9). As discussed previously, fine particles of TiN or other compounds restrict the austenite grain coarsening and act as nucleation sites of ferrite, which results in a decreased fraction of upper bainite. The results presented above show that proper microstructure, and therefore good toughness, could be obtained for high nitrogen steel by balancing heat input to provide a fine transformation product.

8.5 Influence of multi-run welding on HAZ toughness

According to Swedish standard welding practice 25mm plates are normally welded in two or more passes. Investigations (8.3, 8.4) of multi-pass welding of 0.01%Ti, 0.08%V-N plate steels shows a positive effect of the second pass, which allows good toughness even at high heat input. A marked improvement in HAZ toughness after the second pass was observed as compared to the single pass welding with high heat input, cooling time $\Delta t_{8/5}$ = 100s. The ITT_{40J} of 0.013N steel plate decreased by 50 degree to -48°C and for 0.003N steel plate

reached -60°C. The excellent notch toughness properties of the HAZ of high nitrogen plates subjected to thermal simulations of heat input with $\Delta t_{8/5}$<40s and particularly at $\Delta t_{8/5}$=10s can be attributed to the characteristics of the fine ferrite with second phase (FS) (see Fig. 8.12). Thus, the cooling time which gives 50% of fine FS-phase is sufficient to confer good impact notch toughness (see Fig. 8.6 and 8.8) and this seems to be independent of nitrogen as shown by the results in Fig. 8.13. Several investigations showed that V-microalloyed steels gave increased impact transition temperature (ITT) with increasing nitrogen content for high heat input, single pass welds, but rather constant ITT values for low and medium heat input using multi-run welding, as shown in Fig. 8.3 (8.3). During multi-run welding the VN, which is dissolved in the earlier passes, re-precipitates in the subsequent passes and these particles inhibit grain coarsening and allow transformation to fine grained ferrite which results in high toughness.

Mitchell et al. (8.11, 8.12) reported on improvement in the HAZ impact toughness in multi-pass welds with increasing V level up to 0.16%, although the CTOD transition temperature increased slightly at the same time. He also reported that higher heat input (>2kJ/mm) had a positive effect on the CTOD toughness and a slight negative effect on 40J ITT. It was suggested that the improvement in as welded toughness is connected with the formation of a favourable microstructure, intra-granular ferrite. This is in general agreement with our own observation, that the HAZ microstructure at high heat input is usually a mixed structure of fine ferrite with second phases (FS), grain boundary (PF(G)) and intragranular ferrite (PF(I)) (see Figs. 8.7 and 8.12). The poorer toughness of the high heat input HAZ in high N steel was considered to be caused by the presence of a significant volume fraction of coarse grain boundary ferrite in association with precipitation hardening by V(C,N) (8.4). Note also that hot rolling conditions do not affect HAZ structures or properties in these steels to any significant extent.

In multi-pass welding a further complication may arise. The preceding discussion has concerned re-heating the earlier HAZ to temperatures into the fully austenitic range. However, the temperature gradient associated with the later welding pass(es) usually ensures that part of the original CG HAZ becomes heated into the inter-critical (IC) temperature range where it transforms only partially to austenite. In this case the new austenite becomes very rich in carbon, leading to particles of retained austenite/martensite (MA-structure) after cooling. This ‘as-quenched’ high carbon martensite is very hard and brittle and acts as an initiator of fracture either by cracking or by de-cohesion along the boundaries with the softer ferrite matrix. The IC CG HAZ phenomenon can result in a narrow zone of minimum toughness existing a few millimetres from the fusion line. Li and co-workers (8.14-8.16) have examined this fracture behaviour and compared it in plain carbon and microalloyed steels in laboratory simulations of two-pass welding with successive peak temperatures of 1350ºC and 800ºC and with cooling times, $\Delta t_{8/5}$, of 24s in both cases.

The MA phase exists as blocky-like islands as well as elongated stringers, often in conjunction with carbide particles. Close to the fracture surface there are seen to be fractured stringers and de-bonding around larger blocks, indicating that these were probably the mechanisms that had led to the fracture. Charpy impact energy curves for four steels are shown in Fig. 8.14. The base steel composition had 0.09%C, 0.2%Si, 1.4%Mn and 0.005%N. The three microalloyed variants contained additions of 0.05%V, 0.1%V and 0.03%Nb respectively. The lower content of 0.05%V gave an improvement of the toughness as compared with the base C-Mn steel. Increasing vanadium to 0.1%V resulted in an increase in the impact transition temperatures which parallels the characteristics after single pass welding

in Fig. 8.1. The addition of 0.03%Nb also raised the transition temperature. Charpy transition temperatures as functions of the microalloy content are shown in Fig. 8.15 for simulated heat affected structures for both single pass (CG HAZ) and two-pass (IC CG HAZ) welds.

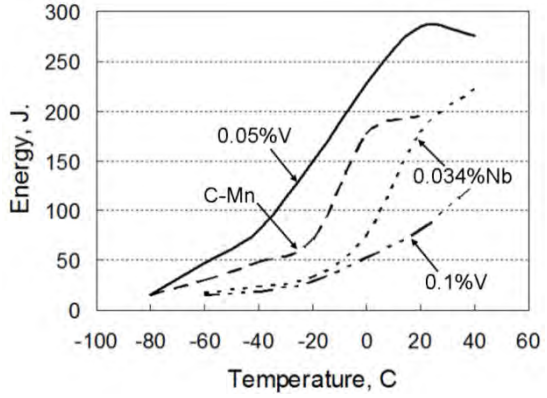

Fig. 8.14 Charpy test results for four steels in IC CG HAZ simulating the behaviour after 2-pass welding (8.16).

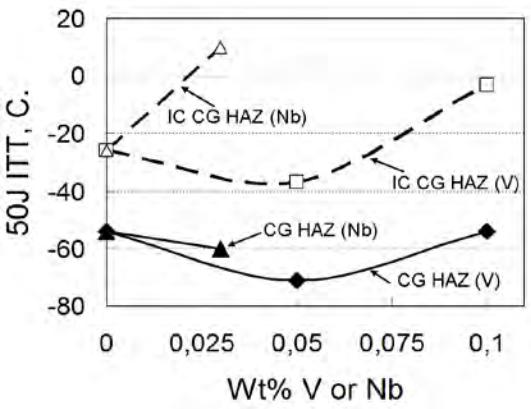

Fig. 8.15 Charpy impact transition temperatures for microalloyed steels after simulated single and 2-pass welding (8.15)

Figure 8.15 demonstrates the serious deterioration in toughness in the inter-critical zone that may take place after 2-pass welding in an example where the peak temperatures were 1350ºC and 800ºC respectively (8.15). The impact transition temperatures are raised by more than 40 degrees as compared to the single pass CG HAZ conditions. Small additions of V have a beneficial influence but this positive effect becomes negated at the higher level of 0.1%V. Similar behaviours to these were seen in the case of CTOD toughness measurements for the same V- and Nb-microalloyed steels (8.15).

8.6 Summary of chapter

- High nitrogen in V-microalloyed steel can be compatible with good weldability, as regards HAZ hardness and toughness, by careful selection of micro-additions and welding parameters.
- There is a general trend of decreasing HAZ toughness with increasing heat input (cooling time). This effect is small in the low nitrogen steels that showed only a slight deterioration in toughness. The transition temperature of the high nitrogen steels (0.013 % N) rises drastically for cooling times above 30-40s.
- The austenite in the HAZ of V- and Nb-steels coarsens significantly during welding. By Ti-micro-additions to V- and Nb-steels this coarsening can be minimised. An increase in nitrogen content in Ti-V-N plates, above the stoichiometric level for TiN suppresses grain coarsening of the HAZ.
- The plate production processing route appears to have an insignificant effect on HAZ toughness.
- Vanadium-microalloyed steels have generally very good toughness properties following welding with 2 or more passes, irrespective of their N-contents; toughness is adversely affected in inter-critically reheated coarse grain heat affected zones (IC CG HAZ) although less so than in C-Mn or Nb-microalloyed steels.

REFERENCES

Section 1

1.1 R. Lagneborg, T. Siwecki, S. Zajac and B. Hutchinson, The role of vanadium in microalloyed steels, Scand. J. Met., **28** (1999) pp. 186-241.
1.2 T.N. Baker, Processes, microstructure and properties of vanadium microalloyed steels, Mater. Sci. Tech., **25** (2009) pp.1083-1107.
1.3 www.Vanitec.org/Publications

Section 2

2.1 T. Gladman, The Physical Metallurgy of Microalloyed Steels. The Institute of Metals, (1997).
2.2 K.J. Irvine, F.B. Pickering and T. Gladman, Grain-refined C-Mn steels. JISI, **205** (1967) pp. 161-182.
2.3 K. Narita, Physical chemistry of the group IVa (Ti,Zr), Va (V,Nb,Ta) and rare earth elements in steel. Trans. ISIJ, **15** (1975) pp. 145-152.
2.4 C. Wagner, Thermodynamics of Alloys., Addison-Wesley Co., Reading, Mass., (1952).
2.5 M. Hillert and J. Staffansson, The regular solution model for stoichiometric phases and ionic melts, Acta Chemica Sc. **24** (1970) pp. 3618-3626.
2.6 S. Zajac, Thermodynamic model for the precipitation of carbonitrides in microalloyed steels. Swedish Institute for Metals Research Report IM-3566, (1998).
2.7 B. Sundman, B. Jansson and J.O. Andersson, ThermoCalc databank system. CALPHAD, **9** (1985) pp. 153-159.
2.8 K. Yvon and E. Parthé, Crystal chemistry of the close-packed transition-metal carbides. Part1, Crystal structure of the zeta-vanadium niobium and titanium carbides. Acta Cryst., **26** (1970) pp. 149-153.
2.9 R.R. Zupp and D.A. Stevenson, The influence of vanadium on the activity of carbon in the Fe-C-V system at 1000°C., correlation of the influence of substitutional solutes on the activity coefficient of carbon in iron-base system. Trans. AIME, **236** (1966) pp. 1316-1323.
2.10 H.A. Wriedt and H. Hu, Chemical metallurgy, a tribute to C. Wagner., Proc. Symp. Chicago, TSM-AIME, Warrendale, PA (1981) pp. 171-194.
2.11 H. Ohtani and M. Hillert, A thermodynamic assessment of the Fe-N-V System. CALPHAD, **15** (1991), pp. 25-39.
2.12 R.W. Fountain and J. Chipman, Solubility and precipitation of boron nitride in iron-boron alloy, Trans. AIME, **224** (1962) pp. 599-606.
2.13 S. Koyama, T. Ishii and K. Narita, Physical chemistry, J. Japan Inst. Metals, 37 (1973) pp. 191-195.
2.14 N. Yoshinaga, K. Ushioda, S. Akamatsu and O. Akisue, Precipitation Behaviour of sulphides in Ti-added ultra low-carbon steels in austenite. ISIJ Int., **34** (1994) pp. 24-32.
2.15 S. Zajac and B. Jansson, Thermodynamics of the Fe-Nb-C-N system and the solubility of niobium carbonitrides in austenite, Metall. Trans., **29B** (1998), pp. 163-176.

Section 3

3.1 S. Zajac, Thermodynamic model for the precipitation of carbonitrides in microalloyed steels, Swedish Institute for Metals Research, Internal Report IM-3566, 1998.
3.2 S. Zajac, R. Lagneborg and T. Siwecki, The role of nitrogen in microalloyed steels. Int. Conf. Microalloying '95, Iron and Steel Society Inc., Pittsburgh, PA, 1995, pp. 321-340.
3.3 W. Roberts, Recent innovations in alloy design and processing of microalloyed steels. Contribution to the 1983 Int. Conf. on Technology and Applications of High Strength Low Alloy (HSLA) Steels, Philadelphia, PA, 1983, pp. 67-84.
3.4 T. Siwecki, A. Sandberg and, W. Roberts, Processing characteristics and properties of Ti-V-N steels. Int. Conf. on Technology and Applications of High Strength Low Alloy (HSLA) Steels, Philadelphia, PA, 1983, pp. 619-634.
3.5 S. Zajac, T. Siwecki, W. B. Hutchinson and M. Attlegård, Recrystallization controlled rolling and accelerated cooling for high strength and toughness in V-Ti-N steels, Metall. Trans., **22A** (1991) pp. 2681-2694.
3.6 B. Lehtinen and P. Hansson, Characterisation of microalloy precipitates in HSLA steels subjected to different weld thermal cycles, Swedish Institute for Metals Research, Internal Report IM-2532, 1989.
3.7 S. Zajac, T. Siwecki and L.-E. Svensson, The influence of plate production processing route, heat input and nitrogen on the HAZ toughness in Ti-V microalloyed steel, Proc. Conf. on Processing, Microstructure

and Properties of Microalloyed and Other Modern Low Alloy Steels, ed. A. J. DeArdo, TMS, Warrendale, PA, 1991, pp.511-523.
3.8 R. Lagneborg, J. Eliasson, T. Siwecki, W.B. Hutchinson and F. Lindberg, Ferrite grain refinement by intragranular nucleation on (Ti,V)N and its application on CSP hot strip steels, Research Report KIMAB-2010-128, 2010.
3.9 S. Sarian, Diffusion of Ti in TiC, J. Appl. Physics **40** (1969) pp. 3515-3520.
3.10 M. L. Baskin, V. I. Tretyakov and I. N. Chaporova, W diffusion in monocarbides of W, Ta and Ti in the solid solution TiC WC and TiC WCTaC, Physics of Metals and Metallography **14** (1962) pp. 86-90.
3.11 M. Prikryl, A. Kroupa. G. C. Weatherly, and S.V. Subramanian, Precipitation behaviour in a medium carbon, Ti-V-N-microalloyed steel, Met. Mat. Trans. **27A** (1996) pp.1149-1165.
3.12 P. Hellman and M. Hillert, On the effect of second-phase particles on grain growth, Scand. J. Metallurgy, **4** (1975) pp. 211-219.
3.13 T. Siwecki, A. Sandberg and W. Roberts, The influence of processing route and nitrogen content on microstructure development and precipitation hardening in vanadium-microalloyed HSLA steels, Swedish Institute for Metals Research, Internal Report IM-1582, 1981.
3.14 L. J. Cuddy, The effect of microalloy concentration on the recrystallization of austenite during hot deformation, Proc. Conf. Thermomechanical Processing of Microalloyed Austenite, TMS-AIME, Warrendale, PA, 1981, pp. 129-140.
3.15 M. Hillert and B. Sundman, A treatment of the solute drag on moving grain boundaries and phase boundaries in binary alloys, Acta Metall., **24** (1976) pp. 731-743.
3.16 J. J Jonas and I. Weiss, Effect of precipitation on recrystallization in microalloyed steels, Metals Science, **13** (1979) pp. 238-245.
3.17 M. G. Akben, T. Chandra, P. Plassiard and J.J. Jonas, Dynamic precipitation and solute hardening in a V microalloyed steel and two Nb steels containing high levels of Mn, Acta Metall., **29** (1981) pp. 111-121.
3.18 M. J. Luton, Interaction between deformation, recrystallization and precipitation in niobium steels, Metal. Trans., **11A** (1980) pp. 411-420.
3.19 S. F. Medina and J. E. Mancill, Influence of alloy elements in solution on static recrystallization kinetics of hot deformed steels, ISIJ Int., **36** (1996) pp. 1063-1069.
3.20 H. S. Zurob, Y. Brechet and G. Purdy, A model for the competition of precipitation and recrystallization in deformed austenite, Acta Mater. **49** (2001) pp.4183-4190.
3.21 L. Bäcke, Modeling the effect of solute drag on recovery and recrystallisation during hot deformation of Nb microalloyed steels, ISIJ Int., **50** (2010) pp. 239-247.
3.22 J. D. Jones and A. B. Rothwell, Controlled rolling of low-carbon niobium-treated mild steels, Proc. Deformation under Hot Working Conditions, ISI Publication **108**, London 1968, pp.78-82, 100-102.
3.23 A. T. Davenport, L.C. Brossard and R.E.Miner, Precipitation in microalloyed high-strength low-alloy steels, J. Metals **27** (1975) pp. 21-27.
3.24 A. T. Davenport, Proc. Conf. Hot Deformation of Austenite, Cincinnati, TMS-AIME 1977, pp.517-536.
3.25 A. J. DeArdo, Modern thermomechanical processing of microalloyed steel: a physical metallurgy perspective, Proc, Conf. Microalloying '95, Pittsburgh, Iron & Steel Soc., 1995 pp.15-33.
3.26 E. J. Palmiere, Precipitation phenomena in microalloyed steels, Proc. Conf, Microalloying '95, Pittsburgh, Iron & Steel Soc. 1995 pp. 307-820.
3.27 H. L. Andrade, M. G. Abken and J. J. Jonas, Effect of molybdenum, niobium and vanadium on static recovery and recrystallisation and on solute strengthening in microalloyed steels, Met.Trans., **14A** (1983) pp.1967-1977.
3.28 I. Kozasu, C. Ouchi, T. Sampei and T. Okita, Hot rolling as a high-temperature thermo-mechanical process, Proc. Conf. Microalloying '75, ed. M. Korchynsky, New York, 1975 pp.120-135.
3.29 T. Siwecki, W.B. Hutchinson and S. Zajac, Recrystallisation controlled rolling of HSLA steels, Int. Conf. "Microalloying '95, Iron and Steel Society Inc., Pittsburgh, 1995, pp.197-212.
3.30 R. Lagneborg, W. Roberts, A. Sandberg and T. Siwecki, Influence of processing route and nitrogen content on microstructure development and precipitation hardening in V-microalloyed HSLA-steels, Proc. Conf. Thermomechanical Processing of Microalloyed Austenite, Pittsburgh, Met. Soc. AIME, 1981 pp.163-194.
3.31 T. Siwecki and S. Zajac, Recrystallization controlled rolling and accelerated cooling of Ti-V-(Nb)-N microalloyed steels, 32nd Mechanical Working and Steel Processing Conf, Cincinnati, USA 1990, pp.441-451.
3.32 S. Gong, The influence of vanadium on the austenite–ferrite transformation in microalloyed steels, Swedish Institute for Metals Research, Internal Report IM-1488 1980.
3.33 W.B. Hutchinson, Microstructure development during cooling of hot rolled steels, Ironmaking and Steelmaking, **28** (2001) pp. 145-151.

3.34 S. Zajac, S.F. Medina and V. Schwinn, Grain refinement by intragranular ferrite nucleation on precipitates in microalloyed steels, (2007) ECSC Final report, EUR 22451EN.
3.35 J-Y. Cho, D-W. Suh, J-H. Kang and H-C. Lee, Orientation distribution of proeutectoid ferrite nucleated at prior austenite grain boundaries in vanadium-added steel, ISIJ Int., **42** (2002) pp. 1321-1323.
3.36 T. Furuhara, J. Yamagushi, N. Sugita, G. Miyamoto and T. Maki, Nucleation of proeutectoid ferrite on complex precipitates in austenite, ISIJ Int., **43** (2003), pp. 1630-1639.
3.37 T. Furuhara, T. Shinyoshi, G. Miyamoto, J. Yamagushi, N. Sugita, N. Kimura, N. Takemura and T. Maki, Multiphase crystallography in the nucleation of intragranular ferrite on MnS+V(C,N) complex precipitate in austenite, ISIJ Int., **43** (2003) pp. 2028-2037.
3.38 D. Hernandez, B. Lopez and J.M. Rodriguez-Ibabe, Intragranular ferrite nucleation in V microalloyed structural steels, International Symposium on Microalloyed Steels (in conjunction with the ASM Materials Solutions Conference), Columbus, OH, 2002, pp. 64-70.
3.39 S.Zajac, W.B. Hutchinson, R. Lagneborg and M. Korchynsky, Ferrite grain refinement in seamless pipes through intragranular nucleation on VN, Proc. 3rdInt. Conf. on Thermomechanical Processing of Steels, 2008, Padua, Italy.
3.40 K. He and D.V. Edmonds, Formation of acicular ferrite and influence of vanadium alloying, Mat. Sci. and Techn., **18** (2002) pp. 289-295.
3.41 S.Zajac, Ferrite grain refinement and precipitation strengthening in V microalloyed steels, proc. 43rd Metal Working and Sheet Processing Conf., ISS, **39** (2001) pp. 497-508.
3.42 C, Garcia-Mateo, C. Capdevilla, F.G. Caballero and C. Garcia de Andrés, Influence of V precipitates on acicular ferrite transformation, Part 1: The role of nitrogen, ISIJ Int., **48** (2008) pp. 1270-1275.
3.43 C, Garcia-Mateo, C. Capdevilla, F.G. Caballero and C. Garcia de Andrés, Influence of V precipitates on acicular ferrite transformation, Part 2: The role of nitrogen, ISIJ Int., **48** (2008) pp.1276-1279.
3.43 C. Capdevilla, C. Garcia-Mateo, J. Chao and G. Caballero, Effects of V and N precipitation on acicular ferrite formation in sulphur-lean vanadium steels, Met. and Mat. Trans., **40A** (2009) pp. 522-538.
3.44 A.O. Kluken, Ö. Grong and J. Hjelen, The origin of transformation textures in steel weld metals containing acicular ferrite, Met. Trans., **22A** (1991) pp. 657-663.
3.55 S.P. Ringer and K.M. Easterling, On the rotation of precipitate particles, Acta Met. and Mater., **40** (1992) pp. 275-283.

Section 4

4.1 F.A. Khalid and D. V. Edmonds, Interphase precipitation in microalloyed engineering steels and model alloy, Mat. Sci. Techn. **9** (1993) pp. 384-396.
4.2 K. Relander, Austenitzerfall eines 0.18%C-2%Mo-Stahles im Temperaturbereich der Perlitstufe, Acta Polytechnica Scand. **34** (1964) pp. 1-80.
4.3 A.T. Davenport and R.W.K. Honeycombe, Precipitation of carbides at austenite/ferrite boundaries in alloy steels, Proc. Roy. Soc. London, **322** (1971) pp. 191-205.
4.4 K. Campbell and R.W.K. Honeycombe, The isothermal decomposition of austenite in simple chromium steels, Metal Science J. **8** (1974) pp. 197-203.
4.5 R.W.K. Honeycombe, Transformation from austenite in alloy steels, Met Trans., **7A** (1976) pp. 915-936.
4.6 R.A. Ricks and P.R. Howell, The formation of discrete precipitate dispersions on mobile interphase boundaries in iron-base alloys, Acta Metall., **31** (1983) pp. 853-861.
4.7 R. Lagneborg and S. Zajac, A model for interphase precipitation in V-microalloyed structural steels, Met. Trans., **32A** (2001) pp. 39-46.
4.8 R. Okamoto and J. Ågren, A model for interphase precipitation based on finite solute drag theory, Acta Mater., **58** (2010) pp. 4791-4803.
4.9 R. Okamoto, A. Borgenstam and J. Ågren, Interphase precipitation in Nb microalloyed steels, Acta Mater., **58** (201) pp. 4683-4790.
4.10 G. Miyamoto, R.Hori, B. Poorganji and T. Furuhara, Crystallographic analysis of proeutectoid ferrite/austenite interface and interphase precipitation of vanadium carbide in medium-carbon steel, Met. Mat. Trans., **44A** (2013) pp. 3436-3443.
4.11 T. Murakami, H. Hatano, G. Miyamoto and T. Furuhara, Effects of ferrite growth rate on interphase boundary precipitation in V microalloyed steels, ISIJ Int., **52** (2012) pp. 616-625.
4.12 J.R. Jang, H.W. Yen, C.Y. Chen and C.Y. Huang, The development of interphase precipitated nanometre-sized carbides in the advanced low-alloy steels, Mater. Sci. Forum, **762** (2013), pp. 95-103.
4.13 S. Zajac, T. Siwecki, M. Korchynsky, Importance of nitrogen for precipitation phenomena in V-microalloyed steels, Int. Symp. on Low Carbon Steels for the 90's 1993 ASM/TSM Materials Week, Pittsburgh, USA, 1993, pp. 139-150.

4.14 R. G. Baker and J. Nutting, The tempering of a Cr-Mo-V-W and a Mo-V steel, Precipitation Processes in Steels, ISI Report No 64, London 1969, pp. 1-22.
4.15 R. M. Smith and D. P. Dunne, Structural aspects of alloy carbonitride precipitation in microalloyed steels, Mater. Sci. Forum, **11** (1988) pp. 166-181
4.16 R. W. K. Honeycombe, Fundamental aspects of precipitation in microalloyed steels, Proc. Int. Conf. on Technology and Applications of HSLA Steels, Philadelphia PA, ASM, 1983, pp.243-250.
4.17 W.C. Johnson, C.L. White, P.E. Marth, P.R. Ruf, S.M. Tuominen, K.D. Wade, K.C. Russell, H.I Aaronson, Influence of crystallography on aspects of solid-solid nucleation theory, Met.Trans., **6A** (1975) pp. 911-919.
4.18 J.L. Lee and H.I. Aaronson, Influence of faceting upon the equilibrium shape of nuclei at grain boundaries, Acta Met., **23** (1975) pp. 799-808.
4.19 J. W. Cahn, The Kinetics of Cellular Segregation Reactions, Acta Met., **7** (1959) pp. 18-28.
4.20 M. Hillert, Proc. Int. Symp. on the Mechanism of Phase Transformation in Crystalline Solids, Monograph and Report Series No.33, Institute of Metals, London, 1969, pp. 231-49.
4.21 R. Lagneborg, Interphase precipitation in incoherent austenite/ferrite interfaces, Swedish Institute for Metals Research, Internal Report, IM 2000-012, 2000.
4.22 W. Roberts, A. Sandberg, The composition of V(C, N) as precipitated in HSLA steels microalloyed with vanadium, Swedish Institute for Metals Research, Internal Report IM-1489, 1980.
4.23 M. J. Schmutz, Research Report to Vanitec from Massachusetts Institute of Technology, 1981.
4.24 W. Roberts, A. Sandberg, and T. Siwecki, Precipitation of V(C,N) in HSLA steels microalloyed with V, Proc. Conf. Vanadium Steels, Krakow, Vanitec, 1980, pp. D1-D12.
4.25 S. Zajac, T. Siwecki and B. Hutchinson, Precipitation phenomena in V-microalloyed 0.15-0.22%C structural steels, Swedish Institute for Metals Research, Internal Report IM-3453, 1996.
4.26 S. Zajac, T.Siwecki, B. Hutchinson and R. Lagneborg, Strengthening mechanisms in vanadium microalloyed steels intended for long products, ISIJ Int., **38** (1998) pp. 1130-1139.
4.27 S. Zajac, T. Siwecki, B. Hutchinson and R. Lagneborg, The role of carbon in enhancing precipitation strengthening of V-microalloyed steels. Int. Symp. Microalloying in Steels: New Trends for the 21st Century, San Sebastian, Spain, 1998, pp. 295-302.
4.28 S. Zajac, The role of nitrogen and carbon in precipitation strengthening of V-microalloyed steels, Swedish Institute for Metals Research, Confidential Internal Report 1997.
4.29 S. Zajac, Kinetics of precipitation during hot rolling and cooling in microalloyed steels, Swedish Institute for Metals Research, Internal Report IM-3568, 1998.
4.30 T. Siwecki, J. Eliasson, R. Lagneborg and B. Hutchinson, Vanadium microalloyed baintic hot strip steels, ISIJ Int., **50** (2010) pp. 760-767.

Section 5

5.1 H. Bruce, Transverse corner cracks in continuously cast microalloyed steels, Swedish Institute for Metals Research, Internal Report IM-2568, (1990) (In Swedish).
5.2 S. Zajac, T. Siwecki, W.B. Hutchinson and M. Attlegård, Recrystallised controlled rolling and accelerated cooling for high strength and toughness in V-Ti-N-steels, Metall. Trans. **22A**, (1991) pp. 2681-2694.
5.3 R. Priestner and C. Zhou, Simulation of microstructural evolution in Nb-Ti microalloyed steel during direct hot rolling, Ironmaking and Steelmaking, **22**, (1995), pp. 326-332.
5.4 C. Zhou and R. Priestner, The evolution of precipitates in Nb-Ti microalloyed steels during solidification and post solidification cooling, ISIJ International, 36, (1996) pp. 326-332.
5.5 D.N. Crowther, The effects of microalloying elements on cracking during continuous casting, Proc Vanitec Symp., Beijing, 2001, pp. 99-131.
5.6 R. Lagneborg, The effect of grain size and precipitation of carbides on the creep properties of Fe-20%Cr-35%Ni alloys, J. Iron and Steel Inst., **207**, (1969) pp. 1503-1506.
5.7 H.G. Suzuki, S. Nishimura and S. Yamaguchi, Characteristics of hot ductility in steels subjected to melting and solidification, Trans. ISIJ, **22**, (1982) pp.48-56.
5.8 B. Mintz and J.M. Arrowsmith, Hot ductility behaviour of C-Mn-Nb-Al steels and its relationship to crack propagation during the straightening of continuously cast strand, Met. Technol., **6**, (1979) pp. 24-32.
5.9 B. Mintz and R. Abushosha, Influence of vanadium on hot ductility of steel. Ironmaking and Steelmaking, **20**, (1993) pp. 445-452.
5.10 B. Mintz and R. Abushosha, The hot ductility of V, Nb/V and Nb containing steels, Mater. Sci. Forum, **284-285** (1998) pp. 461-468.
5.11 L.P. Karjalainen, H. Kinnunen and D. Porter, Hot ductility of certain microalloyed steels under simulated continuous casting conditions. Mater, Sci. Forum, **284-286**, (1998) pp. 477-484.

5.12 D.N. Crowther, M.J.W. Green and P.S.Mitchell, The influence of composition on the hot cracking susceptibility during casting of microalloyed steels processed to simulate thin slab casting conditions, Mater. Sci. Forum, **284-286** (1998) pp. 469-476.
5.13 K.M. Banks, A. Tuling and B. Mintz, Influence of V and Yi on hot ductility of Nb-containing steels of peritectic C contents, Mater. Sci. Tech., **27** (2011) pp.1309-1314.
5.14 J.M. Rodriguez.Ibabe, Thin slab direct rolling of microalloyed steels, Trans-Tech Publications, **33** (2007).
5.15 P.L. Lubensky, S.L. Wigman and D.J. Johnson, High strength steel processing via direct charging using thin slab technology, Proc. Microalloying '95 Iron and Steel Society Inc., Pittsburgh (1995) pp. 225-233.
5.16 T. Siwecki, Surface and structure of thin slab and precipitates in hot strip rolled steel microalloyed with V and Nb, Swedish Institute for Metals Research Confidential Report (1996).
5.17 P.S. Mitchell, D.N. Crowther and M.J.W. Green, The manufacture of high strength vanadium-containing steels by thin slab casting, 41st. Mechanical Working and Steel Processing Conference, Baltimore, USA 2007 pp. 459-470.

Section 6

6.1 T. Siwecki, A. Sandberg, W. Roberts, and R. Lagneborg, The influence of processing route and nitrogen content on microstructure development and precipitation hardening in V-microalloyed HSLA Steels. Proc. Thermomechanical Processing of Microalloyed Austenite, TMS-AIME, Warrendale, USA, 1982, pp.163-192.
6.2 T. Siwecki, A. Sandberg, and W. Roberts, Processing characteristics and properties of Ti- V-N Steels, Proc. Int. Conf. on HSLA Steels – Technology and Application, ASM, Ohio, USA, 1984, pp.619-634.
6.3 M. Korchynsky, New trends in science and technology of microalloyed steels, Proc. Int. Conf. on HSLA Steels-85, Beijing, ASM, 1986, pp.251-257.
6.4 T. Siwecki and S. Zajac, Recrystallization controlled rolling and accelerated cooling of Ti-V-(Nb)-N microalloyed steels, Proc. 32nd Mechanical Working and Steel Processing Conference, ISS-AIME, Warrendale, USA, 1991, pp. 441-451.
6.5 S. Zajac, T. Siwecki, B. Hutchinson and M. Attlegård, Recrystallization controlled rolling and accelerated cooling as the optimum processing route for high strength and toughness in V-Ti-N steels. Met. Trans., **22A** (1991) pp.2681-2694.
6.6 R.M. Fix, A.J. DeArdo And Y.Z. Zheng, Mechanical properties of V-Ti microalloyed steels subject to plate rolling simulations utilizing recrystallization controlled rolling, Proc. Int. Conf. on HSLA Steels-85, Beijing, ASM, 1986, pp.219-227.
6.7 S.W. Lee, W.Y Choo and C.S. Lee, Effects of recrystallization controlled rolling on the properties of TMCP steel for ship building application, Proc. Int. Symp. on Low Carbon Steels for 90`s, Pittsburgh, ASM Intern. M, M&M Soc., 1993, pp.227-234.
6.8 T. Siwecki, B. Hutchinson and S. Zajac, Recrystallization controlled rolling of HSLA steels, Proc. Microalloying-95, Pittsburgh, ISS-AIME, Warrendale, USA, 1995, pp.197-211.
6.9 T. Siwecki and G. Engberg, Recrystallization controlled rolling of steels, Proc. Thermo-Mechanical Processing in Theory, Modelling & Practice, Stockholm, ASM Intern., 1997, pp.121-144.
6.10 A. Tamminen, Development of recrystallization controlled rolling and accelerated cooled structural steels, Proc. Thermo-Mechanical Processing in Theory, Modelling & Practice, Stockholm, ASM Intern., 1997, pp.357-368.
6.11 T. Siwecki, G. Engberg and A. Cuibe, Thermomechanical controlled processes for high strength and toughness in heavy plates and strips of HSLA Steels, Proc. THERMEC, TMS, M,M&M, 1997, pp.757-763.
6.12 T. Siwecki, S. Zajac and B. Ahlblom, The influence of thermo-mechanical process parameters on the strength and toughness in direct quenched and tempered boron-steels (Re>700Mpa), Proc. Physical Metallurgy of Direct Quenched Steels, Materials Week 92, ASM/TMS, Chicago, 1992, pp.213-230.
6.13 A. Blomqvist and T. Siwecki, Optimization of hot rolling and cooling parameters for long products, Swedish Institute for Metals Research, Internal Report IM-3101, 1994.
6.14 W. Roberts, A. Sandberg, T. Siwecki and T. Werlefors, Prediction of microstructure development during recrystallization hot rolling of Ti-V-steels, Proc. HSLA Steels - Technology. and Application, Metals Park, OH, ASM, 1984, pp.67-84.
6.15 T. Siwecki, Modelling of microstructure evolution during recrystallization controlled rolling, ISIJ International**, 32** (1992) pp.368-376.
6.16 T. Siwecki and B. Hutchinson, Modelling of microstructure evolution during recrystallization controlled rolling of HSLA steels, Proc. 33rd Mechanical Working and Steel Processing Conference, Warrendale, USA, ISS-AIME, 1992, pp.397-406.

6.17 S. Pettersson and T. Siwecki, Microstructure evolution during recrystallization controlled rolling of V-microalloyed steels. Swedish Institute for Metals Research Contract Report No 39.190 (1998).
6.18 C.M. Sellars and J.A. Whiteman, Recrystallisation and grain growth in hot rolling, Metal Science, **13** (1979) pp. 187-194.
6.19 F. Kovac, T. Siwecki, B. Hutchinson and S. Zajac. Finishing conditions appropriate for recrystallization controlled rolling of Ti-V-N-steel, Metall. Trans., **23A** (1992) pp. 373-375.
6.20 J.M. Chilton and M.J. Roberts, Microalloying effects in hot rolled low-carbon steels finished at high temperatures, Metall. Trans. **11A** (1980) p.1711-1721.
6.21 G.F. Melloy, How changes in composition and processing affect HSLA steels, Metal Progr. **89** (1966) pp.129-133.

Section 7

7.1 X. Yang, Y. Jin, Q. Wang and G. Zhang, Study of high tensile heavy plate with V-N microalloying technology, Proc. Int. Seminar on Application Technologies of Vanadium in Flat Rolled Sheets, Vanitec, 2006, pp.64-68.
7.2 Q. Sun and Y. Zhang, Hot deformation behaviour and recrystallization controlled rolling of Ti-V-N plate steels, Proc. Int. Seminar on Application Technologies of Vanadium in Flat Rolled Sheets, Vanitec, 2006, pp. 69-74.
7.3 F. Kovac, V. Jurko and B. Stefan, Report, UEM SAV Kosice, 1990.
7.4 J.D. Grozier, Production of microalloyed strip and plate, Proc. Microalloying'75, ed. M. Korchynsky, New York, 1975, pp. 241-250.
7.5 L.K. Chiang, Development and production of HSLA 80ksi (550MPa) steels at Gallatin Steel, Proc. Int. Seminar on Applications of Vanadium in Flat Rolled Steels, Vanitec, 2005, pp. 26-33.
7.6 P.J., Lubensky, S. L. Wigman and D. J. Johnson, High strength steel processing via direct charging using thin slab technology, Proc. Microalloying-95, Pittsburgh, ISS-AIME, Warrendale, USA, 1995, pp. 225-233.
7.7 D.N. Crowther, Vanadium containing high strength strip using thin slab casting, British steel report (1996).
7.8 Y. Li, J.A. Wilson, D.N. Crowther, P.S. Mitchell, A.J. Craven and T.N. Baker, The effects of vanadium, niobium, titanium and zirconium on the microstructure and mechanical properties of thin cast slabs, ISIJ Int., **44** (2004) pp. 1093-1102.
7.9 Y. Li, J.A. Wilson, A.J. Craven, P.S. Mitchell, D.N. Crowther and T.N. Baker, Dispersion strengthening in vanadium microalloyed steels processed by simulated thin slab casting and direct charging Part 1 – processing parameters, mechanical properties and microstructure, Mater. Sci. Tech., **23** (2007) pp. 509-518.
7.10 J.A. Wilson, A.J. Craven, Y. Li and T.N. Baker, Dispersion strengthening in vanadium microalloyed steels processed by simulated thin slab casting and direct charging Part 2 – chemical characterisation of dispersion strengthening precipitates, Mater. Sci. Tech. **23** (2007) pp. 519-527.
7.11 B. Hutchinson, T.Siwecki, J.Komenda, J. Hagström, R. Lagneborg, J.-E. Hedin and M.Gladh, New vanadium-microalloyed bainitic 700 MPa strip steel product, Ironmaking and Steelmaking, **41** (2014) pp. 1-6.
7.12 Y. Caifu, Development of high strength construction rebars, Proc. Int. Seminar on Production/Application of High Strength Seismic Grade Rebar Containing Vanadium, Beijing, 2003, pp. 58-70.
7.13 Y. Caifu, Research, production and application of high strength rebars, Proc. Int. Symp on the Research and Application of High Strength Reinforcing Rebar, Hangzhou, 2003, pp. 124-132.
7.14 D. Russwurm and P. White, High strength weldable reinforcing bars, Conf. Proc. Microalloying ´95, Iron and Steel Society Inc., Pittsburgh, PA, 1995, pp.377-384.
7.15 Magallon, C. Molina, D. Lopez and L. Martinez, Microalloyed steel bars of 590MPa minimum yield strength, Proc. Int. Conf. on Processing, Microstructure, and Properties of Microalloyed and other Modern High Strength Low Alloy Steels, Iron and Steel Soc., Warrendale, USA, 1992 pp.217-222.
7.16 Siwecki and G. Engberg, Recrystallisation controlled rolling of steels, Proc. Conf. Thermo-Mechanical Processing in Theory, Modelling & Practice, Stockholm,1996 ASM Int., 1997, pp.121-144.
7.17 A. Blomqvist and T. Siwecki, Optimisation of hot rolling and cooling parameters for long products, Swedish Institute for Metals Research, Internal report IM-3101, 1994.
7.18 K. Fahlström, B. Hutchinson, J. Kommenda, E. Lindh-Ulmgren and T. Siwecki, Weldability of vanadium-nitrogen steels, Internal Report, KIMAB-2011-553 (2011).
7.19 T.Pan, Z.Wang, C.Yang and Y.Zhang, Chemistry and process optimisation of V- microalloyed N80 seamless tube, 3rd. Int. Conf on Thermomechanical Processing of Steels, Padua, 2008.

7.20 G. Liu, S. Liu, Y. Zhong, Y. Zhang and S. Feng, Microstructure and properties of non-quenched/tempered seamless tubes of medium carbon V-microalloyed steel, Iron and Steel, **40**, Supplement November 2005, pp. 535-541.
7.21 R. Lagneborg, O. Sandberg and W. Roberts, Microalloyed ferrite-pearlite forging steels with improved toughness, Proc. HSLA Steels` 85, Beijing, (1985) pp.863-873.
7.22 R. Lagneborg, O. Sandberg and W. Roberts, Optimisation of microalloyed ferrite pearlite forging steels, Fundamentals of Microalloying Forging Steels, Golden, Colorado, (1986) pp. 39-54.
7.23 G. Krauss, Vanadium microalloyed forging steels, Proceedings of the Vanitec Symposium, Beijing, China, (2001) pp. 50-56.
7.24 Y. Li and D.J. Milbourn, Vanadium microalloyed forging steel, Proceeding of the2nd. International Symposium on Automobile Steel, Anshan, China, (2013) pp. 47-54
7.25 F. Ishikawa and T. Takahashi, The formation of intragranular ferrite plates in medium- carbon steels for hot forging and its effect on the toughness, ISIJ Int., **35** (1995) pp.1128-1133.
7.26 D. Bhattacharya, Machinability of a medium carbon microalloyed bar steel, Conf. Proc. Fundamentals of Microallying Forging Steels, Colorado, USA, (1986) pp. 475-490.
7.27 D.K Matlock, G. Krauss and J.G. Spear, Microstructures and properties of direct- cooled forging steels, J. Materials Processing Technology, **117** (2001) pp.324-328.

Section 8

8.1 P. Hansson and X.Z. Ze, The influence of steel chemistry and weld heat input on the mechanical properties in Ti-microalloyed steels, Swedish Institute for Metals Research, Internal Report IM-2300, 1988.
8.2 P. Hansson, Influence of nitrogen content and weld heat input on Charpy and COD toughness of the grain coarsened HAZ in vanadium microalloyed steels, Swedish Institute for Metals Research, Internal Report IM-2205, 1987.
8.3 S. Zajac, T. Siwecki, B. Hutchinson, L-E. Svensson, and M. Attlegård, Weldability of high nitrogen Ti-V microalloyed steel plates processed via thermomechanical controlled rolling, Swedish Institute for Metals Research, Internal Report IM-2764, 1991.
8.4 S. Zajac, T. Siwecki and L-E. Svensson, The influence of plate production processing route, heat input and nitrogen on the toughness of Ti-V-microalloyed steel, Int. Symp. On Low Carbon Steels, Pittsburgh, USA, TSM (1993) pp. 511-523.
8.5 J.T. Bowker, R.F. Orr, G.E. Ruddle and P.S. Mitchell, The effect of vanadium on the parent plate and weldment properties of accelerated cooled API 5LX100 steels, 35th Mechanical Working and Steel Processing Conference, Pittsburgh (1973) pp. 403-412.
8.6 K. Fahlström, B. Hutchinson, J. Kommenda, E. Lindh-Ulmgren and T. Siwecki, Internal report, Swerea KIMAB-2011-553 (2011).
8.7 P.H.M. Hart, The influence of vanadium microalloying on the weldability of microalloyed steels, Welding and Cutting, **55** (2003) pp. 204-210.
8.8 N.E. Hannerz, Weld metal and HAZ toughness and hydrogen cracking susceptibility of HSLA steels influenced by Nb, Al,V,Ti and N, Proc. Conf. Welding of HSLA (Microalloyed) Structural Steels, Rome (1976) pp. 365-385.
8.9 MNC Handbook nr. 15 Welding of Steels, SIS, 1986.
8.10 N.E. Hannerz and B.M. Jonsson-Holmqvist, The influence of vanadium on heat affected zone properties of mild steel, Metal Science, **8** (1974) pp. 228-234.
8.11 P.S. Mitchell, W.B. Morrison and D.N. Crowther, The effect of vanadium on the mechanical properties and weldability of high strength structural steels, Low Carbon Steels for the 90`s, ASM/TSM, Pittsburgh, USA, (1990), pp. 337-334.
8.12 P.S. Mitchell, P.H.M. Hart, and W.B. Morrison, The effect of microalloying on HAZ toughness, Microalloying 95, ed. M. Korchynsky et. al., I&SS, Pittsburgh, USA, (1995), pp. 149-162.
8.13 H. Beladi and W.B. Hutchinson, Deakin University, Australia, un-published work (2013).
8.14 Y. Li, D.N. Crowther, M.J.W. Green, P.S. Mitchell and T.N. Baker, The influence of vanadium in microalloyed steels on the properties and microstructure of the intercritically reheated coarse grained zone, Thermomechanical Processing of Steels, IOM, vol. 1 (2000), pp.69-78.
8.15 Y. Li, D.N. Crowther, M.J.W. Green, P.S. Mitchell and T.N. Baker, The effect of vanadium and niobium on the properties and microstructure of the intercritically reheated coarse grained heat affected zone in low carbon microalloyed steels, ISIJ International, **41** (2001) pp. 46-55.
8.16 Y. Li and T.N. Baker, Effect of morphology of martensite-austenite phase on fracture of weld heat affected zone in vanadium and niobium microalloyed steels, Mater. Sci. Techn., **26** (2010) pp. 1029-1040.